

Double-barrier membranes: coupling hydrophilic coatings with biocidal Ag-MOFs for sustainable (bio)fouling mitigation and biofilm inhibition

Original

Double-barrier membranes: coupling hydrophilic coatings with biocidal Ag-MOFs for sustainable (bio)fouling mitigation and biofilm inhibition / Pejman, Mehdi. - (2022 Feb 25), pp. 1-110.

Availability:

This version is available at: 11583/2957750 since: 2022-03-09T10:24:32Z

Publisher:

Politecnico di Torino

Published

DOI:

Terms of use:

Altro tipo di accesso

This article is made available under terms and conditions as specified in the corresponding bibliographic description in the repository

Publisher copyright

(Article begins on next page)



ScuDo
Scuola di Dottorato - Doctoral School
WHAT YOU ARE. TAKES YOU FAR



1
2
3
4
5
6
7
8
9
10
11
12
13
14
15
16
17
18
19
20
21

Doctoral Dissertation
PhD Program in Civil and Environmental Engineering (34th Cycle)

Double-barrier membranes: coupling hydrophilic coatings with biocidal Ag-MOFs for sustainable (bio)fouling mitigation and biofilm inhibition

Mehdi Pejman

Supervisor

Prof. Alberto Tiraferri

External Advisor

Prof. Ahmad Rahimpour

Doctoral Examination Committee:

1- Prof. Naser Tavajohi

2- Dr. Fatima Seyedpour

Politecnico di Torino

(14.02.2022)


1 This thesis is licensed under a Creative Commons License, Attribution - Non-commercial -
2 Nonderivative Works 4.0 International: see <http://www.creativecommons.org>. The text may be
3 reproduced for non-commercial purposes, provided that credit is given to the original author.

4
5
6
7
8
9

10
11 I hereby declare that the contents and organisation of this dissertation constitute my own original
12 work and does not compromise in any way the rights of third parties, including those relating to the
13 security of personal data.

14
15
16
17
18
19
20

21
22
23
24
25
26
27


.....
Mehdi Pejman
Turin, (14.02.2022)

1
2
3
4
5
6
7
8
9
10
11
12
13
14
15
16
17
18
19
20
21
22
23
24
25
26

1 **Summary**

2 This thesis revolves around the use of novel nanomaterials and various coating
3 techniques with the aim of improving the capability of polymeric membranes in water and
4 wastewater purification processes.

5 The exponential growth in human population and the consequent increased water demand
6 for use in industry, agriculture, and drinking together with limited fresh water sources has made
7 inevitably clear the need to treat and re-use our consumed water. One of leading technologies to
8 produce high-quality water streams is membrane technology. Despite widespread use of reverse
9 osmosis membranes since their inception, fouling remains the major setback in membrane
10 operations and significantly reduces membrane operability and life-span. Fouling occurs when
11 feed contaminants such as e microorganisms, precipitates, and organic load block membrane
12 pores or deposit on its surface, severely impacting water permeability and/or selectivity.

13 There have been several measures taken to combat fouling, and its most nefarious
14 version, biofouling. Since fouling propensity heavily depends on membrane surface chemistry
15 and morphology, tailoring the surface of membranes has been a popular pathway of equipping
16 membranes with antifouling capacity. One of the most effective methods of anti-biofouling
17 mitigation methods in membranes, is attaching biocides to their surface, notably antimicrobial
18 metals, and silver in particular. Issues with silver anchoring includes the subsequent leaching and
19 a lack of compatibility with the polymeric matrix of the membrane. In that regard, silver-
20 containing metal-organic-frameworks (Ag-MOFs) could remedy both those issues. These
21 structures have proven to be stable, membrane-compatible (due to their organic linker), and
22 tunable (several choices for metal nodes and organic linkers).

1 While anchoring metals can help organic fouling mitigation, an effort to incorporate more
2 potent antifoulants into/onto the membrane surface will lead to a membrane with coupled
3 antifouling/anti-biofouling capabilities. This approach will lead to a “double-barrier” membrane
4 with specialized defensive forces against two specific foulant types (organic and microbial).
5 Zwitterions and acrylic acid could provide such antifouling components; the former due to
6 forming a strong hydration layer with immense water affinity, and the latter through carboxyl
7 groups known as potent hydrophiles.

8 In this research, polymeric membranes were surface-functionalized using Ag-MOFs as
9 anti-biofoulants, coupled with an antifouling agent, i.e., zwitterions or acrylic acid. Modified
10 membranes were characterized using various techniques; surface morphology, roughness,
11 hydrophilicity, electrical charge, and most importantly, successful anchoring of modifying agents
12 was verified through spectroscopy tools. These membranes were then tested in osmotic (forward
13 osmosis) and pressure-driven (ultrafiltration) processes. The effect of functionalization was
14 evaluated in terms of membrane transport parameters and these membranes were subsequently
15 tested against model organic and microbial foulants during long term filtration experiments to
16 measure the efficacy of surface-functionalized membrane against fouling and biofouling,
17 respectively. For forward osmosis (FO), water flux to reverse solute flux (the main indicator for
18 transport trade-off in FO) remained mostly unaffected or became slightly improved. For
19 ultrafiltration (UF) membranes, water permeation was generally reduced due to the rising
20 thickness of the membrane active layer due to foulant deposition. The collective effect of a
21 “double-barrier” coating resulted in 80% and 87% of flux preservation during organic and
22 microbial fouling in FO, respectively. For UF, steady-state flux values reached up to 13 times
23 that of the pristine membrane, and long-term heavy organic foulant filtration experiments

1 resulted in up to 20% of flux recovery post-cleaning in MOF-containing samples compared to
2 zero for the pristine membranes.

3 Antibacterial resilience of silver-containing membranes was further investigated through
4 confocal microscopy, heterotrophic plat count, and SEM imaging. MOF-containing membranes
5 displayed impressive antimicrobial activity reaching 90% and 95% inactivation rates against
6 *E.coli* and *S. aureus*, respectively . Silver leaching was evaluated over bi-weekly or monthly
7 periods to measure the released amount of silver into the containing solution. These tests attested
8 to the strength and stability of immobilized Ag-MOFs onto the membrane surface, with leaching
9 degrees well below WHO safety guidelines (0.1 mg/l).

10 This research was dedicated to investigating the potential of Ag-MOFs to be used as
11 surface functionalization agents as anti-biofoulants for polymeric water treatment membranes.
12 This research shows the efficacy of MOFs could be more pronounced when used in conjunction
13 with pre-grafted hydrophilic layers; this approach led to improved surface features, provided
14 more binding sites for the MOFs while acting as antifoulants themselves and collectively
15 shielded the membrane from organic and microbial fouling in a “double-barrier” mode. Fouling
16 was significantly reduced, and membrane transport parameters were preserved (osmotically
17 driven) or enhanced (pressure-driven).

18

19

20

21

22

1

2

3 **Acknowledgments**

4 Financial support for this work was provided through the PhD scholarship from MIUR

5 and Politecnico di Torino

6

1

2

3 **Dedication**

4 I would like to humbly dedicate this thesis to my loving wife, Mina, who has been my
5 rock and salvation throughout the years and the primary source of support in my scientific
6 endeavors. This thesis is the fruition of our **relentless collective** endeavors, on a sacred mission
7 to a fulfilled and accomplished life. I hope this effort do justice to her fortitude, wisdom, and
8 grace, for these are the assets I treasure above all else in this world.

9

TABLE OF CONTENTS

1		
2	1. Introduction	1
3	1.1 Membranes and water treatment.....	1
4	1.2 Fouling	2
5	1.3 Membrane surface engineering	3
6	1.4 MOFs and other materials	4
7	1.5 Research hypotheses.....	5
8	2. Materials and methods	9
9	2.1. Reagents	9
10	2.2 Synthesis of Ag-MOFs.....	10
11	2.3 Surface modification of membranes.....	10
12	2.4 Characterization of materials and membranes.....	17
13	2.5 Membrane filtration: transport parameters, fouling and biofouling protocols.....	18
14	2.6 Evaluation of antibacterial activity in membranes	20
15	2.7 Stability of silver ions on the membranes	22
16	3. Results and discussion	24
17	3.1 Physio-chemical characterization of membranes and functionalization verification	24
18	3.1.1 Attenuated total reflection- Fourier transform infrared spectroscopy (ATR-FTIR).....	24
19	3.1.2 X-ray photoelectron spectroscopy (XPS)	27
20	3.1.3 Energy Dispersive X-Ray Analysis (EDX), X-Ray Diffraction (XRD).....	32
21	3.1.4 Zeta potential.....	35
22	3.1.5 Contact angle.....	36
23	3.2 Morphological properties of modified membranes and Ag-MOFs	37
24	3.2.1 Scanning Electron Microscopy (SEM), Transmission electron microscopy (TEM), Atomic Force	
25	Microscopy (AFM).....	37
26	3.2.2 Ag-2MI nanocrystals	44
27	3.3 Antibacterial properties, biofilm inhibition	46
28	3.4 Membrane performance metrics: FO transport, UF separation, (bio)fouling investigation.....	55
29	3.5 Silver stability on membranes	70
30	4. Conclusions	74
31	5. Suggestions	76
32	References	77
33		

1. Introduction*

1.1 Membranes and water treatment

The rapid and ever-present growth of the world population places a massive burden on our water resources. It is possible to facilitate access to available water and better manage our produced wastewater through desalination and wastewater reuse [1]. Also, industrial activities are increasing and presenting us with a variety of emerging (micro)pollutants which are discharged into our water sources through wastewater, necessitating perpetual innovativeness in our purification approaches [2]. Membrane-based technologies provide efficient and relatively cheap mechanisms that enable the production of high-quality water from different feed sources. Specifically, forward osmosis (FO) is an innovative process that makes use of thin-film composite (TFC) membranes, utilizing the concept of osmosis, that has attracted substantial academic and industrial interest recently. TFC FO membranes are highly water-permeable membranes with excellent salt rejection [3]. These membranes have captured interest for a variety of applications, such as wastewater treatment [2] and seawater/brackish water desalination [4,5]. On the other hand, ultrafiltration (UF) is also widely used for the treatment and pre-treatment of contaminated waters, employing an external source of applied pressure to drive water through the membrane [6,7]. The majority of UF membranes are synthesized from polymers, mostly polysulfone and polyethersulfone. The pore size of UF membranes denies passage to a wide spectrum of pollutants, including medium to high molecular weight compounds, suspended particles, bacteria, and viruses [6]. Despite a great potential for widespread applications, membrane-based processes remain restricted in use due to fouling. This

* Part of the content discussed in this chapter, with permissions, has been previously published in [41,42,63,127]

1 phenomenon robs membranes of its optimum water productivity and permeate quality, while
2 simultaneously reducing the membrane lifespan and increasing the operational cost of filtration
3 [8,9].

4 **1.2 Fouling**

5 Fouling occurs when retained microorganisms, colloidal particles, organic matter, and
6 scaling agents deposit either at the membrane surface or within its pores [10]. Fouling
7 predominantly occurs through adsorption, chemical interaction, cake layer formation, and pore
8 blocking [11], with rates and degrees correlated with factors such as foulant concentration in
9 feed and membrane surface pore distribution [12]. Amongst all forms of fouling, biofouling
10 seems to be the most challenging one [13]. Bio-fouling, referred to as the “Achilles’ heel” of
11 membrane processes, occurs when microorganisms adhere onto the membrane surface and
12 generate a new bio-layer, called biofilm [14]. The biofilm produces a potent barrier against mass
13 transport, which is shared by all fouling types, and in addition to the hydraulic resistance of the
14 membrane which hinders water passage, necessitates the application of a larger driving force
15 (applied external pressure in pressure-driven processes or dosing higher draw solutes in osmotic
16 processes) to maintain productivity. Immobilizing antimicrobial agents via surface modification
17 of membranes is a substitute to adjusting process hydraulics or constant dosage of materials
18 (becoming almost entirely useless due to extremely fast proliferation of biofilms) in handling
19 biofouling through preemptively increasing the antimicrobial activity, surface hydrophilicity, and
20 by reducing the surface roughness of the membrane [15,16]. Several routes have been tried over
21 the years to implement these agents onto/into the membrane matrix, including cross-linking
22 [17,18], in-situ covalent functionalization [19,20], layer-by-layer assembly [17,21], direct
23 deposition of metal ions and nanoparticles [22,23], and surface grafting [24,25].

1 **1.3 Membrane surface engineering**

2 Fouling potential directly relates to membrane material and more specifically, with its
3 surface morphology and chemistry. That is why surface science is an indispensable approach to
4 fouling mitigation, and vast research work on membrane modification is dedicated to it [26].
5 Tailoring the membrane surface has proven quite reliable in improving its performance and
6 sustaining surface integrity over prolonged filtration periods for a variety of foulant feeds.
7 Understanding and designing the solid-liquid interface of water and the membrane could lead to
8 not only reduced fouling, but less required energy input for the treatment process [27], less
9 chemical waste and a less frequent need for membrane cleaning.

10 One way to mitigate/postpone biofouling is the surface modification of the membrane
11 through anchoring biocidal agents [28]. Silver-based materials have been reported to impart
12 effective anti-biofouling properties when applied as surface modification agents to membranes
13 due to the strong and broad antimicrobial activity of silver against bacteria, fungi, and viruses
14 [29]. In-situ surface functionalization of the commercial polyamide (PA) membranes with silver
15 nanoparticles thus appeals as a viable solution since it requires less silver as opposed to direct
16 silver dosing into the feed solution, and therefore, is less wasteful and more cost-effective.
17 Logically, this approach minimizes the silver-induced health risks and bacterial resistance [30],
18 and also renders the silver regeneration process much easier [31]. However, silver leaching due
19 to little resistance to washing [22,32,33] as well as incompatibility issues between inorganic
20 materials and the organic membrane matrix, (costing membrane its selectivity [34]) pose some of
21 the major concerns with silver nanomaterials. In this respect, the use of metal organic
22 frameworks (MOFs) is a promising candidate for a more rational use of silver.

23

1 **1.4 MOFs and other materials**

2 MOFs consist of organic ligands connected by metal ions to form one-, two-, or three-
3 dimensional coordination networks [35,36]. Their key advantage over other structures is their
4 tunability by a wide array of different metals and/or organic linkers. Also, their organic backbone
5 may ameliorate the interaction with the polyamide active layer of TFC membranes compared to
6 other fully inorganic structures such as silver nanoparticles, avoiding compatibility issues. MOFs
7 tend to release metal ions (release-killing) [37] and hence, Ag-MOFs have been investigated for
8 antimicrobial application by several researchers [38–40]. Multiple immobilization techniques
9 have been experimented with and studied, such as surface grafting [24,25], layer by layer
10 assembly [17,21] in-situ surface functionalization, and direct deposition of MOFs [41,42].

11 MOFs provide a reservoir of uniformly distributed biocidal metal ions on a membrane
12 surface, prevent aggregation of nanomaterials, and maintain their antimicrobial activity for a
13 prolonged time [43]. Also, in these structures, the organic frame can act as a barrier against high
14 rates of metal loss [11,44]. A specifically attractive surface modification approach is represented
15 by the coupling of the antimicrobial property of Ag-based MOFs with the antifouling activity
16 provided by highly hydrophilic materials such as zwitterions [45–47]. Zwitterions are overall
17 neutral compounds with an equal number of positively and negatively charged functional groups.
18 This architecture produces a strong binding property with water molecules, forming a strong
19 hydration layer [48], favoring the passage of water. For this reason, several methods have been
20 used thus far to introduce zwitterions at the membrane surface, including surface-initiated
21 polymerization [49], grafting [50], and coating [51]. It is worthy of mention that the separation
22 properties of the membrane are defined by the uppermost few nanometers of its thickness,
23 therefore, applying surface-modifications in the post-fabrication stage seems to be one of the

1 most efficient strategies, as evidenced by our previous successful studies following the same
2 approach [41,42].

3 **1.5 Research hypotheses**

4 The hypothesis of the first study is that different zwitterions can be effectively applied to
5 the membrane surface in combination with Ag-MOFs to impart enhanced antifouling properties
6 coupled with added antibacterial activity to the membrane surface. The functionalization impacts
7 the transport parameters of the membranes; however, it needs to preserve its transport parameters
8 at the minimum to be considered an effective approach. In order to investigate the effects and
9 consequences of modification, Ag-based MOFs were combined with carboxyl (COO^-) and sulfur
10 (SO_3^-)-containing zwitterions to develop novel antifouling/anti-biofouling TFC membranes via
11 chemical grafting on the membrane surface; firstly, the zwitterionic layer is grafted, followed by
12 immersion under an Ag-MOFs solution. In addition to transport parameters assessment and
13 characterization of the membrane surface, fouling and biofouling tests were also conducted to
14 reveal the potential effect of the modifying agents.

15 The second study picks one zwitterion (COO^- -containing) and focuses on investigating
16 the effects of the simultaneous introduction of Ag-MOFs and said zwitterion for combined
17 functionalization of a polyamide membrane. To this end, carboxyl-rich zwitterions are grafted
18 onto the polyamide, and then a simple dipping procedure is adopted to promote the effective in-
19 situ growth of silver-based MOFs for the first pathway. Second pathway introduced a suspension
20 of zwitterion/MOF as the base grafted layer, followed by the Ag-MOFs in-situ growth mode,
21 replicating the first pathway. Surface characterization and transport analysis studies were
22 conducted like the previous study. For both studies, the antimicrobial activity of functionalized
23 membranes was assessed through both plate count and confocal microscopy. Ultimately, the

1 antifouling/anti-biofouling capability of the membranes was discussed based on their flux
2 behavior in medium-term filtration experiments. To conclude, the rate of silver release was also
3 measured to assess the efficacy of the grafting method on silver stability and consequently,
4 silver-related environmental health and safety concerns.

5 For the third study, UF membranes were functionalized under UV-irradiation grafting
6 instead, accomplished either via “grafting to” or “grafting from” technique. In “grafting to”, end-
7 functionalized polymer molecules react with functional groups on the surface in order to form
8 tethered chains [52]. The “grafting from” technique, however, starts at the substrate level by
9 (normally covalently) attached initiator groups. As a result, molecules of a second desirable
10 monomer can easily spread into and across the established grafted first layer, allowing for higher
11 degrees of uniformity and density of the final coated layer [52,53]. One of the best known
12 “grafting from” pathways, initially introduced by Ma et al. (34) to modify polypropylene
13 membranes, is realized through a 2-step process to form a secondary layer of polymeric surface
14 via UV grafting, mediated with benzophenone (BP) as a photo initiator [54]. Therefore, such
15 grafting practice using carefully selected monomer pair can lead to potent imparted features, with
16 uniform and distribution potentially for a lengthy period. The feature in demand for the purposes
17 of this study is antifouling membranes. For this research, polymeric UF membranes are
18 functionalized with Ag-MOFs through BP-assisted UV photo-grafting of acrylic acid (AA),
19 much similar to the zwitterion-Ag-MOF strategy employed for the FO membranes. First, BP was
20 used as a photo-initiator for UV-grafting of AA onto the membrane, thus preparing the surface
21 for in-situ MOFs synthesis. The grafted AA layer itself combats fouling through added
22 hydrophilicity to the surface while also providing a reactive site for Ag-MOF immobilization,
23 forming the “defensive” barrier [55–57]. These AA-seeded membranes are thus functionalized

1 with Ag-MOFs to impart additional antibacterial activity, realizing the “offensive” aspect of
2 modification. Immobilizing a hydrophilic base layer via the “grafting from” pathway leads to an
3 impressive increase in Ag binding sites and thus, potentially more favorable loading degree
4 leading to more efficient MOF-assisted antifouling as indicated by our past studies [41,42]. To
5 our knowledge, this effort was the first work to accommodate Ag-MOFs onto the membrane
6 surface by exploiting the capacity of AA UV photo-grafting.

7 A fourth study, focusing on FO, was briefly discussed to aid with the illumination of
8 antibacterial properties. Seeing as *E. coli* is not known to generate strong biofilms, another
9 microorganism, *P. aeruginosa*, was investigated as a microbe with wide infectivity and robust
10 biofilm formations to verify the actual inhibition/mitigation rates demonstrated by the same Ag-
11 MOFs used in other three studies. Of course, Ag-MOFs were incorporated into the m-
12 phenylenediamine (MPD) solution as part of integration into the TFC membrane PA selective
13 layer and there was no hydrophilic coating prior or after MOF introduction. The sole objective of
14 this inclusion was to magnify the resilience these Ag-MOFs provide to the membranes in
15 combating strong and fast-proliferating biofilms.

16 FO and UF membranes were comprehensively characterized to verify the presence of
17 newly grafted molecules and investigate the newly obtained physio-chemical properties. A cross-
18 flow and a dead-end filtration setup were built to be used to evaluate the performance of FO and
19 UF membranes, respectively, in terms of UF water flux and permeability for FO, FO reverse
20 solute flux (selectivity) and UF retention of a high-concentration humic acid feed, and fouling
21 behavior during long-term filtration periods. Notably, their antibacterial properties were
22 investigated and fully discussed based on the results obtained from disc inhibition zone and
23 confocal microscopy methods, followed by measuring the silver release rate.

1 This thesis focuses on research on producing membranes with maximized surface
2 potency in terms of antifouling and anti-biofouling with strong biofilm inhibition, through
3 implementing a double-barrier coating strategy for osmotic and pressure-driven membranes and
4 processes.

5

6

7

8

9

10

11

12

13

14

15

16

17

18

1 **2. Materials and methods**[†]

2 This research is based on two articles studying FO membranes, and one focusing UF
3 experiments. The reagents and materials have significant overlaps with primary focus on MOFs
4 and a hydrophilic coating, however, pathways of modifications and of course, methods of
5 performance evaluation naturally differ due to process differences. They will each be expanded
6 upon in this section of the thesis.

7 **2.1. Reagents**

8 Silver nitrate (AgNO_3) was used as the source of metal, with 2-methylimidazole (2MI) as
9 the organic linker, and ethanol as a solvent for the synthesis of silver-based metal organic
10 frameworks (Ag-MOFs). For the preparation of the grafting solutions to be used on FO
11 membranes, *N,N*-diethylethylenediamine (DEDA), potassium persulfate, and sodium
12 metabisulfite were used. 3-bromopropionic acid (BPA) and 1,3-propane sultone (PS) were used
13 as two types of COO^- -based and SO_3^- -based zwitterions. For pH adjustment, nitric acid (HNO_3)
14 and sodium hydroxide (NaOH) were used. Sodium chloride (NaCl) was used in the preparation
15 of the draw solution (DS) to conduct the FO filtration tests. KCl was used to prepare background
16 solutions for streaming potential measurements. Commercial TFC PA FO membranes from
17 Porifera (Porifera, Inc., CA) were used as the baseline pristine membranes soaked in 1% Sodium
18 metabisulfite solution for 24 h, then immersed in water until use.

19 For UF tests, we used similar material sources for the synthesis of Ag-MOFs; AgNO_3 ,
20 2MI, water and ethanol. Benzophenone (BP) was used as the photo-initiator, in a UV chamber
21 (Dymax ECE 5000) deploying an irradiation wavelength within the UV-A range (averaged at

[†] Methods and protocols discussed in this chapter, with permissions, have been previously published in [41,42,63,127]

1 365 nm) utilized to house the membranes for surface modification. Acrylic acid (AA) was used
2 as a hydrophilic monomer as a hydrophilic pre-graft layer to Ag-MOFs. Commercial M-PS20-
3 GPET UF membranes from Nanostone Water were immersed in aqueous solution at pH 11
4 overnight to wash off any coating agent before functionalization to be used as pristine baseline
5 membranes. Deionized water (DI) was used for all purposes during FO and UF
6 experimentations. Except for AA and ethanol (Acros Organics), other reagents were purchased
7 from Sigma-Aldrich and all were used as received.

8 **2.2. Synthesis of Ag-MOFs**

9 Preparation of Ag-MOFs in the original powder form was adapted from previously
10 reported protocols [58,59]. AgNO₃ (0.6 g) was dissolved in 90 mL of deionized (DI) water to
11 prepare the metal solution, while the ligand solution was prepared by using a 90 mL ethanol
12 solution containing 2MI (1.05 g). The two solutions were separately stirred and ultra-sonicated in
13 a bath for 15 min and 2 min, respectively. Then, the ligand solution was slowly poured into the
14 stirring metal solution followed by 30 min of additional stirring. The mixture was then kept
15 stagnant for 3 h for the formed MOFs to precipitate. The resulting suspension containing the
16 precipitates was washed several times using DI in order to remove the unreacted substances.
17 Next, the precipitate was centrifuged twice at 8000-10000 rpm with one round of rinsing with
18 ethanol after each round. Finally, the powder was collected and dried in an oven for 18 h at 60
19 °C.

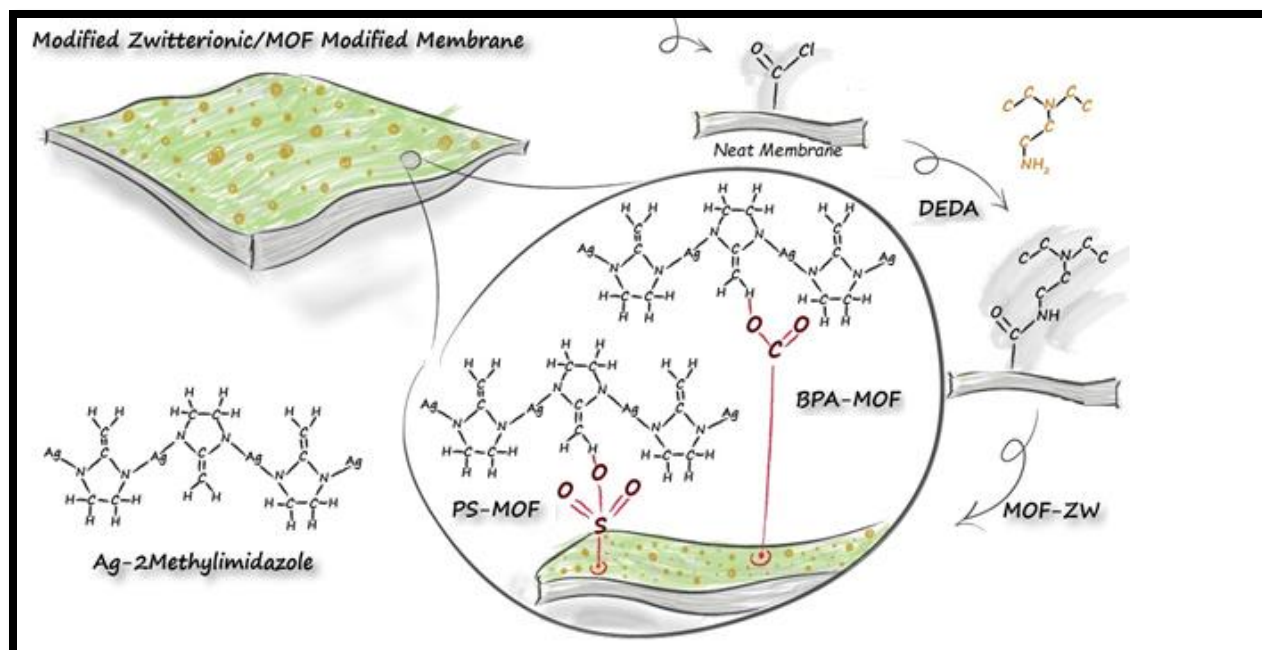
20 **2.3. Surface modification of membranes**

21 For the purposes of this research, several modification protocols were adapted, and each
22 were investigated through different pathways to optimize said protocols. For the FO membranes,
23 zwitterions were grafted as a hydrophilic bedding to bind Ag-MOFs. This approach was realized

1 through following the protocol from a recent study by Yi *et. al* [46]. An aqueous solution
2 containing DEDA (2% wt.), potassium persulfate (0.03% wt.), and sodium metabisulfite (0.02%
3 wt.) at pH 5 was slowly poured and kept on top of the rubber-framed membrane surface at room
4 temperature for 60 min, which resulted in DEDA-grafted membrane via an amidation reaction
5 between the carboxyl groups on the membrane surface and DEDA amine functional groups.

6 In our first study [42], we experimented with BPA and PS as the pre-grafted zwitterionic
7 layer to investigate their independent and collective effects with MOFs on the membrane surface
8 features and performance behavior. DEDA-grafted membranes were immersed under a PS
9 aqueous solution (5% wt., pH 5.0) or a BPA aqueous solution (5% wt., pH 5.0), for 20 h at 40
10 °C, to graft SO_3^- -based or COO^- -based zwitterions, respectively. These membranes are referred
11 to as “TFC-PS” and “TFC-BPA”, respectively. Membranes functionalized with Ag-MOFs were
12 fabricated with the same procedure except that 0.05 wt.% of Ag-MOFs was added to the PS
13 aqueous solution (dubbed as “TFC-PS-MOF”) and to the BPA solution (thus dubbed “TFC-
14 BPA-MOF”). A mixture of NMP (10 wt.%) and DI (90 wt.%) was used as a solvent to prepare
15 the zwitterionic solution for TFC-BPA-MOF to avoid agglomeration and precipitation.
16 Unmodified pristine membranes were referred to as “TFC0” for the purposes of this project. The
17 functionalization strategy was schematically visualized and is reproduced here from the Journal
18 of Membrane Science in Scheme 1 [42].

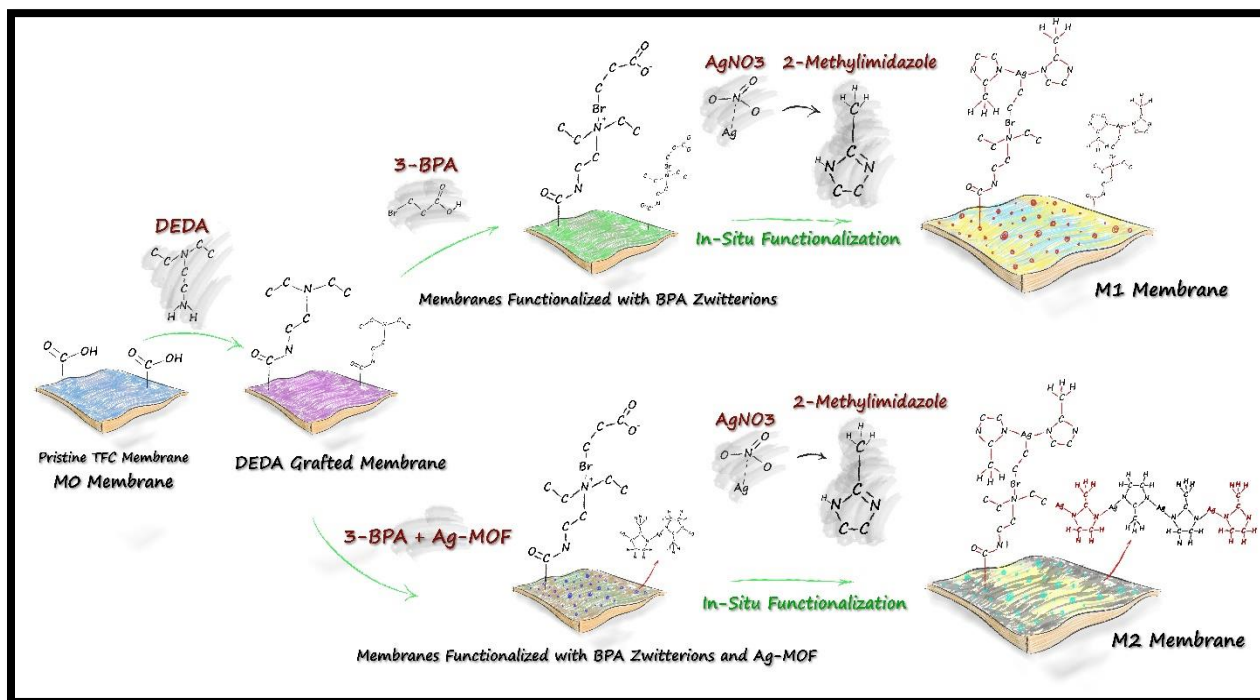
19



1
 2 **Scheme 1.** Schematic illustration of the surface functionalization with BPA and PS zwitterions and Ag-
 3 MOFs

4 Based on the favorable results from this study, it was decided to further investigate this
 5 approach by exploring one of the more promising modification strategies in the next project
 6 [41]; employing in-situ growth instead of direct deposition which was explored in the previous
 7 study. Membranes were grafted with DEDA first, then subject to two different fabrication
 8 methods. For this study we only worked with BPA, being the more challenging of the two
 9 zwitterions based on previous experience (more difficult dispersion in MOF solution) and to
 10 keep the bed layer conditions constant. Some samples were obtained by covering the DEDA-
 11 grafted surfaces with a BPA aqueous solution (5 wt%, pH 5.0), for 20 h at 40 °C, labeled as
 12 “M1”. The next batch were instead obtained by covering the DEDA-grafted surfaces with a
 13 solution containing both BPA (5 wt. %, pH 5.0) and Ag-MOFs (0.05 wt. %), which were then
 14 labeled as “M2”. Again, here a mixture of N-Methyl-2-pyrrolidone (NMP, 10 wt.%) and water
 15 (90 wt.%) was needed (minimized NMP by experimentation) as a solvent for better dispersion of

1 Ag-MOFs in the BPA solution. The final stage was the in-situ formation of Ag-MOFs on top of
 2 both M1 and M2. To this aim, a metal solution (1.5 wt. % in 180 mL DI) and a ligand solution
 3 (2.5 gr in 160 mL ethanol) were separately prepared. The membranes, M1 and M2, were then
 4 both immersed under the metal solution followed by the ligand solution, each time for 30 min.
 5 The samples were finally heat-cured at 50 °C for 1 hr to finish the procedure. Here, the surface
 6 functionalization pathway is reproduced from the study in ACS Applied Materials and Interfaces
 7 and presented as Scheme 2 [41].



8
 9 **Scheme 2.** Illustrative scheme of the steps involved in the preparation of the M1 and M2
 10 membranes, through grafting BPA (with Ag-MOFs for M2) and a subsequent 2-stage in-situ growth
 11 with Ag-MOFs

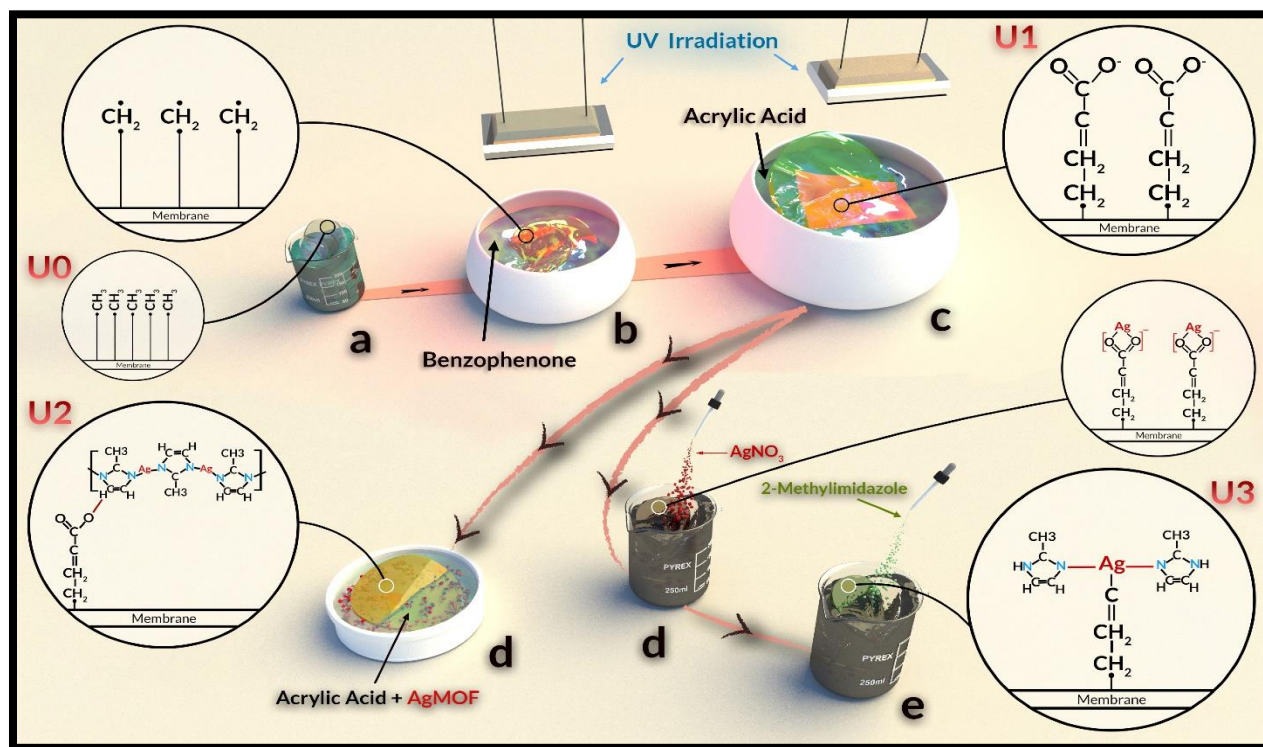
12 These two studies exploited the potential of zwitterions to bind metal ions due to the
 13 presence of the negative functional groups [47,60]. Abundant residual carboxyl functional
 14 groups present on the BPA-modified surface can thus act as active sites and promote nucleation

1 of Ag⁺ ions [61]. Upon silver nucleation, organic 2-MI was applied to coordinate with Ag⁺ ions,
2 and to self-assemble networks of Ag-2MI MOFs [28]. Ag-2MI contains amide functional groups,
3 thus these structures are capable of coordinating with Ag⁺ ions and form highly stable Ag-2MI
4 MOFs on the zwitterionic pre-grafted layer [60,62].

5 In our most recent study [63], the potential of UV-irradiation to graft layers of desired
6 characteristics was explored. As thoroughly outlined before, UV irradiation was used to graft BP,
7 to be followed by grafting AA monomers as the hydrophilic bedding layer to immobilize Ag-
8 MOFs. Different membrane functionalization pathways were investigated, producing a total
9 number of five sets of samples. The pristine polysulfone (PSf) UF membrane was referred to as
10 U0. This procedure was carried out in two stages: in the first step, the membranes were
11 immersed in a methanol solution containing 0.3 wt.% of BP for 30 min. BP-soaked membranes
12 were then irradiated in the UV chamber for 5 min. In the second stage, the BP-activated
13 membrane samples were immersed in 5 wt.% of AA solution for 30 min. The AA-soaked
14 membranes were then again UV irradiated for 5 min, leading to U1 membranes.

15 Further two sets of membranes, U2 and U3, saw the introduction of Ag-MOFs into the
16 preparation procedure, following two separate modification pathways. The first step of
17 modification, i.e., UV-mediated BP grafting, was conducted similarly to U1, while the
18 introduction of AA and Ag-MOFs in the next stage of modification would be performed
19 differently. In the first adapted pathway, 0.1 wt.% of Ag-MOFs powder (synthesized following
20 the previously established protocol) was dispersed in AA solution and poured on top of the BP-
21 grafted membranes before a second UV irradiation, producing U2 samples. In the second chosen
22 pathway, Ag-MOFs were simply in-situ grown on top of U1 membranes to obtain U3
23 membranes. In-situ formation of Ag-MOFs was done based on the same proportions and

1 procedures established in the previous study [41]. Nucleation of Ag^+ on top of the photo-grafted
 2 membrane surface is realized through negative carboxyl functional groups [64,65], a mechanism
 3 similar to BPA as the zwitterionic layer. All UV-irradiated samples were subsequently rinsed
 4 several times with methanol and dried at 50 °C for 1 h. To understand the individual effects of
 5 each modifying agents, Ag-MOFs were also in-situ grown over the surface of pristine PSf U0
 6 membranes, without any intermediate functionalization either with BP or AA. These samples
 7 were labeled as U4. The step-by-step functionalization procedures for this membrane collection
 8 are illustrated in Scheme 3 [63], reproduced from my published paper in the Chemical
 9 Engineering Journal.



10
 11 **Scheme 3.** Illustration of membrane modification steps to obtain different membrane surface
 12 modifications. U0: pristine PSf membrane; U1: AA photo-grafted membrane; U2: Ag-MOFs-coated AA
 13 photo-grafted membrane; U3: in-situ synthesized Ag-MOFs on the surface of AA photo-grafted
 14 membrane; U4 (not shown in the figure): in-situ synthesized Ag-MOFs on the surface of pristine PSf
 15 membrane. [63]

1
2
3
4
5
6

Readers are referred to consult table 1, where all the details and modification components corresponding to all the studied pristine and surface-functionalized membranes for this research are tabulated for ease of access.

Table 1. Details and specifications of all membranes studied for the purposes of this research

Membrane ID	Study	Characteristics
TFC0	FO #1	Pristine commercial PA membrane
TFC-BPA	FO #1	TFC0 grafted with BPA solution
TFC-BPA-MOF	FO #1	TFC0 grafted with BPA solution, followed by immersion under Ag-MOFs solution
TFC-PS	FO #1	TFC0 grafted with PS solution
TFC-PS-MOF	FO #1	TFC0 grafted with PS solution, followed by immersion under Ag-MOFs solution
M0	FO #2	Pristine commercial PA membrane
M1	FO #2	M0 grafted with BPA solution, followed by 2-step in-situ growing of Ag-MOFs
M2	FO #2	M0 grafted with mixed BPA and Ag-MOFs solution, followed by 2-step in-situ growing of Ag-MOFs
U0	UF	Pristine commercial PSf membrane
U1	UF	U0 immersed under AA solution, then UV-irradiated
U2	UF	U0 immersed under AA and Ag-MOFs solution, then UV-irradiated
U3	UF	U1 with 2-step in-situ growing of Ag-MOFs
U4	UF	U0 with 2-step in-situ growing of Ag-MOFs

7
8
9

1 2.4. Characterization of materials and membranes

2

3 The membranes prepared for the purposes of this research were thoroughly and
4 comprehensively characterized using a variety of techniques and devices to verify the success of
5 functionalization with different modifying agents utilized. The surface chemistry was
6 investigated through attenuated total reflection Fourier transform infrared spectroscopy (ATR-
7 FTIR, Nicolet iS50 FT, Thermo Fisher Scientific, USA), set between 500 and 4000 cm^{-1} . Surface
8 morphology was observed using scanning electron microscopy (SEM, JEOL 7000, JEOL, USA)
9 equipped with energy-dispersive X-ray spectroscopy (EDX, JEOL 7000, JEOL, USA) for
10 elemental analysis. A 5-nm gold layer was coated on the membranes using a sputter coater
11 (Leica EM ACE600, USA) before measurements for each study. Further investigation of surface
12 topology and roughness analysis was provided via atomic force microscopy (AFM, Bruker
13 Dimension Edge, USA) and results were summarized in terms of Ra (average roughness) and
14 R_{RMS} (root-mean-squared roughness). Contact angle measurements (DSA 100, KRÜSS,
15 Germany) of water droplets on five randomized spots was performed for each sample as an
16 indicator of membrane wettability.

17 The spectra of the crystalline patterns corresponding to the MOF particles were
18 investigated via X-ray powder diffraction (XRD) using a diffractometer (Bruker D8, Germany),
19 with a Cu $K\alpha$ radiation in 2θ mode from 0° to 60° . X-ray photoelectron spectroscopy (XPS) was
20 performed with a Kratos spectrometer (Axis 165 XPS/ Auger, Shimadzu, Japan) equipped with a
21 100 μm monochromatic Al K(alpha) X-ray in order to identify the functional groups present on
22 the membrane surfaces. Membrane surface chemistry was further explored using Raman
23 spectroscopy, measured on a DXR Raman spectroscope (Thermo Scientific, U.S.A) equipped
24 with a red excitation laser operating at 633 nm. Stokes Raman spectra were collected in the 100-

1 2000 cm^{-1} range with a spectral resolution of 1.0 cm^{-1} . Zeta potential measurements were
2 performed using a SurPASS Electrokinetic solid surface streaming potential analyzer (Anton
3 Paar, Graz, Austria), across a 3-11 pH range. All the streaming zeta potential measurements were
4 conducted in a background electrolyte solution composed by 1 mM KCl at 25 °C and using HCl
5 (0.05 M) and NaOH (0.05 M) as acid and base for pH adjustment, respectively.

6 **2.5. Membrane filtration: transport parameters, fouling and biofouling protocols**

7 The transport parameters of the FO membranes i.e., the water permeance (A), the salt
8 permeability coefficient (B), and the structural parameter of the support layer (S), were measured
9 using a cross-flow FO unit with a cell containing a membrane coupon with a net surface area of
10 30 cm^2 . The system included two gear pumps circulating the NaCl draw solution (DS) and the
11 feed solution (FS) on the two sides of the membrane at a cross-flow velocity of 20 cm/s .
12 Deionized water and NaCl solutions with various concentrations (0.5, 1, 1.5, and 2 M) were used
13 as the FS and DS, respectively. The method proposed by Tiraferri et al. [66] was applied to
14 determine the membranes transport parameters. This methodology comprises a single FO
15 experiment divided into four stages, each employing a different concentration of DS. The
16 experimental water and reverse salt fluxes measured in each stage are fitted to the corresponding
17 FO transport equations by performing a least-squares non-linear regression, using A, B, and S as
18 regression parameters.

19 Dynamic fouling experiments for forward osmosis process were conducted to evaluate
20 the organic and microbial fouling propensity of the membranes, based on a previously
21 established protocol in literature [59]. For organic fouling, sodium alginate (SA), a
22 polysaccharide, was selected as a model organic foulant [67–69]. The foulant solution was
23 prepared by dissolving 250 mg/L of the SA powder in DI. Initial feed and draw volumes of 3 L

1 were utilized for the fouling experiments. Prior to the addition of the foulant, the permeate flux
2 was allowed to stabilize at the value of $20 \pm 1 \text{ L m}^{-2}\text{h}^{-1}$ using the designated concentration of
3 DS for a corresponding experiment. The FO system was then left to operate for 24 h at a cross-
4 flow velocity of 8.5 cm/s, while recording the permeate flux continuously using an electronic
5 balance. For the biofouling assessment, the same protocol was followed by using *E. coli* bacteria,
6 replacing SA, at a concentration of 10^7 CFU/L . The foulant concentrations during these
7 experiments represent conditions of accelerated fouling and are significantly higher than those
8 encountered in typical operation to test these modified membranes against harsh conditions
9 [70,71].

10 UF membranes were on the other hand, tested using typical procedures employed for
11 pressure-driven membrane filtration processes. Membrane coupons with an effective area of 3.8
12 cm^2 were used in a dead-end cell (model 8010, Amicon). Pressure was applied with a pressurized
13 nitrogen gas tank and the membrane cell was kept stirring at 200 rpm during all stages of
14 filtration. The membranes were initially compacted using DI as feed solution under 4 bar applied
15 pressure for 2 h to reach a steady flux. Subsequently, DI water permeation flux was measured
16 and recorded at 2 bar for 1 h (J_{w1}). A 200 ppm humic acid (HA) solution containing 10 mM
17 NaCl, 0.1 mM NaHCO_3 (pH 7), and 0.5 mM CaCl_2 was used as model foulant solution to
18 evaluate HA filtration parameters such as flux (J_p), rejection, and fouling behaviour, with an
19 initial flux of $600 \pm 100 \text{ L m}^{-2}\text{h}^{-1}$ under a 3 bar applied pressure in HA filtration stage for both
20 pristine and modified membranes. The water permeability coefficient, PWP ($\text{L m}^{-2}\text{h}^{-1}\text{bar}^{-1}$), and
21 the rejection rate of HA were determined using equations (1) and (2):

$$22 \quad PWP = \frac{J_{w1}}{\Delta p} \quad (1)$$

$$23 \quad R\% = \left(1 - \frac{C_p}{C_f}\right) \times 100 \quad (2)$$

1 where Δp is the transmembrane pressure applied, $R\%$ is the solute rejection rate, and C_p
2 and C_f are the solute concentrations in the permeate and feed solution, respectively. Membranes
3 were physically washed with DI water for 10 min after the completion of HA filtration stage and
4 were tested again to investigate the flux recovery for 1 h (J_{w2}) using DI water as feed under a 2
5 bar pressure. The flux recovery ratio (FRR%) as a typical fouling propensity indicator was
6 measured for all membranes based on the following formula:

$$7 \quad FRR\% = \left(\frac{J_{w2}}{J_{w1}} \right) \times 100 \quad (3)$$

8 Fouling was deconstructed for further illumination as total fouling ratio ($R_t\%$), reversible
9 fouling ratio ($R_r\%$), and irreversible fouling ratio ($R_{ir}\%$), all calculated using the formulas below:

$$10 \quad R_t(\%) = \left(1 - \frac{J_p}{J_{w1}} \right) \times 100 \quad (4)$$

$$11 \quad R_{ir}(\%) = \left(1 - \frac{J_{w2}}{J_{w1}} \right) \times 100 \quad (5)$$

$$12 \quad R_r(\%) = \left(\frac{J_{w2} - J_p}{J_{w1}} \right) \times 100 \quad (6)$$

13 Above-mentioned equations were extracted based on previous studies on UF filtration
14 performance assessment [72–74]. All fluxes are reported in the normalized format (relative to the
15 starting flux measured for each membrane) for easier comparative analysis of fouling behaviour
16 among all membranes.

17 **2.6. Evaluation of antibacterial activity in membranes**

18 Antibacterial activity of Ag-MOFs is one of the main attractions of utilizing them as
19 surface modification agents for membranes used in water treatment. Here, the exact procedure
20 first reported in my first study is presented [42]. To this purpose, *E. coli* was used as the model
21 gram-negative bacterial microorganism to investigate the antimicrobial properties of the surface-
22 functionalized membranes. The *E. coli* was cultured overnight in trypticase soy broth (TSB) by
23 incubating at 37 °C with proper shaking. Freshly prepared TSB was inoculated with the

1 overnight culture of *E. coli* and was again incubated at the same temperature for 3 hours. In these
2 studies, a total of three methods were deployed to monitor and investigate the antibacterial
3 properties of the membranes. Heterotrophic plate count and confocal microscopy were used to
4 determine the relative survival of unattached bacteria exposed to the surfaces of the MOF-
5 containing membranes and the survival of attached bacteria on the membrane surfaces,
6 respectively; SEM was used to determine the morphological conditions of bacterial cells.

7 For heterotrophic plate count experiments, the bacteria culture was centrifuged at 6000
8 rpm for 3 minutes and a bacterial pellet was obtained, the pellet was then re-suspended in a
9 sterile 1X phosphate buffer solution (PBS) and the final bacterial solution of 10^7 CFU/mL
10 concentration was achieved. For each membrane, 1×1 cm² of the membrane-active surface was
11 exposed to the bacterial solution (1 mL) in Petri dishes and was incubated at 37 °C for 1 h with
12 shaking. The 1×1 cm² samples were then washed with sterile 10 mL of PBS to wash away the
13 unattached bacterial cells from the membranes. This rinse solution was then plated on the
14 trypticase soy agar plates and these plates were again incubated for 1 day at 37 °C (without
15 shaking) to determine the viability of the unattached cells. The number of viable cells was
16 finally counted in terms of colony-forming units (CFUs).

17 For confocal microscopy tests, LIVE/DEAD™ BacLight™ Bacterial Viability Kit
18 (ThermoFisher Scientific) was used to determine the viability of the attached cells on the
19 membranes. SYTO 9 and Propidium Iodide (PI) were used to investigate the proportion of
20 attached cells that were viable and non-viable, respectively. After microbial exposure,
21 membranes were stained with PI and SYTO9 stains and were incubated in the darkroom for 15
22 min. Then, the membranes were again washed in sterile PBS to get rid of the extra staining
23 material, before being analyzed under a microscope. The membranes were then mounted on

1 glass slides and examined under a Nikon C2 Laser Scanning Confocal Microscope. An EGFP
2 laser at 495-547 nm was used for SYTO 9 and a TRIC laser at 566-624 nm was used for PI
3 stains' excitation. The SYTO 9 caused the live cells to fluoresce green while caused the dead
4 cells to fluoresce red. At a magnification of 60X lens at a scanning speed of half-frame per
5 second, a digital image capture system was used to take 18 images on different spots of each
6 membrane sample to count the total dead and live bacteria. Two sets of membrane samples were
7 used to determine the viability of the bacteria on the membranes and the average was reported.

8 For the SEM images, the membrane samples exposed to bacteria were washed with 2.5%
9 glutaraldehyde, again washed with PBS and sterile DI water, and then successively washed with
10 different percentages of laboratory-grade ethanol to enable clear imaging of the healthy viable
11 bacterial cells and damaged bacterial cells on the tested membranes. A Thermo Scientific™
12 Apreo scanning electron microscope (SEM) was used for the image capture of the live-dead
13 bacterial situation of the cells on the membranes.

14 For disc inhibition tests used on the UF membranes, a bacterial suspension with 10^6
15 CFU/mL of either *E. coli* or *S. aureus* was spread on a petri dish containing trypticase soy agar.
16 Membrane discs with a diameter of 12 mm were then placed with the active layer facing
17 downward in the middle of the petri dish and incubated for 18 h. A Canon 1200d camera was
18 used to take pictures of the inhibited area on the membranes.

19 **2.7. Stability of silver ions on the membranes**

20 Silver stability is a major factor to consider when used as a modification agent as it can
21 directly affect health and safety of humans, flora, fauna, and specifically aquatic life. To evaluate
22 the stability/release of silver ions, membrane coupons (4 cm²) were incubated in 20 mL of DI
23 water under mild shaking in batch mode, followed by acidification using a 1% nitric acid

1 aqueous solution and shaking (100 rpm) for 30 days. Water samples were analyzed daily for up
2 to 15 or 30 days using inductively coupled plasma mass spectrometry (ICP-MS, 143 NEXION
3 300D, PerkinElmer) to determine the leached Ag^+ concentration in the solution [75].

4

5

6

7

8

9

10

11

12

13

14

15

16

17

1 **3. Results and discussion**[‡]

2 **3.1. Physio-chemical characterization of membranes and functionalization verification**

3 The success of membrane functionalization with various modifying agents was verified
4 using different spectroscopic and morphological techniques. These techniques provide evidence
5 as to the quality and quantity of agent immobilization, their independent physio-chemical
6 conditions, and the resulting characteristics of the membranes post-functionalization.

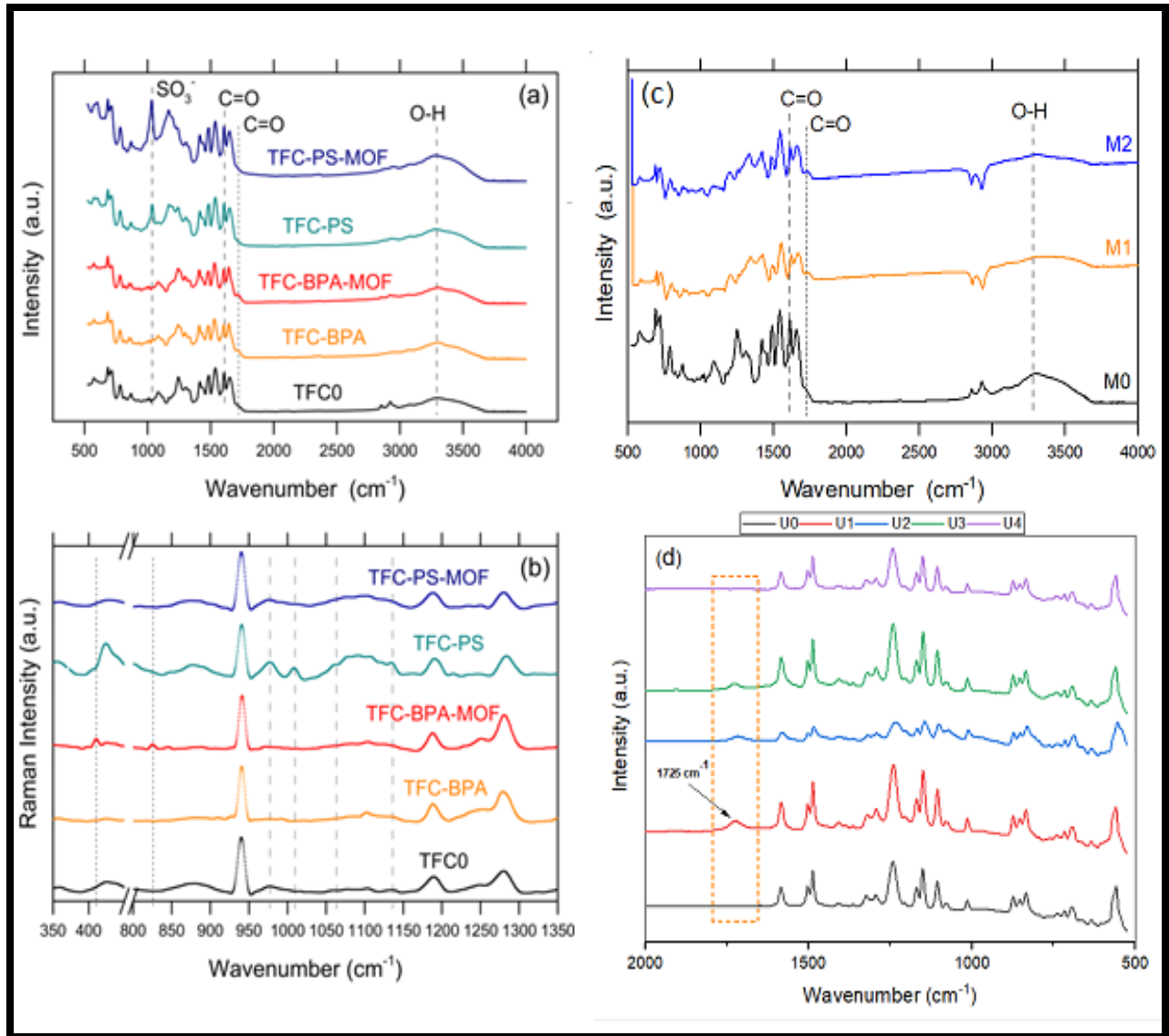
7 **3.1.1 ATR-FTIR**

8 Infrared spectroscopy provides insight regarding the surface functional groups present on
9 top of the unmodified and modified samples, and hence was used for all three studies on FO and
10 UF membranes (Fig. 1). The peak observed at around 3300 cm^{-1} in all five spectra of both FO
11 studies (TFC-PS, TFC-PS-MOF, TFC-BPA, TFC-BPA-MOF, M1, and M2) is due to O–H
12 stretching [5,13]. The absorption peak at around 1620 cm^{-1} for all samples corresponds to the
13 stretching vibration of C=O of the amide group, inherent of PA forward osmosis membranes
14 [76]. A peak detected at 1730 cm^{-1} is associated to C=O stretching of the carboxyl group,
15 potentially indicative of BPA, suggesting the presence of C=O functional group of BPA on the
16 surface of TFC-BPA, TFC-BPA-MOF, M1, and M2 membranes in the two studies employing
17 this carboxyl-containing zwitterion [77,78]. Peak indicating the presence of PS zwitterions on the
18 surface of TFC-PS and TFC-PS-MOF in the Journal of Membrane Science (JMS) study can be
19 observed at wavenumber 1030 cm^{-1} , assigned to the O=S=O functional group of PS [46]. Raman
20 spectroscopy was also exploited in the JMS study to further verify the presence of these
21 compounds on the membrane surfaces (Fig. 1b). The peaks around 980 cm^{-1} , 1010 cm^{-1} , and

[‡] Data and discussion provided in this chapter, with permissions, have been previously published in [41,42,63,127]

1 1065 cm^{-1} are attributed to the symmetric stretching modes of SO_3 , coupled with the peak around
2 1127 cm^{-1} attributed to an asymmetric stretching mode of SO_3 [79–81], indicative of PS
3 presence particularly on TFC-PS without the probable diluting effect of Ag-MOFs, having
4 different Raman modes. The peak around 410 cm^{-1} in the spectrum of TFC-BPA-MOF sample is
5 correlated to the stretching mode of C-Br bonding [81]; another peak around 825 cm^{-1} is also
6 assigned to the stretching vibration of C-Br bonding [82], both of which are indicative of BPA
7 presence on the TFC-BPA-MOF membrane.

8 UF membranes were also characterized with ATR-FTIR to verify the presence of AA on
9 the membrane surfaces to ascertain the presence of carboxyl groups needed to bind Ag-MOFs.
10 Certain peaks were detected at 1150 cm^{-1} , 1324 cm^{-1} , 1242 cm^{-1} , 1489 cm^{-1} , and 1585 cm^{-1}
11 which are characteristic peaks of PSf; these peaks are respectively ascribed to symmetric and
12 asymmetric stretching vibrations of O=S=O [82,83]; asymmetric stretching of O-C-O [84], and
13 the aromatic ring stretching pertaining the last two [84,85]. Most importantly, the peak at 1725
14 cm^{-1} , present only in the spectra of U1, U2, and U3, is the characteristic peak for the carbonyl
15 group (C=O stretching) [57,76]. This peak is indicative of the AA carboxyl groups since it does
16 not pre-exist in U0 pristine membrane and we know AA was not used to modify U4 as well.



1
 2 **Figure 1.** Detection of zwitterions and AA pre-graft functional groups on the surface of the membranes:
 3 (a) ATR-FTIR spectra for TFC0 to TFC-PS-MOF: peaks indicating the successful immobilization of BPA
 4 and PS; (b) Raman spectra for TFC0 to TFC-PS-MOF: short dash and long dash lines indicates the
 5 Raman shift associated with SO₃⁻ and C-Br modes, respectively; (c) ATR-FTIR spectra for M1 and M2,
 6 verifying the presence of C=O containing BPA; and (d), ATR-FTIR spectra for U0-U4, indicative of AA
 7 presence on AA-treated U1-U3

8

9

1 3.1.2 XPS

2 Surface chemical composition of modified membranes can be further illuminated via X-
3 ray photoelectron spectroscopy. The XPS survey spectra obtained from TFC0, TFC-BPA, TFC-
4 PS, TFC-BPA-MOF, TFC-PS-MOF (Fig. 2), M0-M2 (Fig. 3), and U0-U4 (Fig. 4) are provided
5 below. The XPS survey spectra in Fig. 3 and 4 show three dominant peaks around 284, 399, and
6 530 eV for all the PA membranes, used in the FO studies. These bands correspond to the
7 predominant elements of carbon (C 1s), nitrogen (N 1s), and oxygen (O 1s), respectively [86,87].
8 Regarding C 1s, the peak at around 284.6 eV is assigned to C–C, C=C, and C–H bonds; the peak
9 around 286.2 eV is ascribed to C–N, C-Br, C–O, C-O-C, and C-O-H bonds; and the peak
10 approximately at 288.5 eV is ascribed to O-C=O and C=O bonds [34,36,88]. Finally, regarding O
11 1s, the peak around 530 eV is reportedly attributed to N-C=O, O-C=O, and C=O bonds; and the
12 peak around 532 eV may be associated with O-C=O and C-O-H bonds [88].

13

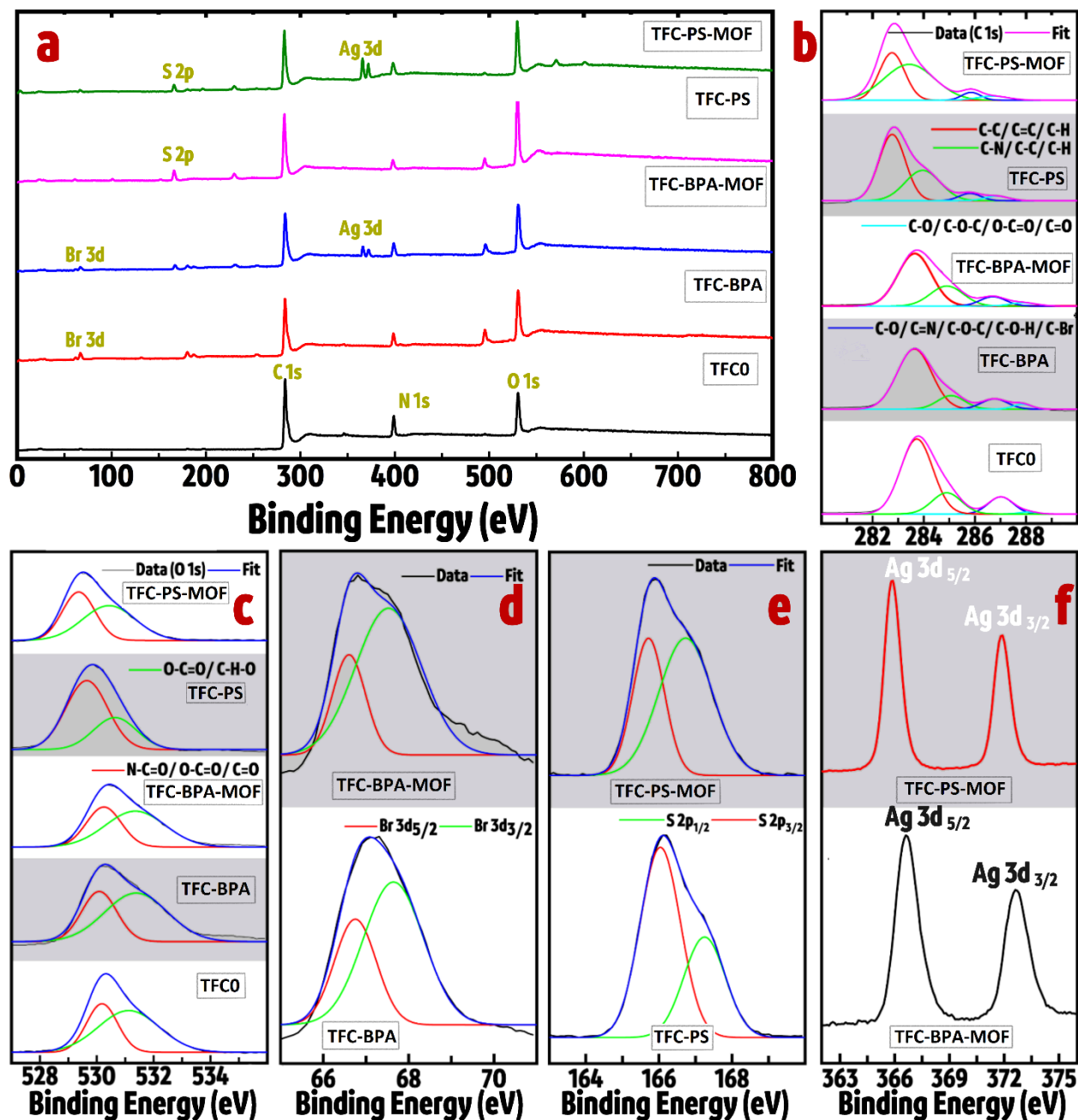
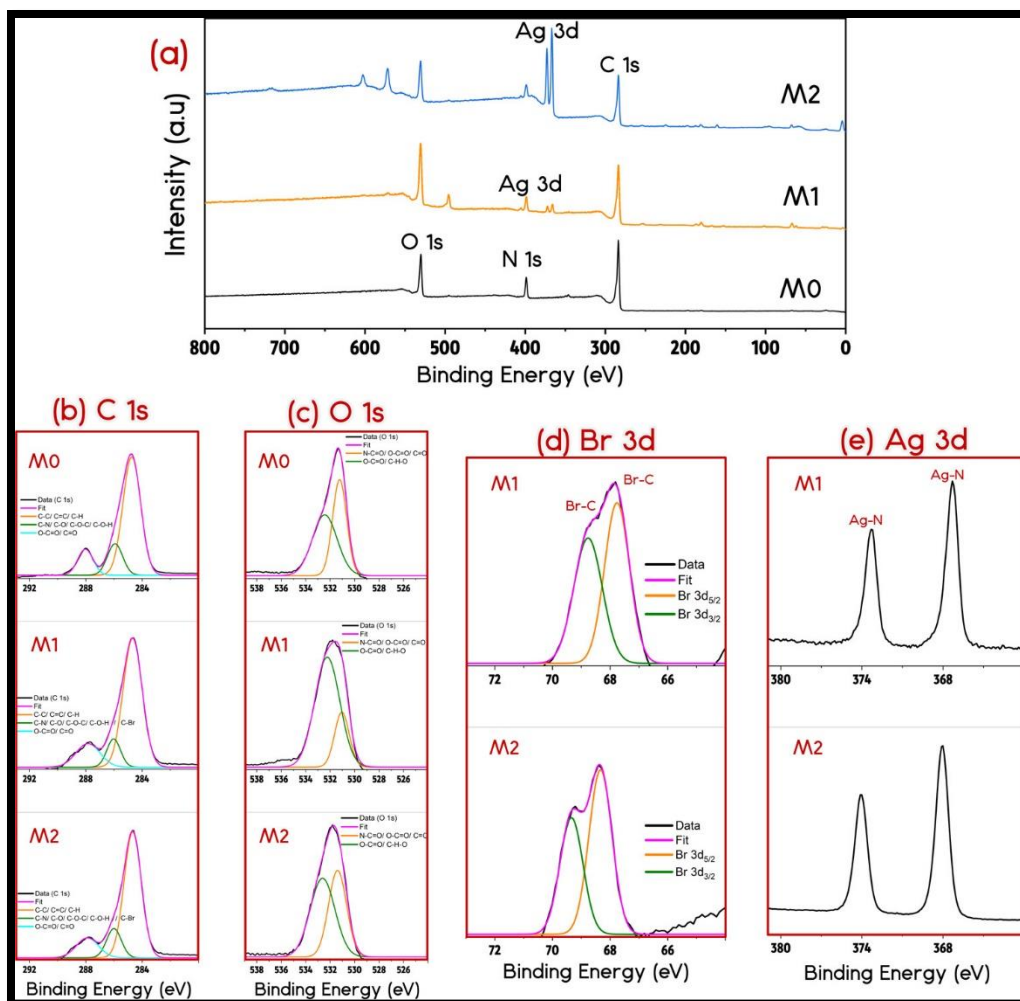


Figure. 2 a) XPS spectra of the TFC FO membranes. The corresponding peaks for C 1s, N 1s, O 1s, Br 3d, S 2p, and Ag 3d are marked, b) Deconvoluted high-resolution XPS spectra in C 1s range for membranes (TFC0-TFC-PS-MOF), in addition to their corresponding bonds shown in the legend, c) Deconvoluted high-resolution XPS spectra in O 1s range for the membranes, in addition to their corresponding bonds shown in the legend, d) Deconvoluted high-resolution XPS spectra in Br 3d range for TFC-BPA and TFC-BPA-MOF, e) Deconvoluted high-resolution XPS spectra in S 2p range for TFC-

1 PS and TFC-PS-MOF, and f) Deconvoluted high-resolution XPS spectra in Ag 3d range for TFC-BPA-
2 MOF and TFC-PS-MOF.

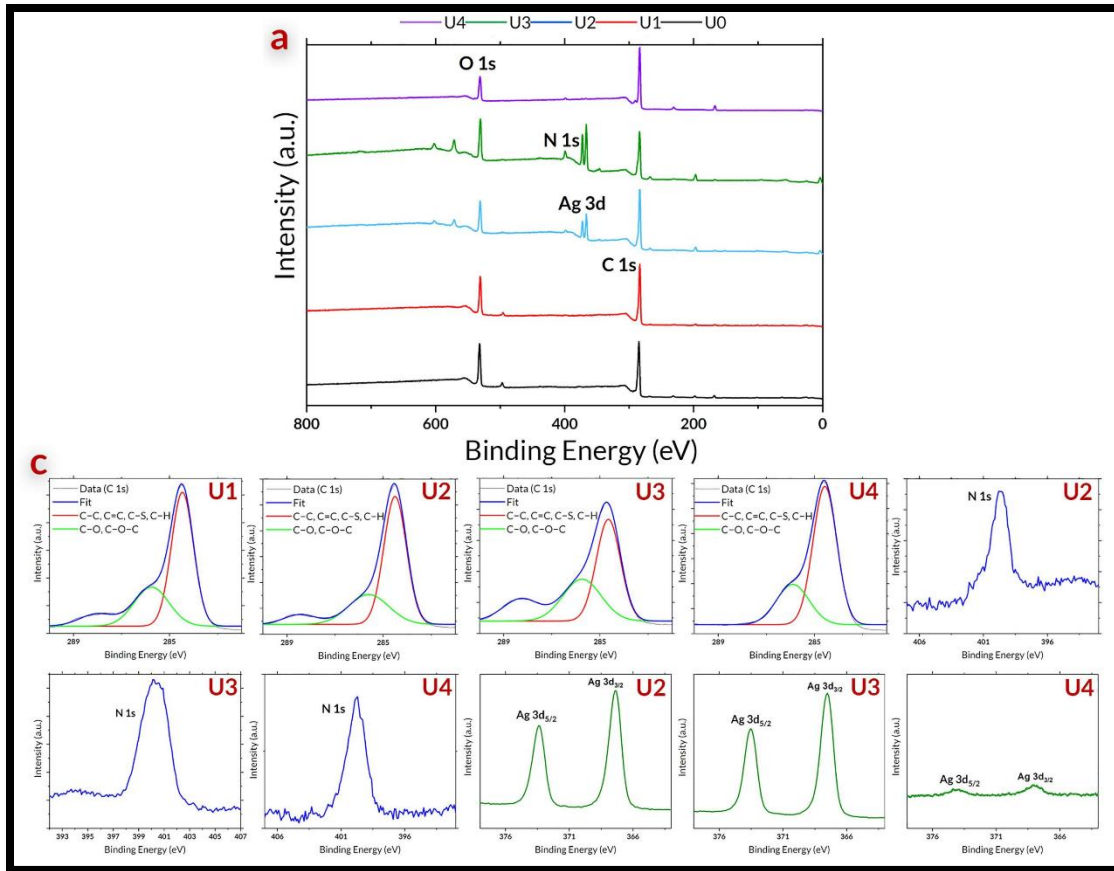
3 A peak associated to C–Br centered approximately at 67 eV (Fig. 2d) and 68.5 eV (Fig. 3d)
4 verifies the presence of BPA on the surface of TFC-BPA, TFC-BPA-MOF, M1, and M2
5 membranes grafted with this zwitterion. The Br 3d peak deconvolutes to Br 3d_{5/2} and Br 3d_{3/2}
6 bonds at 67.7 eV and 68.7 eV, respectively, for M1, and 68.3 eV and 69.3 eV for M2 [28,29,89];
7 accordingly this peak is deconvoluted to Br 3d_{5/2} and 3d_{3/2} bonds at 66.8 eV and 67.6 eV,
8 respectively, for TFC-BPA, and 66.6 eV and 67.5 eV for TFC-BPA-MOF [90,91]. For the PS-
9 grafted membranes, the S bonds at around 166 eV for TFC-PS and TFC-PS-MOF hint at the
10 successful grafting of these zwitterions [92–94]. Detected S bonds at around 166 eV for TFC-PS
11 and TFC-PS-MOF (Fig. 2e) shows the successful grafting of PS zwitterions on the membranes’
12 surfaces; this peak is further decomposed to S2p_{3/2} and S2p_{1/2} bonds at 165.7 eV and 166.7 eV
13 for TFC-PS, and 166.0 eV and 167.3 eV for TFC-PS-MOF, respectively [92,94]. The occurrence
14 of Ag 3d_{5/2} and Ag 3d_{3/2} peaks on M1 and M2 (Fig. 3e) which are primarily indicative of Ag–N
15 bonding happened around 367.5 eV and 373.5 eV [22,32,33], respectively; similarly, Ag 3d_{5/2}
16 and Ag 3d_{3/2} bonds for TFC-BPA-MOF and TFC-PS-MOF emerged at around 366 eV and 372
17 eV (Fig. 2f). It is noteworthy that Ag peaks obtained in M2 appear stronger and more
18 pronounced compared to M1 due to the fabrication route including an additional step of Ag-
19 MOF loading for M2, prior to in-situ growth. These results hint at the validity of the hypothesis
20 that zwitterion structures with negative functional groups might be effective in interacting with
21 metal ions [47,60], as active sites to bind Ag⁺ [95] to enhance its loading rate.



1
 2 **Figure 3.** (a) XPS spectra; and (b-e) fitted C 1s, O 1s, together with Br 3d and Ag 3d peaks regions for
 3 M0, M1, and M2 membranes.

4 XPS spectra of U2, U3, and U4 were also obtained to measure and compare the extent of
 5 Ag-MOFs presence among these samples in a semi-quantitative manner (Fig. 4). Similar to PA
 6 FO membranes, all membranes showed peaks for carbon (C) and oxygen (O). The peak centered
 7 at 284.6 eV in the C 1s spectrum and its deconvolution is assigned to C–C, C=C, C–S, and C–H
 8 bonds [96,97] (may also be assigned to C–N for U2, U3, and U4 [65]) and the peak around 286.2
 9 eV is associated to C–O and C–O–C bonds [86]. All these bonds are inherent in of PSf and were
 10 accordingly detected in the spectra of all pristine and modified membranes. The appearance of

1 two prominent silver signals at about 367.5 and 373.5 eV, assigned to Ag 3d_{5/2} and 3d_{3/2}, were
2 probably indicative of the Ag–N bonding [11,75], proving the existence of Ag-MOF on the
3 silver-containing membranes. Here, again, Ag peaks were more intense for U2 and U3 than U4
4 (respectively, 22 and 42 times larger based on the area under the curve), implying a denser Ag-
5 MOFs deposition or formation on these two membranes; implying that much like negatively-
6 charged zwitterions, using AA as a pre-grafted layer for subsequent coating with Ag-MOFs can
7 lead to functionalization maximization and enhancement. It is also worthy of note that U3
8 contained about two times more Ag on the surface compared to U2, suggesting that the in-situ
9 growth of Ag-MOFs on AA carboxyl active sites is superior to direct deposition in terms of Ag
10 uptake and possibly MOF network coordination and structuring. Another metric to verify MOF
11 existence is all the membranes but U0 and U1 showed the peak assigned to nitrogen (N 1s) from
12 2-MI [65,100] at 400 eV [101,102]. Notably, the green peak in C 1s at around 288.5 eV was
13 found only in the spectra of U1, U2, and U3, and may be attributed to C=O and O–C=O bonds
14 [86]. The C=O bond is likely related to AA incorporation; justifiably, this peak did not appear in
15 the spectra of U0 and U4 where no AA was used in the modification procedure. Results of XPS
16 spectra certify the validity of the hypothesis that structures with negative functional groups might
17 be effective in interacting with metal ions [47,60], as active sites to bind Ag⁺ [95] to enhance its
18 loading rate.

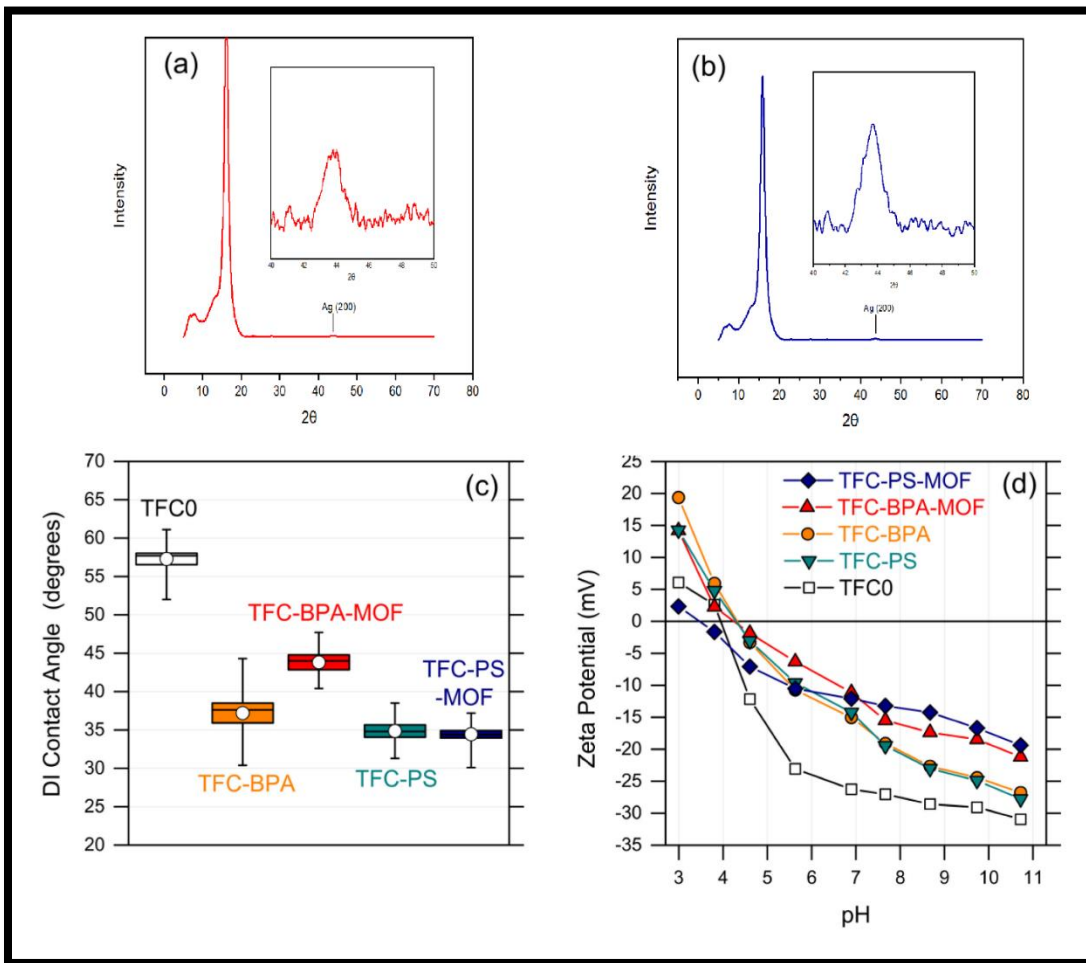


1
 2 **Figure. 4** (a) XPS survey spectra; and (b) high resolution deconvoluted XPS peaks of U0-U4 membranes.

3 **3.1.3 EDX, XRD**

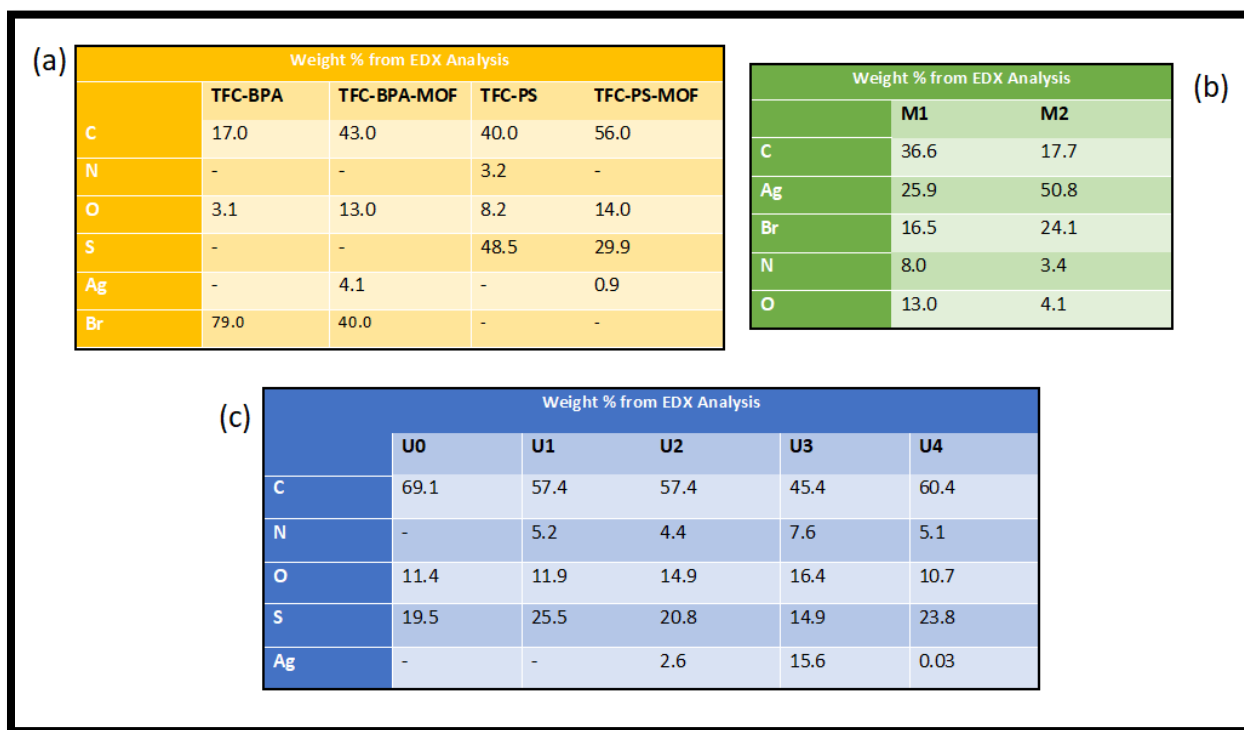
4 Further evidence as to the presence of Ag-MOFs on the membranes' surfaces could be
 5 provided via EDX and XRD analyses. These results corroborate the successful verification of all
 6 membranes with silver; EDX elemental distribution and peaks were also obtained and presented
 7 for better clarity. Specifically, it is observed from the EDX table for the UF membranes that our
 8 hypothesis regarding the enhanced Ag loading as a result of AA favorable binding conditions
 9 (U3 > U2 >> U4) was further confirmed (Fig. 6c). There was also the observation that the pre-
 10 existence of Ag-MOFs on the membrane could enhance further MOF loading, probably through
 11 coordination, even more so than the effect of favorable hosting sites provided by BPA carboxyl

1 groups ($M2 > M1$). This could also negatively imply aggregation of MOFs and loss of a more
 2 uniform zwitterion-Ag-MOFs double-layer, which will be explored in silver leaching
 3 monitoring. Based on the EDX results of the study with both PS and BPA, it is worthy of
 4 mention that the Ag concentration in TFC-BPA-MOF is significantly higher than that pertaining
 5 to TFC-PS-MOF, suggesting a potentially higher affinity of carboxyl groups as silver binding
 6 sites compared to sulfonic groups.



7
 8 **Figure 5.** Physio-chemical characteristics of the surface of the membranes: (a) XRD spectrum of
 9 TFC-BPA-MOF, and b) TFC-PS-MOF, both with inset graphs highlighting the peak related to Ag (200);
 10 (c) statistics of contact angles of DI water droplets sitting on the membrane surface; (d) zeta potential
 11 measured as a function of pH, measured in a 1 mM KCl solution.

1 XRD analysis was also conducted for the PA FO membranes. Results shows an Ag (200)
 2 characteristic peaks on both TFC-BPA-MOF and TFC-PS-MOF membranes (Fig. 5a, b). The Ag
 3 (111) and Ag (220) peaks observed for M1 and M2 (Fig. 8L) also corroborate the presence of
 4 silver nanoparticles on the modified samples. The presence of peaks at 54.5°, 77° and 89° on
 5 these two spectra possibly indicate a crystalline structure of the coated MOFs, as suggested by
 6 previous studies [103].

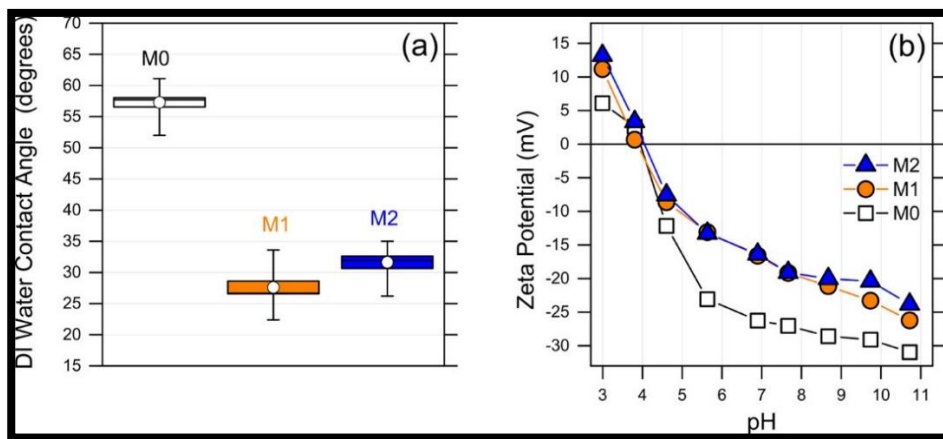


7
 8 **Figure. 6.** EDX analysis in terms of weight percentage of the various elements for a) TFC0, TFC-BPA-
 9 TFC-BPA-MOF, TFC-PS, TFC-PS-MOF; b) M1 and M2; and c) U0, U1, U2, U3, U4

10
 11
 12
 13

3.1.4 Zeta potential

The surface zeta potentials were measured over the pH range of 3 to 11 for PA FO and PSf UF membranes. The pristine PA membrane (TFC0 and M0) displayed negative potentials for pH values above the pK_a of carboxyl groups which has been reported at around 4.4-4.9 [104,105] (Fig. 5d and Fig. 7b). The existence of overall electrically neutral zwitterions caused an upward shift towards neutral zeta potential values. This effect was more visible for the Ag-containing TFC-BPA-MOF and TFC-PS-MOF membranes compared to TFC-BPA and TFC-PS, probably due to the addition of positively charged silver. This upward move is also partially a contribution of 2MI; the organic linker has a basic secondary amine group which could cancel out some of the membrane surface's negative charge. The same trend was observed for M1 and M2 compared to the pristine M0. Overall, keeping an overall negative surface charge at neutral pH territory and simultaneously minimizing the exposed density of carboxyl groups is a valid strategy for the membrane to both wield electrostatic repulsion against organic and biological foulants and minimize the odds of carboxyl interaction with Ca²⁺ and other multivalent cations, which has been reported to promote the formation of dense fouling layers [106,107].



16
17 **Figure. 7.** (a) Results of contact angles measurements of DI water on the membranes; (b) zeta
18 potential of the surfaces as a function of pH in 1 mM KCl at room temperature.

1 All PSf UF samples similarly displayed negative zeta potentials as they were exposed to
2 environments with pH above 3, with U3 and U4 having the highest potential values in the neutral
3 range (Fig. 11h). Zeta potential values indicate the strength of their electrical double-layer
4 repulsion and so are positively linked with solute retention [108]. All modified samples managed
5 to maintain their overall negative potential originally present in the pristine U0, with U3 and U4
6 exhibiting a negative surface potential of higher magnitude around the neutral pH range. The
7 same principle of utilizing a negative surface potential for electrostatic repulsion of organic and
8 biological foulants is logically applicable and deemed favorable here as well.

9 **3.1.5 Contact angle**

10 The wettability of the surfaces is directly associated with antifouling activity in terms of
11 mitigation of the foulant deposition rate and hence was investigated with water contact angle
12 measurements for all studied membranes. The results show a notable decline from 57° for TFC0
13 membrane to approximately 37°, 44°, 35°, and 34° for TFC-BPA, TFC-BPA-MOF, TFC-PS, and
14 TFC-PS-MOF, respectively (Fig. 5c). This reduction can be justified due to the presence of
15 COO⁻ and SO₃⁻ containing zwitterions and positively charged silver ions increasing the
16 membrane affinity with water droplets. Similarly, an estimated average angle reduction of 50%
17 was obtained for both M1 and M2 compared to the pristine M0 (Fig. 7a). This trend could be
18 similarly attributed to the moieties of BPA, the amide bonds, and silver ions, leading to an
19 enhanced membrane hydrophilicity.

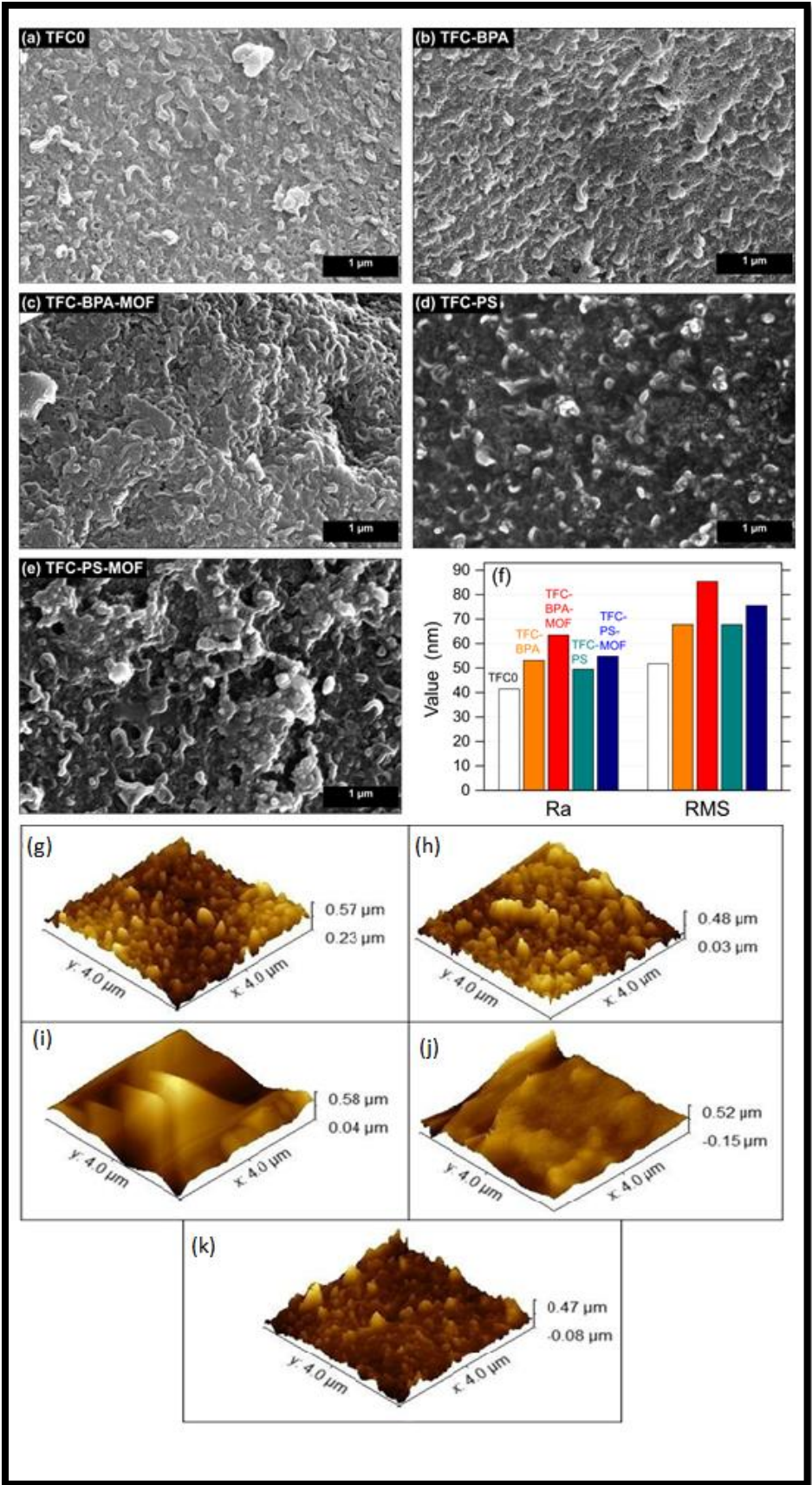
20 The same trend was observed for CA measurements on the UF membranes (Fig. 10a),
21 with the best value achieved for U3, i.e., for the membrane with the complete functionalization
22 package which was in-situ growing of MOFs on the top of BP-activated and AA-coated samples.
23 Actually both U2 and U3 (containing both Ag-MOFs and AA) displayed lower contact angle

1 values and higher wettability compared to U1 (solely AA) and of course U0 (non-functionalized)
2 and U4 (solely Ag-MOFs), suggesting that both the anionic polymer and the MOFs contributed
3 to the imparted hydrophilicity. Higher wettability in U3 compared to U2 is likely due to the
4 higher Ag-MOFs density on the surface of U3 (EDX) [109,110], probably due to a more efficient
5 MOF loading procedure. The observed pattern was associated with the presence of ionic silver in
6 MOFs similar to the case of FO membranes, but also the carboxyl groups in AA [111,112].

7 **3.2 Morphological properties of modified membranes and Ag-MOFs**

8 **3.2.1 SEM, TEM, AFM**

9 The rate and behavior of deposition of foulants onto the membrane is heavily defined by
10 the surface morphology and roughness parameters,. Therefore, SEM was used to capture
11 micrographs corresponding to pristine and surface-functionalized membranes in all studies for
12 this research. SEM micrographs of the pristine commercial TFC membranes for our FO studies
13 show the typical ridge-and-valley structure of PA membranes prepared by interfacial
14 polymerization between MPD and TMC [106,113] . These ridge-and-valley structures were
15 slightly altered after grafting PS and BPA in both studies; these changes became more obvious
16 subsequent to Ag-MOFs introduction. Careful observation of the SEM micrographs
17 corresponding to TFC-BPA-MOF and TFC-PS-MOF revealed nodules as the result of Ag-MOFs
18 incorporation (Fig. 8a-e). Similarly, these nodules assumed apparent granule and floc-like
19 formation on the surface of M1 and M2 membranes following MOF introduction (Fig. 9a, b, d,
20 g, h). The stochastically distributed white spots on the surface of M1 and M2 membranes can be
21 ascribed to the Ag-MOFs, with a more apparent thickness of a white layer on M2 as suggested
22 by High-magnification micrographs (right-side, Fig. 9), as a result of more Ag-MOFs
23 incorporation during M2 preparation [114].



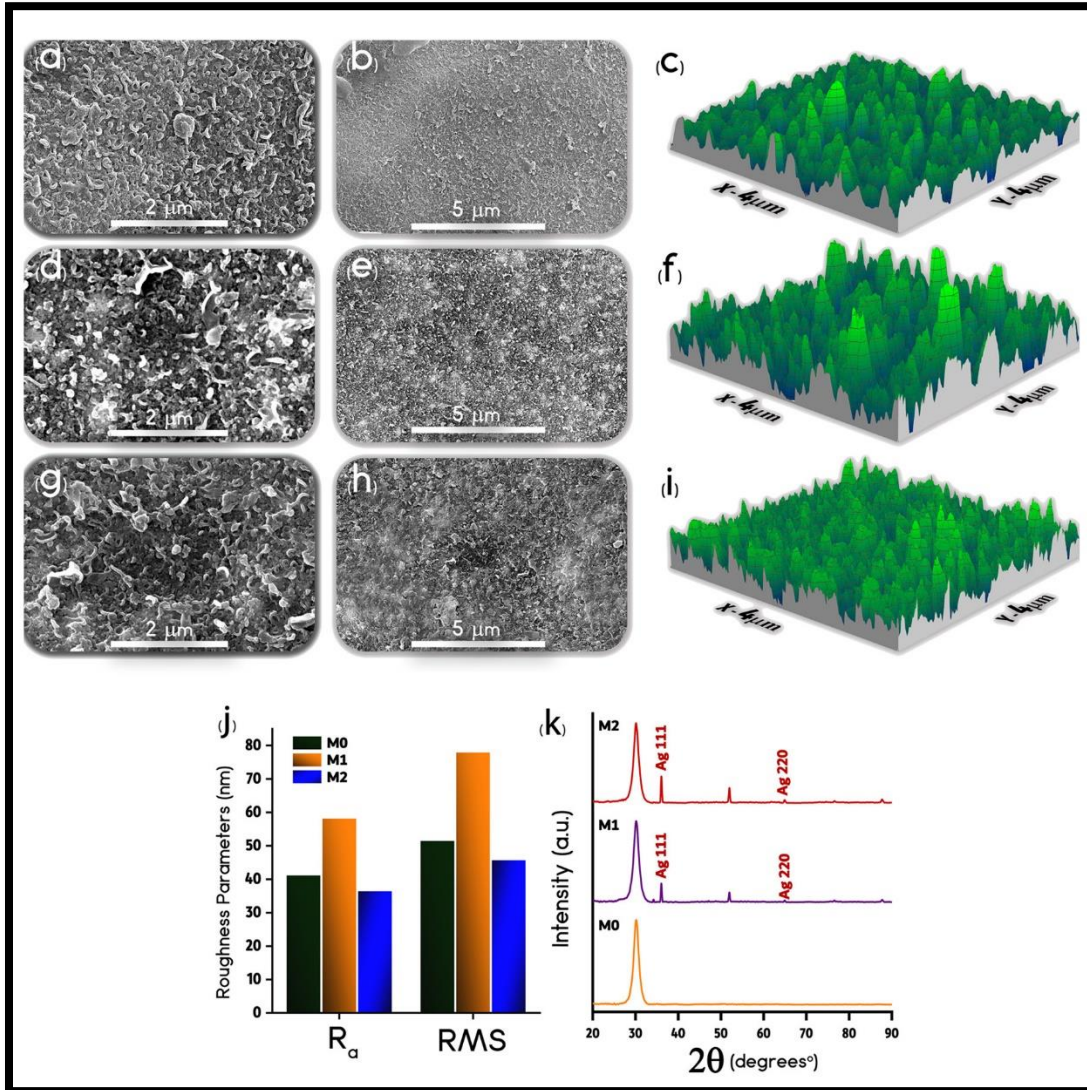
1 **Figure. 8.** (a-e) Representative SEM micrographs and (f) roughness parameters of the pristine and
2 functionalized membranes; AFM 3D images of g) pristine and functionalized membranes h) TFC-BPA, i)
3 TFC-BPA-MOF, j) TFC-PS, k) TFC-PS-MOF

4

5 Atomic force microscopy measurements were a general confirmation of the SEM
6 observations. AFM roughness scans and the extracted parameters, R_a (average roughness) and
7 R_{RMS} (root-mean-squared roughness), are provided as a complimentary tool in surface
8 morphology investigations. Functionalization resulted in a generally increased roughness for
9 membranes. This change was less significant when only PS or BPA were grafted, while it was
10 more remarkable when Ag-MOFs were added, probably corresponding to the nodules observable
11 in SEM micrographs (Fig. 8f-k).

12 For the other PA membrane set, M0 and M2 membranes exhibited close R_a and R_{RMS}
13 values, whereas M1 displayed a surge in surface roughness (Fig. 9c, f, i, k). A rougher surface
14 for M1 compared to M0 is perfectly in accordance with the SEM micrographs. The similarity
15 between M0 and M2 roughness values could stem from the procedure deployed for the
16 preparation of M2. An additional inclusion of Ag-MOFs in the BPA solution (as opposed to a
17 mere post-BPA in-situ growth, deployed for M1) might have promoted a more homogeneous,
18 uniform-layerd MOF growth, producing a smoother surface. It is noteworthy that larger
19 roughness is typically reported as a cause for increased fouling propensity; however, surface
20 roughness can cause an intensification of the initial wettability of the membrane as suggested by
21 the Wenzel model, be it more biased towards hydrophilic or hydrophobic. It can therefore be
22 concluded that roughness can enhance the wettability of a hydrophilic surface. Hence, it could be
23 argued that the coupled impacts of a reduced contact angle (increased water affinity) and

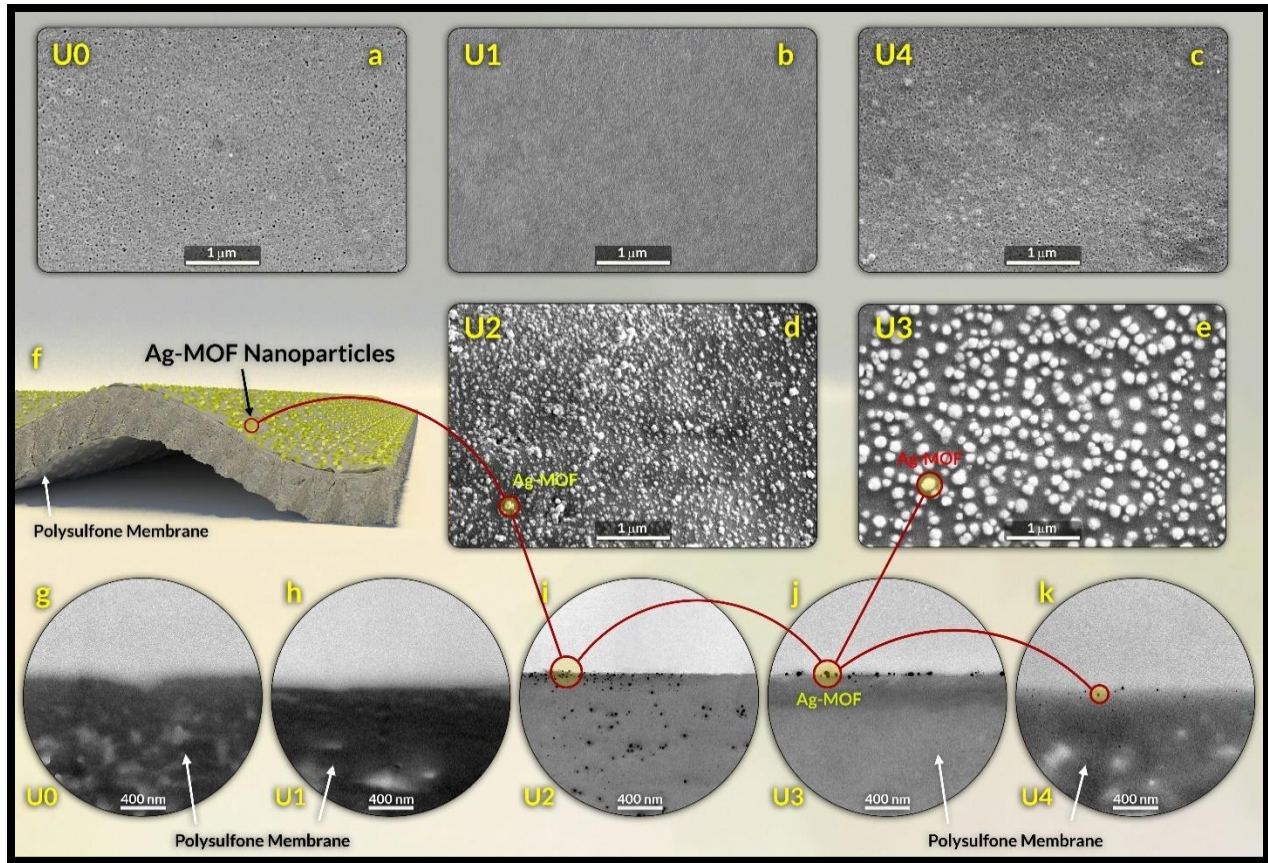
1 heightened roughness can synergistically lead to a more wettable surface for the MOF-containing
2 membranes [110].



3
4 **Figure. 9.** Representative surface SEM micrographs of (a and b) M0, (d and e) M1, and (g and h) M2. 3D
5 AFM scans of (c) M0, (f) M1, and (i) M2. (j) Roughness parameters of all the membranes measured with
6 the AFM. (k) XRD patterns of the various membranes. The broad peak at $2\theta = 30^\circ$ corresponds to
7 amorphous glass [115,116], which was used as the sample holder during XRD measurements.

8 UF membranes were prepared in a more diverse set of pathways to isolate the impact of
9 MOFs and the way they were deployed. As evident in representative SEM micrographs (Fig.

1 10a-e), multitudes of white aggregates were visible solely on the surface of MOF-containing U2,
2 U3, and U4 samples. There was a similar observation with the TEM micrographs of U2, U3, and
3 U4 displaying a randomized number of black dots (Fig. 10g-k). These white aggregates and
4 black dots could justifiably be attributed to Ag-MOFs. There was an understandable difference in
5 the Ag-MOFs resulting formations on U2 as opposed to U3. U2 displayed a bed of smaller-sized
6 MOFs (~10-50 nm) due to being deposited from an AA suspension; however, the surface of U3
7 was covered with larger cluster-like MOFs (~50-200 nm), which were in-situ grown separately
8 on a pre-grafted AA layer. It is noteworthy that unlike U3, Ag-MOFs were also observed under
9 the surface of U2; possibly due to the suspension seepage through the membrane pores. This
10 movement would be possible given that the average surface pore size of the commercial PSf
11 membranes was measured as 39 ± 15 nm. On the other hand, Ag-MOFs solely observable on the
12 surface of U3 would provide a fully deployable layer of biocidal reservoirs at the
13 membrane/liquid interface where the interactions will happen. This observation could act as a
14 testimony for the in-situ growth over direct deposition of a MOF suspension.

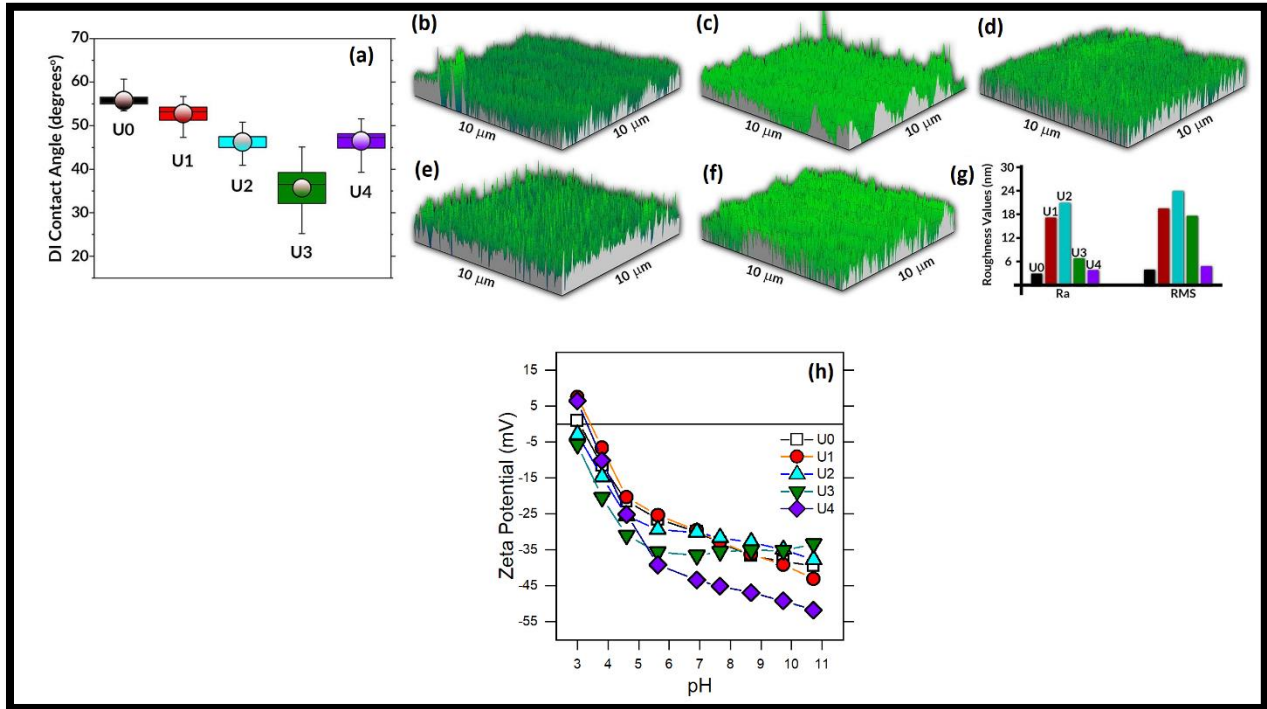


1
2

3 **Figure. 10.** (a-e) SEM micrographs and (g-k) TEM micrographs of pristine and surface-modified
4 membranes, and (f) schematic 3D illustration of the UF membranes modified with Ag-MOFs.

5 AFM was also deployed for a more quantitative analysis of the UF membrane surfaces
6 (Fig. 11b-g). All four of the modified samples gained in roughness compared to U0, in
7 accordance with SEM observations. U2 displayed slightly more of a roughness gain compared to
8 U3; this result could be justified due to a possible MOF aggregation as a result of rapid
9 deposition, while the in-situ growth employed for U3 possibly provided a more still condition for
10 a slow “MOF crystallization” phenomenon which allows for larger clusters that stay immobilized
11 on the membrane surface. Here again, the decision regarding higher hydrophilicity should be
12 based on roughness data in conjunction with CA results; For example, U2 is more wettable (due
13 to AA and MOFs) but rougher due to a non-uniform coated layer. Also, U3 is more wettable than

1 U4 (solely MOFs), but due to bulkier coating, it has a higher roughness. Morphological analyses
 2 seem to favor the in-situ growth method of MOF immobilization which doesn't allow seepage
 3 through pores and avoid aggregation.



4
 5 **Figure 11.** (a) Statistics of the contact angle of water droplets; 3D AFM images of (b) U0, (c) U1, (d)
 6 U2, (e) U3, and (f) U4 membranes; (g) AFM roughness parameters; and (h) zeta potential measurement
 7 results for the UF membranes

8
 9 Results from physio-chemical and morphological characterization of TFC PA membranes
 10 revealed that immobilizing a layer of Ag-MOFs onto a pre-grafted zwitterionic layer equips the
 11 modified membranes with enhanced features in terms of water affinity, surface roughness, and
 12 Ag-MOFs formation and loading. It can also be implied that these enhancements will be more
 13 pronounced when in-situ modification pathway is applied, compared to direct deposition, so that
 14 there would not be a competition for binding sites between BPA or PS and Ag-MOFs, but rather
 15 the zwitterionic layer would enhance MOF loading. The differences between gained surface

1 features of TFC-BPA-MOF and M1, and M2 (same zwitterions, different methods) are a
2 testimony to that efficacy.

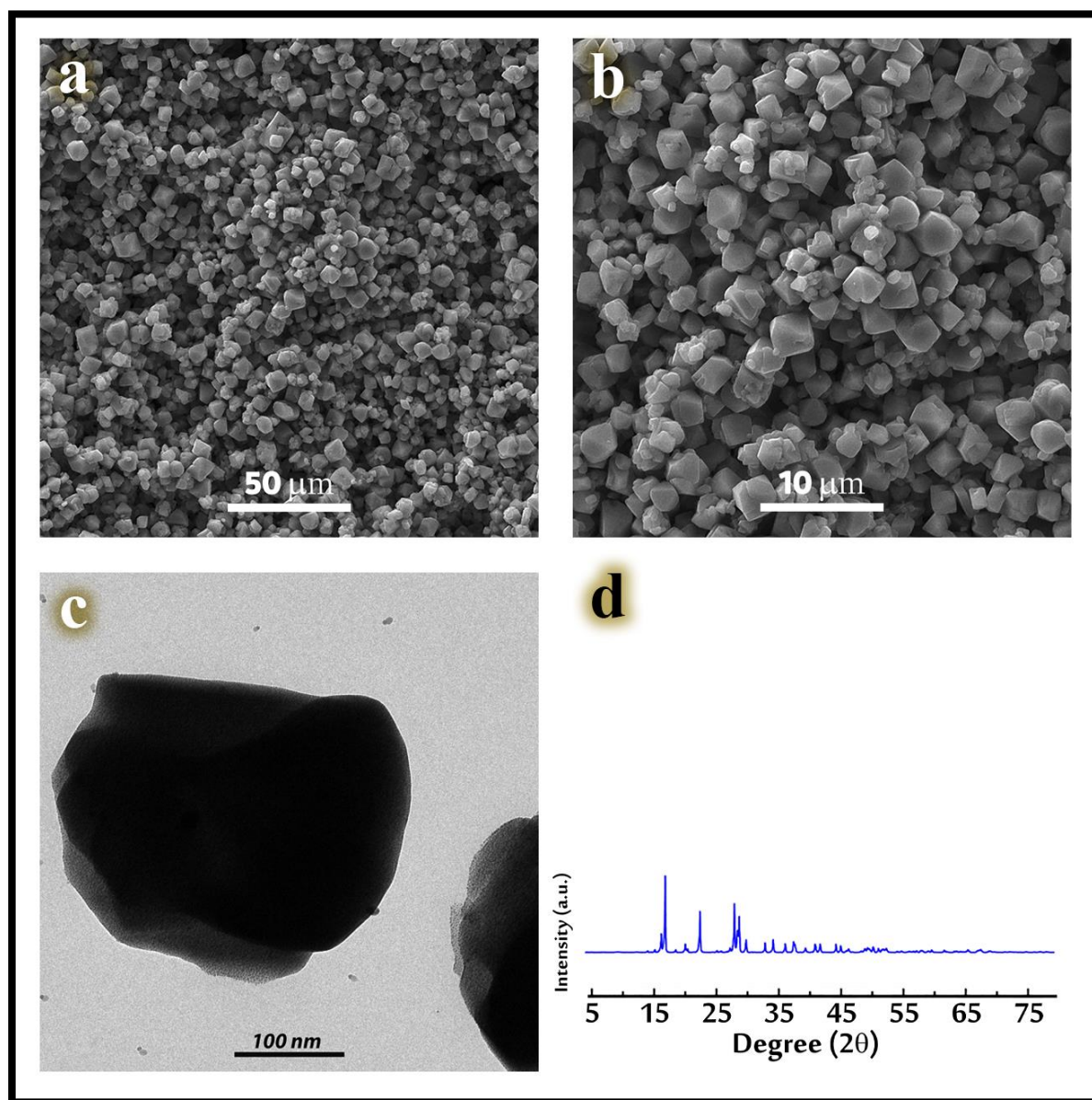
3 Similar trend can be observed for the PSf UF membranes. U3 gained a more favorable set
4 of collective surface characteristics compared to U2 (both membranes had AA and Ag-MOFs).
5 Again, here it was also evident that not having to compete for active hosting sites on the
6 membrane surface, realized via the in-situ growth method, promoted better surface
7 characteristics similar to the PA TFC membranes. It is noteworthy that U4 (No AA used) barely
8 outperformed pristine U0 in terms of silver loading. From all three studies, it can be concluded
9 with strong evidence that a layered modification strategy coupled with the in-situ growth of Ag-
10 MOFs produced the best surface features, most probable to outperform other samples in terms of
11 transport and long-term fouling experiments.

12 **3.2.2 Ag-2MI nanocrystals**

13 The Ag⁺ ion affinity with the N-donor ligands including imidazole-based linkers can be
14 exploited to form supramolecular silver-based building blocks with morphologically favorable
15 structures. Hence, silver concentration within these structures naturally plays a major role in
16 determining the degree of bacterial inactivation. Representative FE-SEM, TEM images, and
17 XRD spectrum (Fig. 12) of these structures are extracted from a recent study on three different
18 silver-Based metal azolate frameworks including Ag-2MI, deployed for the purposes of this
19 research [117].

20 It has been also reported that the shape of Ag nanoparticles is heavily influential in the
21 degree to which it can induce toxicity to microbial entities [118]. As suggested by the octahedral
22 nanocrystal of Ag-2MI, these sharp edges enable Ag-2MI nanoparticles to effectively engage
23 with the bacteria and cause a charge imbalance in the cell membrane, leading to a lethal increase

1 in intracellular oxygen moieties. Another important factor in AgNP antibacterial activity is the
2 rate of release which can be tuned by the choice of organic linker; which incidentally can possess
3 antimicrobial features itself such as 2MI [119], which will further expanded on in the
4 antibacterial section of this thesis.

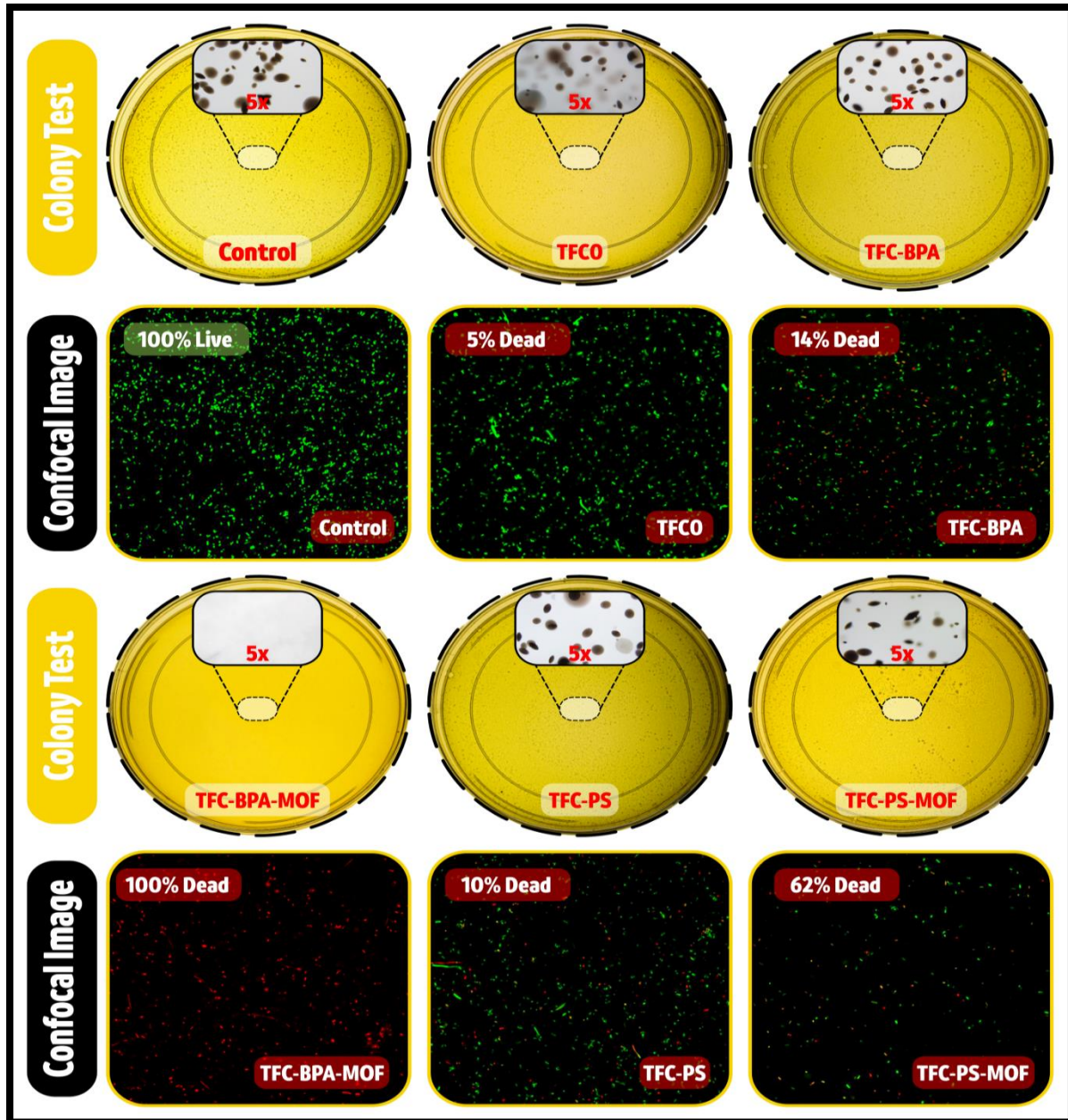


5
6 **Figure. 12.** (a and b) FE-SEM images at different magnifications, (c) TEM image, and (d) XRD spectrum
7 corresponding the Ag-2MI structure (extracted from *Tailoring the Biocidal Activity of Novel Silver-*
8 *Based Metal Azolate Frameworks* [117])

1 3.3 Antibacterial properties, biofilm inhibition

2 For the FO studies, plate count and confocal microscopy were employed to determine the
3 antimicrobial characteristics of the membranes, using the gram-negative *E. coli* as a surrogate for
4 biofouling organisms. Using the culture-based pour plating method, the TFC-BPA-MOF
5 membrane yielded approximately 100% *E. coli* inactivation from an original solution containing
6 10^7 *E. coli* CFU/mL (Fig. 13). The TFC-PS-MOF membrane yielded a significant 62%
7 annihilation of *E. coli*. The non-MOF-containing TFC-BPA and TFC-PS membranes displayed
8 small bacterial inactivation rates of 10% and 14%, respectively, while the corresponding rate for
9 the pristine TFC0 was 5%, denoting a lack of antibacterial properties as compared to the
10 modified membranes. The confocal microscope was used to take fluorescence images of bacteria
11 after *E. coli* exposure of the membrane and staining the membrane with SYTO9 and PI, the
12 standard stains used to differentiate viable and non-viable cells under confocal microscopy,
13 respectively. The live:dead (green:red) ratio was subsequently calculated and used to describe
14 the relative degree of membrane's ability in compromising the integrity of bacterial cells. This
15 ratio was very high (approximately 100) for the TFC0 membrane, i.e., meaning there were 100
16 *E. coli* bacteria were allowed to live for every killed bacterium. In an eye-catching contrast, this
17 ratio was 0.01 for the TFC-BPA-MOF sample, translating to only one living bacterium per every
18 100 dead bacteria (approximately 99% die-off). The TFC-PS-MOF membrane demonstrated a
19 live-to-dead ratio of 0.33, annihilating three bacteria per every living bacterium (75% die-off).
20 These ratios were 6.66 (13% die-off) and 5.22 (16% die-off) for TFC-BPA and TFC-PS,
21 respectively. The results from microscopy are consistent with those obtained during plate count,
22 hailing Ag-MOFs as the obvious biocidal agents. The same analysis procedure was implemented
23 for M0, M1 and M2 samples in the second study as they are much similar in surface chemistry

1 and modification scheme in general (Fig. 14). For the M0 samples, no red-stained cells (denoting
2 dead bacteria) were visible under the microscope, corroborated by the abundance in colonies
3 (roughly 10^4 CFU/mL as opposed to the 10^7 CFU/mL in the control plate) as represented in the
4 plate count results. M1 and M2 demonstrated an expectably improved antibacterial capacity for
5 the attached microorganisms, with the live-to-dead ratio of 1.38 and 0.31 for M1 and M2,
6 yielding 42.0% and a more remarkable 76.3% of bacterial inhibition, respectively. These
7 numbers were backed by heterotrophic plate count of the unattached cells, showing no viable
8 bacterial colonies on the plates. SEM imaging was provided for a better insight into the bacterial
9 situation on top of M0, M1 and M2 membranes. These images (Fig. 14c₁-c₃) also attested to the
10 presence of healthy (green) *E. coli* cells on M0 and damaged (red) *E. coli* cells upon exposure to
11 M1 and M2.



1
 2 **Figure. 13.** Results of antimicrobial activity tests for pristine and functionalized membranes tested with
 3 gram-negative *E. coli* using heterotrophic plate count and confocal microscopy.

4 Bacterial annihilation or inactivation done by Ag-MOFs could be presumably done
 5 through multiple pathways, most importantly via breaking through the outer cell membrane,
 6 causing a seepage of cellular matters [120]. Factors such as higher Ag⁺ content coupled with a
 7 more uniform presence of Ag-MOFs on the surface of M2 ensured a relatively higher chance of

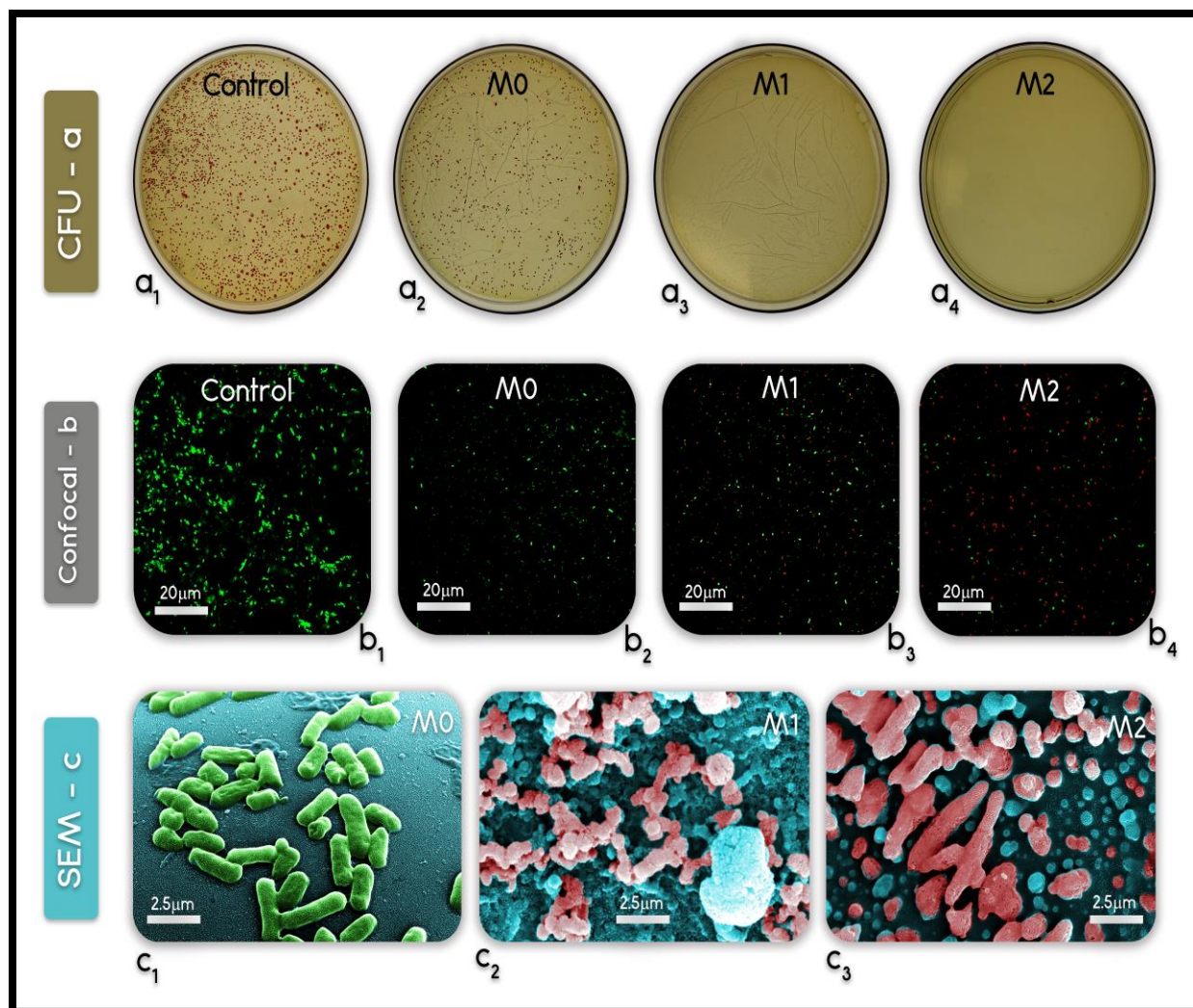
1 lengthy and direct *E. coli* exposure to silver ions, justifying the higher antimicrobial activity
2 observed for M2 samples as opposed to M1 which was lacking in both factors [60].

3 The antibacterial activity demonstrated by these membranes cannot be solely ascribed to
4 the multiple mechanisms of silver in action. There is evidence reported in the literature regarding
5 imidazole and its derivatives to have various antiviral, antibacterial and antifungal effects
6 [66,75]. As described earlier and pointed to by a recent study by our colleagues investigating
7 three imidazole-based Ag-MOFs (Ag-imidazole, Ag-2 methylimidazole, Ag-benzimidazole),
8 Ag-2 methylimidazole displayed the highest antibacterial activity, resulting from its relatively
9 higher silver content and an octahedral nanocrystal structure with sharp bacteria-engaging edges
10 [60].

11 Probable antibacterial mechanisms in action obtained via MOF immobilization can be
12 summed up as follows:

- 13 • The controlled release of the Ag⁺ whether in cation form or as small MOF fragments is
14 the predominant antibacterial mode of action of these structures, directly dependent on
15 the Ag⁺ density and kinetics of release [68,69].
- 16 • The properties of the organic linker which in the case of 2MI, has complimentary
17 antimicrobial activity to contribute to that of Ag⁺; a phenomenon that might be justified
18 due to the reactive oxygen species of 2MI [121].
- 19 • The crystal size and morphology of the nanostructure; a crystal size in the order of
20 nanometres, more specifically 200-700 nm in the case of Ag-2MI MOFs [60], and
21 possessing a sharp-edged octahedral nanostructure shape makes them into ideal biocidal
22 candidates for intake by bacterial cells via endocytosis and pinocytosis [122].

23



1
 2 **Figure. 14.** Representative results of antimicrobial activity against *E. coli* for control and
 3 functionalized membranes: (a) heterotrophic plate count of cells suspended in the solution in contact
 4 with the sample surfaces; (b) live/dead microscopy images of cells attached to the sample surfaces;
 5 (c) SEM images of bacteria upon contact with the membranes.

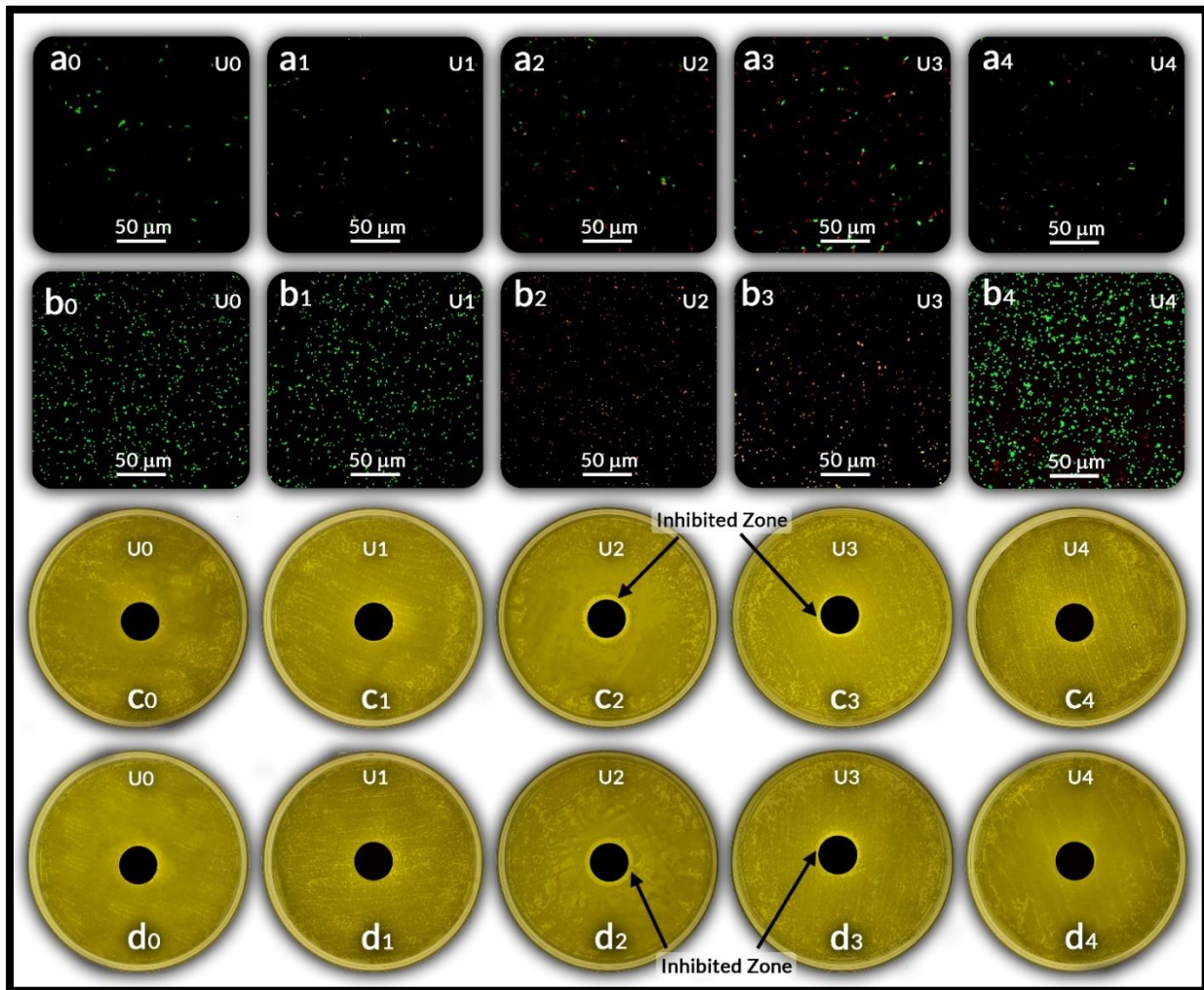
6 The antibacterial activity of the UF membranes was tested by confocal microscopy and
 7 inhibition zone analysis using *E. coli* and *S. aureus* as gram-negative and gram-positive model
 8 bacteria, respectively (Fig. 15a, b). There was almost no antibacterial resistance from U0 upon
 9 microbial contact induced from the bacterial suspensions (Fig. 15a₀, b₀). By contrast, these
 10 numbers amounted to 80% and 90% of *E. coli* inactivation for U2 and U3, respectively, with
 11 even more remarkable activity against *S. aureus* with a 95% inactivation rate. U1 and U4

1 neutralized a humbling 10% and 17% of *E. coli*, together with 3% and 13% of *S. aureus*,
2 respectively. Disc inhibition zone tests were carried out to provide a more thorough insight into
3 the antibacterial activity of the membranes (Fig. 15c, d). Only U2 and U3 exhibited inhibited
4 areas around the membrane, in accordance with the results observed in microscopy viability
5 tests.

6 An inhibition zone forms around the membranes upon the unleashing of biocides by the
7 membranes [123]. An Inhibition zone does not create long-term antibacterial property by itself
8 [124,125]; although, it ensures the inactivation of attached bacteria which is essential for
9 maintaining antibiofouling activity and biofilm formation [2]. Confocal and inhibition zone tests
10 may together provide a comprehensive insight into the performance of portions of silver-
11 containing agents that are: 1) strongly (mostly covalently) surface-bound, and 2) released from
12 the biocidal reservoirs, respectively. Hence, confocal microscopy shines a light on the status of
13 firmly-attached microorganisms, which in turn corresponds to the performance of the strongly-
14 bound biocides on the membrane surface [126]. On the other hand, inhibition zone analysis is a
15 shorter-term strategy, and more focused on prevention of microbial attachment through silver
16 release; therefore, potentially relaxing the microbial burden on the bound silver reserves. Hence,
17 a balanced release within a generally highly stable and strongly-attached structure becomes
18 paramount. In the upcoming section discussing silver release rate (Fig. 21), it is discussed and
19 shown that U2 displayed almost three times higher Ag^+ release rate than U3. This was in
20 accordance with the relatively thicker inhibition zone around U2 and higher dead:live (red:green)
21 bacterial ratio of U3 as observed in the confocal results. This difference could well be justified
22 due to differences in the modification pathways corresponding to U2 and U3. In U3, Ag-MOFs
23 were layer by layer grown in-situ on the membrane (able to slowly form properly coordinated

1 covalently-bonded networks) while U2 possessed Ag-MOFs that were synthesized in advance
2 and later immobilized on the membrane (irregular structures with weaker fast-formed bonds and
3 potentially possible aggregation). This difference could have resulted in a more stable Ag-MOFs
4 on top of U3, as opposed to more loosely-bound Ag-MOFs formed on U2 surface, which
5 beautifully explains the U3 superiority phenomenon. As it can be seen in Fig. 19, better
6 performance of U3 in fouling test also supports this idea that attachment of Ag-MOFs on U3 is
7 stronger than U2.

8



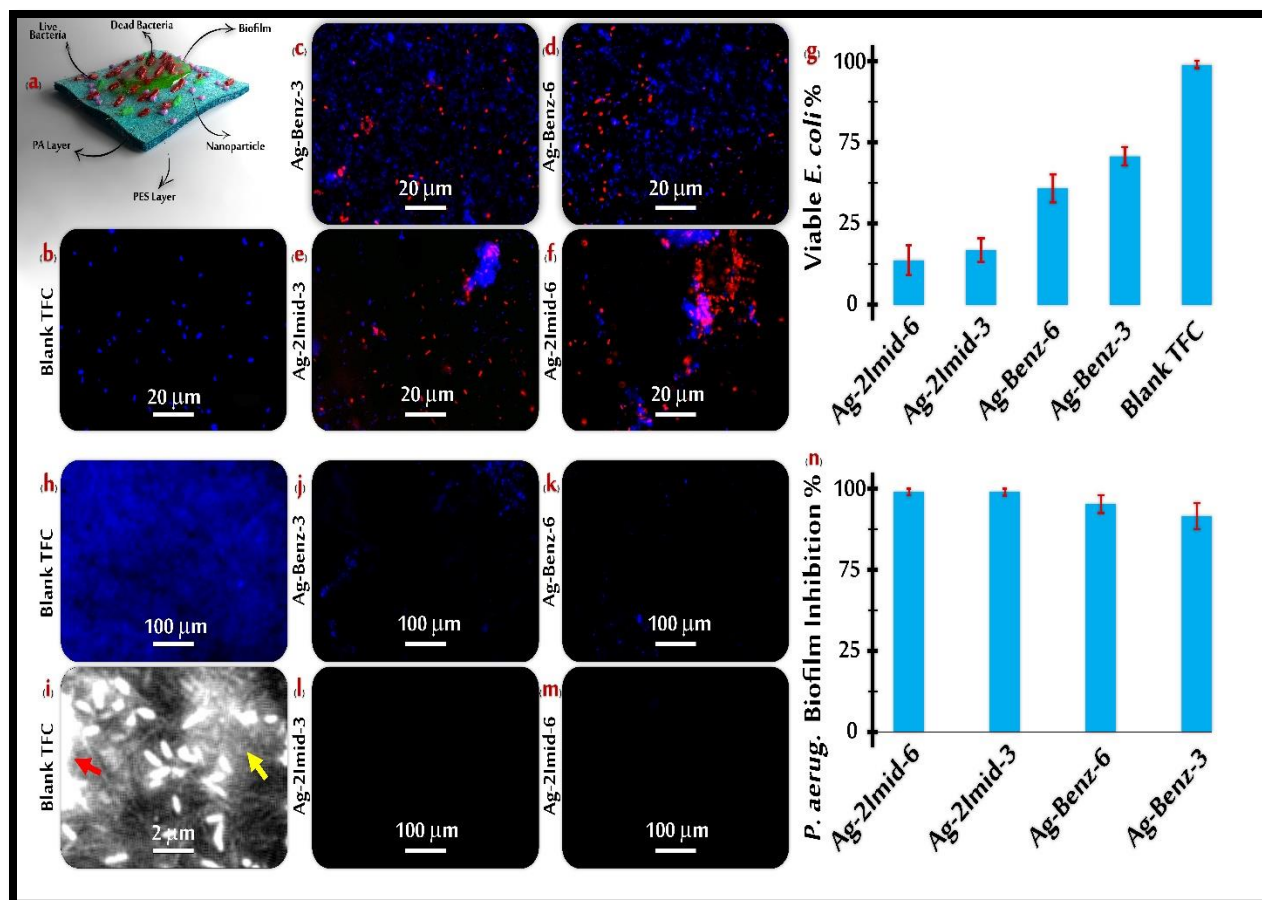
9

1 **Figure. 15.** Assessment of the antibacterial activity of the membranes. Confocal images of the
2 membranes upon surface contact with suspensions of (a) *E. coli*, and (b) *S. aureus*. Representative disc
3 inhibition zones of the membranes with (c) *E. coli*, and (d) *S. aureus*. U0 (a0, b0, c0, and d0), U1 (a1, b1,
4 c1, and d1), U2 (a2, b2, c2, and d2), U3 (a3, b3, c3, and d3), and U4 (a4, b4, c4, and d4).

5 The ability of the membranes modified with Ag-2MI MOFs to inhibit the formation of a
6 biofilm by pathogenic bacteria (*P. aeruginosa*), a ubiquitous Gram-negative strain with wide
7 infectivity was investigated as part of a separate study by our group [127]. This microorganism
8 has the ability to produce robust biofilm structures that ease infection and boost the organism's
9 ability to tolerate antimicrobial treatment and host defenses [128]. Instead of surface
10 modification of PA membranes with Ag-MOFs, two biocidal MOFs made from 2MI and
11 benzimidazole (benz) were incorporated into the active layer of the membranes by including 0.03
12 and 0.06% wt. of these materials in the MPD solution needed for interfacial polymerization.
13 Figure 15h displays a healthy *P. aeruginosa* biofilm formed on the blank TFC membrane within
14 48 h. In this experiment, 4',6-diamidino-2-phenylindole (DAPI) stained both bacterial cells and
15 extracellular polymeric substances (EPS) within the biofilm structures. Cells and EPS are
16 indicated by a yellow and red arrow, respectively (Fig. 16i). The fabricated TFN membranes,
17 displayed strong resistance towards bacterial proliferation, with only small pieces of thin
18 biofilms (10-50 μm wide) observable (Fig. 16j, and k). This phenomenon was even more
19 suppressed for the 2Imid- TFN membranes (Fig 16l, and m), which are the exact MOF type used
20 for the purposes of this thesis. Biofilms were semi-quantitatively evaluated by measuring the
21 fractional blue area in each field-of-view (FOV): Ag-Benz-3, Ag-Benz-6, Ag-2Imid-3, and Ag-
22 2Imid-6 TFN membranes resulted in ~90%, 95%, 99%, and 99% inhibition of biofilm formation,
23 respectively. The results were similar for *E. coli* inactivation as well. Briefly, bacterial cells were
24 stained with DAPI (blue, signifying intact cells) and PI (red, only observed if bacterial

1 cytoplasmic membrane is compromised); viability results showed 60%, 47%, 22%, and 18% of
2 the cell population was live after exposure to Ag-Benz-3, Ag-Benz-6, Ag-2Imid-3, and Ag-
3 2Imid-6 TFN membranes, respectively. As evident, 2MI yielded better antimicrobial activity
4 against planktonic cells and biofilms, which prompted its use for our next-generation studies on
5 FO and UF membranes.

6 There was no hydrophilic pre- or post-coating introduced for this set of membranes and
7 the method for MOF implementation is selective layer incorporation (which renders membranes
8 prone to surface defects) instead of post-fabrication coating (usually less damage to the selective
9 layer), both situations unlike those in previous studies. It is thus speculated that the excellent
10 inhibition data obtained from this investigation holds up, if not outperformed, by other
11 membranes with less invasive modification schemes and a hydrophilic supplemental layer which
12 assists in keeping (bio)foulants at bay, and thus, lessens the rate and impact of microbial
13 deposition.



1
 2 **Figure. 16.** (a) Illustration of biofilm formation and mitigation on membranes; (b-f) fluorescence imaging
 3 results obtained upon exposure of *E. coli* planktonic cells to the antibacterial membranes. The dead
 4 bacteria cells are colored in red while the live bacteria are in blue. (g) Percentage of viable *E. coli* cells;
 5 (h-m) *P. aeruginosa* biofilm formed on the membranes. Blue spots represent the biofilm. (n) Resulting
 6 percentage of biofilm inhibition by the membranes.

7
 8 **3.4 Membrane performance metrics: FO transport, UF separation, (bio)fouling**
 9 **investigation**

10 Membrane modifications could result in modest to significant changes to transport
 11 parameters in FO membranes; these alterations could result in water flux enhancements up to the
 12 limits imposed by inherent FO membrane parameters such as concentration polarization [129]
 13 and operational conditions including channel hydrodynamics in the FO setup, , but mostly they

1 can induce structural defects due to faulty modification routes, leading to heightened
2 permeability in exchange for compromised selectivity of the active layer. Filtration experiments
3 were thus conducted to evaluate the effectiveness of the surface-functionalized membranes for
4 the FO process conditions in the two studies. The water flux (J_w) and the reverse solute flux (J_s)
5 values were measured using a range of DS concentrations (0.5 to 2M). PA membranes exposed
6 to PS generally displayed a stronger spike in water flux values relative to pristine membranes,
7 compared to BPA-functionalized samples. Actually, PS-modified membrane pair (with and
8 without MOFs) outperformed the BPA-modified membrane pair in terms of productivity (Fig.
9 17). It is very reasonable to argue that zwitterions (both PS and BPA) would enhance water
10 permeability for both surface-functionalized membrane pairs, realized through raised water
11 affinity via a strong hydration layer; this phenomenon might have been materialized on an
12 excessive level in the case of BPA, leading to a dense and heavy zwitterionic layer grafted onto
13 the active membrane layer and subsequently, add to the entry barrier for water molecules due to
14 a thickened layer. This rationalization was visually demonstratable by the SEM micrographs.
15 Overall, it seemed that the alliance formed between silver ions and the functional groups of BPA
16 and PS (COO^- and SO_3^-) seemed to have led to the creation of a more favorable structure in
17 terms of water affinity, demonstrated by the higher fluxes of TFC-BPA-MOF and TFC-PS-MOF
18 membranes compared to values corresponding to TFC-BPA and TFC-PS membranes,
19 respectively.

20 A general upwards movement in reverse solute flux was observed for the surface-
21 functionalized membranes compared to the pristine membrane, except for TFC-PS, which
22 showed no significant change. This upward shift in solute flux permeability may be partly
23 justified due to the reduced negative charge of the membrane surface after functionalization with

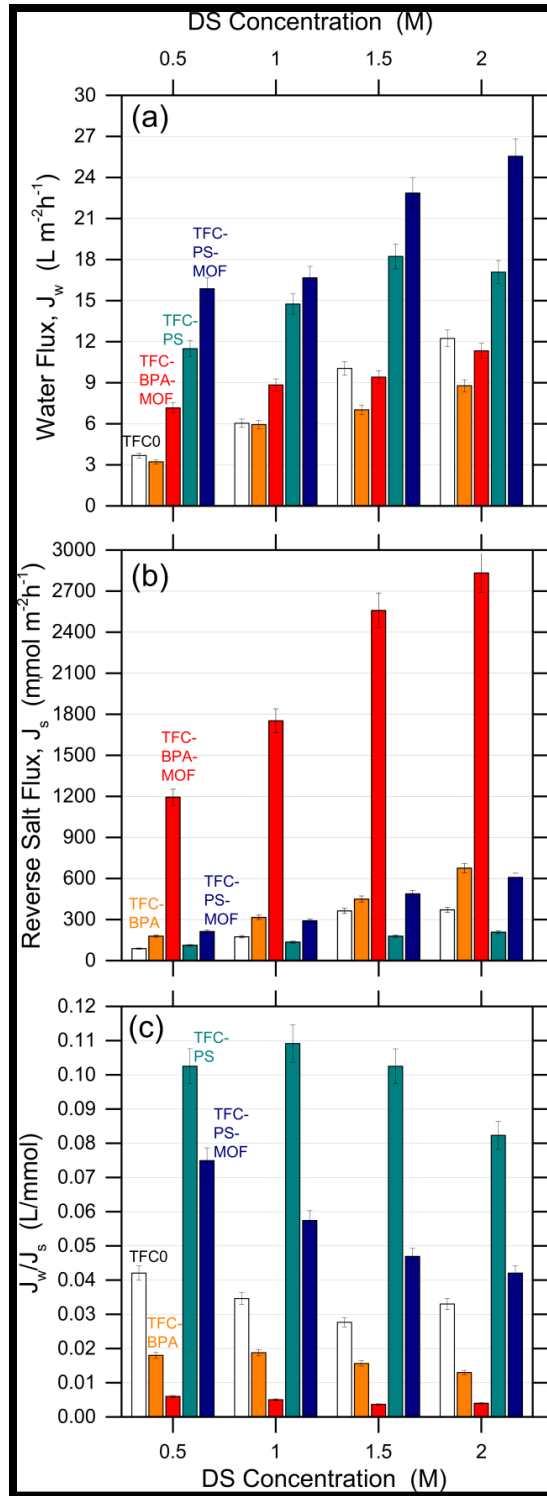
1 zwitterions and Ag-MOFs; zwitterions are overall neutrally-charged as discussed, and Ag-MOFs
2 displayed an added positive charge to the membrane surface as demonstrable by the zeta
3 potential results. This structural change can lead to a reduction in the electrostatic repulsion at
4 the membrane selective layer/feed interface, leading to a higher solute permeability (B) and
5 therefore, a higher reverse solute flux. The somewhat considerable increase of reverse solute flux
6 observed for TFC-BPA-MOF sample may be specifically ascribed to the addition of BPA-based
7 Ag-MOFs to the membrane surface, which can lead to change in charge distribution [77]. There
8 was also a great deal of difficulty regarding agent dispersion when preparing the BPA-MOF
9 solution; a negligible amount of NMP was dosed into the solution (which was minimized
10 experimentally), which might have had some part in creating defects on the membrane active
11 layer. The J_w/J_s ratio, or reverse solute flux selectivity (RSFS), is the comprehensive parameter
12 which is indicative of both membrane productivity (water flux) and selectivity (solute flux), and
13 defined as the volume of water produced per mass of draw solute lost due to reverse salt
14 diffusion [130–132]. Higher values reflect membranes with overall improved transport and
15 perm-selectivity [133]. As observed, TFC-PS and TFC-PS-MOF exhibited a relatively
16 significant enhancement in terms of RSFS values, while TFC-BPA and TFC-BPA-MOF samples
17 failed to perform well in that regard, even when measured against TFC-0. These FO performance
18 results can lead to the conclusion that BPA zwitterions might not be as potent in improving
19 membrane transport parameters as PS zwitterions, and that the addition of Ag-MOFs generally
20 resulted in some sacrifice in selectivity in exchange for higher productivity levels.

21 As displayed by EDX results (Fig. 6a), BPA proved to be a more favorable host for
22 binding Ag-MOFs, however, our method resulted in performance data that was less in favor of
23 BPA-MOF combination, compared to PS-MOF. The presumed higher favorability of BPA with

1 regards to Ag-MOFs receptiveness to the level of potentially creating too dense of a MOF layer
2 leading to a less favorable surface charge and the fact that a strong solvent was needed to
3 disperse the zwitterionic solution, prompted us to re-use BPA in the next study as the more
4 potent zwitterionic bed layer while re-think the immobilization strategy to maximize the added
5 features and performance benefits.

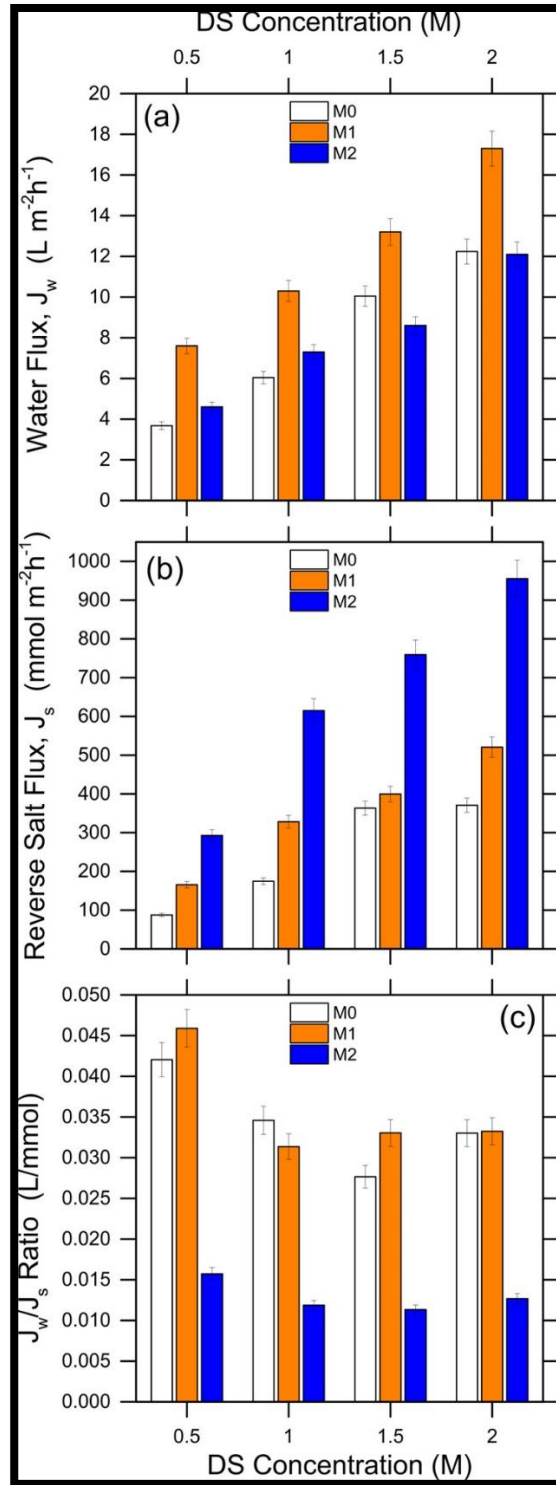
6 Similar FO experiment were conducted for the second study, focused solely on BPA-
7 MOF-modified membranes, employing the in-situ growth method instead of somewhat failed
8 direct deposition (for this specific combination of materials) (Fig. 18). The water flux (J_w) saw a
9 spike upon functionalization via both pathways used to prepare M1 and M2, which can safely be
10 ascribed to an increased hydrophilicity in the active membrane surface and the consequently
11 stronger affinity with water molecules. Similar to our observation for TFC-BPA-MOF, the less
12 pronounced improvement for M2 might be due to the formation of a denser covering layer,
13 leading to a higher resistance for water passage, compounded by a slightly lower wettability
14 compared to M1 [134]. The reverse solute flux (J_s) of both M1 and M2 membranes increased
15 relative to the pristine M0. Similar to BPA- and PS-modified pairs in the previous study, the
16 increased reverse salt flux is potentially partly due to the more neutralized surface charge of the
17 membranes leading to less electrostatic repulsion and a higher solute permeability. This spike is
18 more intense in the case of M2 sample, which managed to preserve a significantly lower degree
19 of the pristine M0's salt selectivity. Readers are respectfully reminded that for M2, there was a
20 preliminary inclusion of Ag-MOFs in the BPA solution, which necessitated the minimal use of
21 NMP for achieving a more homogenous dispersion of Ag-MOFs within the BPA solution. This
22 result potentially unveils the degree of NMP-induced deterioration of the membrane structure,
23 which outweighs any potential gain in productivity levels.

1 RSFS values (J_w/J_s ratio) showed resilience with even slight improvements in some draw
2 concentrations for M1, which is indicative of uncompromised transport parameters. M2 on the
3 other hand, demonstrated a relatively lessened perm-selectivity, naturally due to poor solute
4 selectivity. As explained, this phenomenon was resulted by an increased thickness of M2 active
5 layer as a result of excessive MOFs loading (creating a transport barrier to water) as well as
6 NMP-induced defects in the BPA grafting stage.



1

2 **Figure. 17.** Performance of the pristine TFC and functionalized membranes in FO filtration tests at
 3 various DS concentrations: a) FO water flux, J_w , b) FO reverse salt flux, J_s , c) water flux to salt flux ratio,
 4 J_w/J_s .



1

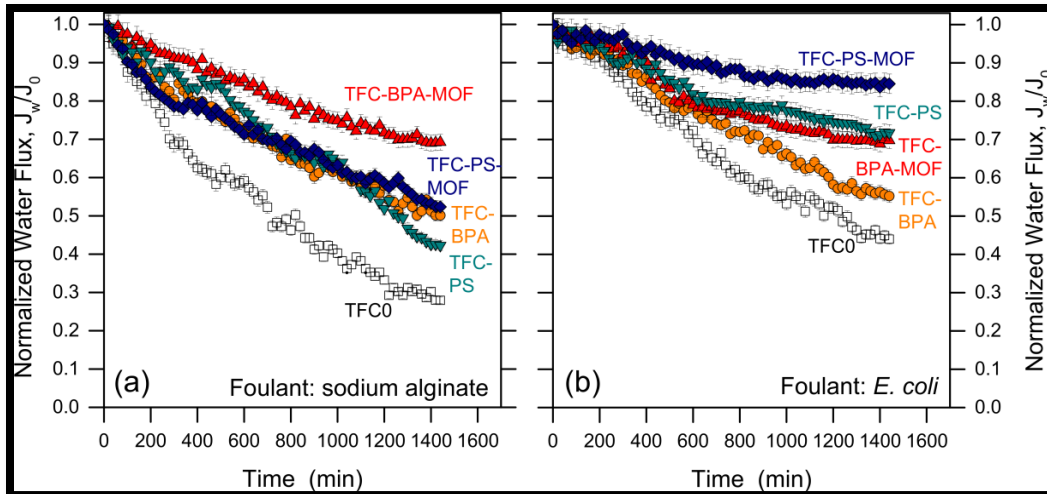
2 **Figure. 18.** FO transport parameters of pristine and functionalized membranes, measured with a lab
 3 filtration setup and in tests using different NaCl concentrations. (a) Permeate flux, J_w ; (b) reverse
 4 NaCl flux, J_s ; (c) ratio of permeate flux over NaCl flux, J_w/J_s .

1 Fouling tests were conducted using sodium alginate (SA) as model organic foulant and *E.*
2 *coli* as model biofoulant for both FO studies. SA is a polysaccharide and one of the main
3 components of extracellular polymeric substances. For both studies, the water flux started to
4 decrease substantially soon after the introduction of SA into the FS. This decrease was
5 specifically pronounced for the pristine membranes; however, the surface-functionalized
6 membranes exhibited a less intense flux decline. This result could be justified by the presence of
7 a more hydrophilic surface on the functionalized membranes that created a denser hydration
8 layer, which hampered foulant deposition on the membrane surface [135]. The presence of Ag-
9 MOFs on the TFC-BPA-MOF and TFC-PS-MOF membranes also seemed to lead to a relative
10 improvement in antifouling propensity compared to membranes solely modified by zwitterions
11 (Fig. 19a). It has been reported that the presence of 2-methylimidazol in the structure of Ag-
12 MOFs might add to the strength of the hydration layer on the membrane/feed interface [136].
13 Similarly, the flux decline became almost non-existent for M1 and M2 membranes after roughly
14 7 h, proving them to be even stronger membrane products in terms of fouling resistance (Fig.
15 20a). This phenomenon was a potent indicator of the impact a different coating strategy would
16 bring about, making it even more impressive (particularly with the transport-calibrated M1)
17 given the fact that these two samples employed BPA which was the weaker of the zwitterionic
18 pair in terms of transport and fouling performance. The results of biofouling experiments were
19 obtained and plotted besides those corresponding to organic fouling. As expected, introducing *E.*
20 *coli* into the feed solution caused a major downward flux movement in time due to deposition
21 and possible biofilm formation on the membrane surface. This phenomenon was somewhat
22 disrupted for the surface-functionalized membranes, and generally more pronounced in the case
23 of TFC-BPA-MOF and TFC-PS-MOF with respect to TFC-BPA and TFC-PS samples,

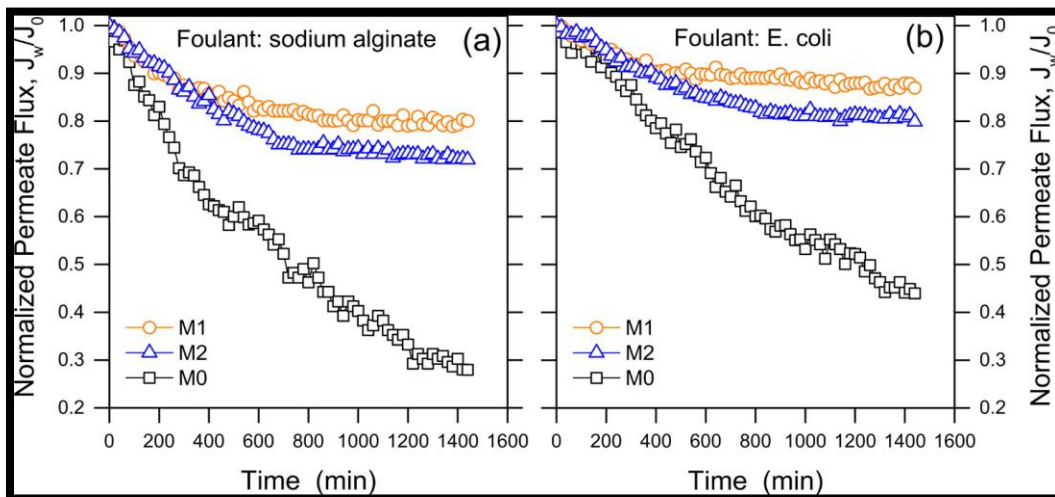
1 obviously due to the presence of Ag-MOFs possessing anti-microbial activity (Fig. 19b).
2 Specifically, these four functionalized membranes managed to retain between 42-69% and 55-
3 84% at the end of fouling and biofouling experiments, respectively. The corresponding figures
4 were 28% (fouling) and 44% (biofouling) for the pristine TFC0 membrane, showing a noticeable
5 enhancement. In the BPA-focused FO study, M1 and M2 maintained 80% and 72% of the initial
6 flux in the organic fouling tests, and 87% and 80% in the bio-fouling tests. Comparing to the
7 corresponding fluxes of 28% and 44% pertaining to the pristine M0 (which was the same as
8 TFC0), indicating a remarkable fouling mitigation brought about by a more efficacious surface
9 modification. These results were similarly ascribed to higher water affinity, particularly for M1
10 [135], and (primarily in the biofouling tests) to the activity of silver that inactivated bacteria
11 efficiently (Fig. 20b). Theoretically, the membrane with a higher surface loading of silver, i.e.,
12 M2, should have demonstrated a better anti-biofouling performance. However, for both foulants
13 (SA, and *E. coli*) M1 membranes displayed a better flux resilience. This phenomenon could be
14 rationalized with a relatively faded presence of zwitterions on the M2 surface due to the more
15 aggressive loading of Ag-MOFs. Higher accessibility of zwitterions to the water molecules at the
16 membrane/feed interface would increase the density of the formed hydration layer, which in turn
17 works unfavourably towards bacterial adhesion. Finally, different silver-based materials used for
18 biofouling mitigation in FO membranes are tabulated (table 2) following approaches
19 implemented for surface functionalization in comparison with this study, extracted from a recent
20 work on Ag-MOFs [137].

21

22



1
 2 **Figure. 19.** Flux decline due to fouling in FO experiments for the pristine and the surface-modified
 3 membranes; a) organic fouling by sodium alginate at a concentration of 250 mg/L, b) microbial
 4 biofouling by *E. coli* with an initial concentration of 10^7 CFU/L.



5
 6 **Figure. 20.** Antifouling performance of the pristine and of the surface-modified membranes during
 7 FO filtration tests. The model foulants were: (a) sodium alginate at a concentration of 250 mg/L and
 8 (b) *E. coli* at an initial concentration of 10^7 CFU/L. All the points are the average of two
 9 experiments.

10

11

1 **Table 2.** A comparison of different approaches and bacterial spectrum applied for antibacterial
 2 assessment in FO membranes

Year	Substrate material	Anti-biofoulant agent	Modification approach	Bioufoulant	Key feature of functionalization	Ref.
2020	PA-TFC	Ag-MOFs on zwitterionic coating	In-situ growth	<i>E. coli</i>	<ul style="list-style-type: none"> - Relatively simple approach - quick reaction time in room temperature without using dangerous solvents - excellent increase in hydrophilicity (50% reduction in contact angle) - no detrimental effect on membrane transport parameters - substantial antibacterial activity (42% and 76% inactivation) - sustainable antibiofouling mitigation during a 24 h operation without physical cleaning (87% flux retention throughout the biofouling test) 	This research [41]
2020	PA-TFC	Ag-MOFs on zwitterionic coating	Direct deposition	<i>E. coli</i>	<ul style="list-style-type: none"> - coupled defensive (hydration layer) and offensive (silver release) approach - increased hydrophilicity - maintain membrane integrity (for PS-modified samples) - 75-99% bacterial inactivation - Steady-state flux reached during 24h with no cleaning (70-85% flux retention achieved) 	This research [42]
2014	CTA	Ag NPs regenerated by TiO ₂	In situ growth	ATP	<ul style="list-style-type: none"> - moderate enhanced hydrophilicity - increased roughness - effective inhibition of bacteria growth 	[138]
2015	PA-TFC	Ag-GO nanocomposite	Click chemistry reaction	<i>E. coli</i>	<ul style="list-style-type: none"> - super-hydrophilic properties - significant bacterial activity reduction due to the synergetic effect of the Ag-GO nanocomposite - no adverse effect on the membrane transport properties 	[139]
2015	PA-TFC	Ag-GO nanocomposite	EDC/NHS coupling In situ reduction	<i>E. coli</i> , <i>E. faecalis</i>	<ul style="list-style-type: none"> - enhanced silver loading and stability due to GO presence - increased surface hydrophilicity - 98% antibacterial activity - 75% antibacterial activity after regeneration 	[86]
2015	PAN	Ag NPs	In situ reduction	<i>E. coli</i>	<ul style="list-style-type: none"> - very high antimicrobial activity against <i>E. coli</i> for 14 days under laboratory conditions 	[140]
2016	PA-TFC	Ag NPs on PDA coating	In situ growth	<i>E. coli</i> , <i>S. aureus</i>	<ul style="list-style-type: none"> - enhanced hydrophilicity (contact angle of 40.6°) - increased roughness - strong sustainable antibacterial properties 	[141]

					against <i>E. coli</i>	
2017	PA-TFC	Ag-GO nanocomposite	EDC/NHS coupling	<i>P. aeruginosa</i>	<ul style="list-style-type: none"> - slight reduction in surface roughness - significant decrease in bacterial attachment and viability - 30% water flux decline during dynamic biofouling 	[109]
2017	PA-TFC	Ag NPs Zwitterionic nanocomposite	ATRP grafting	synthetic wastewater supplemented <i>P. aeruginosa</i>	<ul style="list-style-type: none"> - smoother membrane surface - remarkable increased hydrophilicity (contact angle of 21°) - 95% antibacterial activity - 46% increase in dead cells biovolume - 60% decrease in EPS content - 8% water flux decline 	[43]
2017	PA-TFC	Silica NPs Zwitterionic nanocomposite	ATRP grafting	<i>E. coli</i>	<ul style="list-style-type: none"> - high surface hydrophilicity and reduced surface roughness - improved antifouling property - reduced water flux decline (17%) - PSBMA-TFC membrane showed drastic increased in antibiofouling resistance (96% reduction of the number of attached <i>E. coli</i>) 	[142]
2018	PA-TFC	BSA capped Ag NPs	Grafting	<i>E. coli</i>	<ul style="list-style-type: none"> - slight improvement water permeability and salt rejection - low release rate and excellent stability during filtration - excellent antibacterial and high biofouling resistant properties 	[143]
2018	PA-TFC	Ag NPs on PDA coating	In-situ reduction	synthetic wastewater supplemented <i>P. aeruginosa</i>	<ul style="list-style-type: none"> - improved hydrophilicity - good stability of Ag NPs and 96.1% antimicrobial activity after 24 h of cross-flow test - really low water flux decline - proper antibacterial activity in both static and dynamic conditions - efficient biofouling mitigation during long-term operation 	[106]
2018	PA-TFC	Ag NPs Zwitterionic nanocomposite	Grafting In-situ reduction	<i>E. coli</i>	<ul style="list-style-type: none"> - increased hydrophilicity, high water flux, and excellent selectivity - simultaneous improvement of antiadhesive property - 96% antibacterial activity - significant biofouling resistance and long-term antibiofouling 	[120]

2019	PA-TFC	Ag-MOFs	In-situ growth	synthetic wastewater supplemented <i>P. aeruginosa</i>	<ul style="list-style-type: none"> - uniform distribution of Ag-MOFs on the PA layer - irreversible binding of Ag-MOFs to the TFC surface - slight reduction in both the salt and water permeability - nearly 100% antibacterial activity - high antibiofouling performance 	[144]
------	--------	---------	----------------	--	--	-------

1 Long-term ultrafiltration tests were also conducted to measure the viability of surface
2 modifications applied to the UF membranes and to evaluate the potentially gained advantages in
3 terms of both salt selectivity and fouling-induced flux decline. The PWP of pristine membranes
4 was measured to be within the 1500 and 2500 L m⁻¹h⁻¹bar⁻¹ range, with variability probably
5 stemming from differences in surface porosity and pore size among different selected and cut
6 portions of the flat sheet TFC commercial membrane. The modified membranes exhibited
7 instead less PWP variations, which were also more consistent among the different sets of
8 functionalization, namely, 1200 ± 260 L m⁻¹h⁻¹bar⁻¹. These results are rationalized with the
9 possibility that not only did the additional AA and/or Ag-MOFs layers on U2, U3, and U4
10 membranes provided an equalizing effect in terms of surface morphology, but they also
11 introduced some resistance (through a thickened active layer) to water permeation and
12 represented the main factor affecting mass transport, thus overriding the variability of the
13 underlying membrane [145].

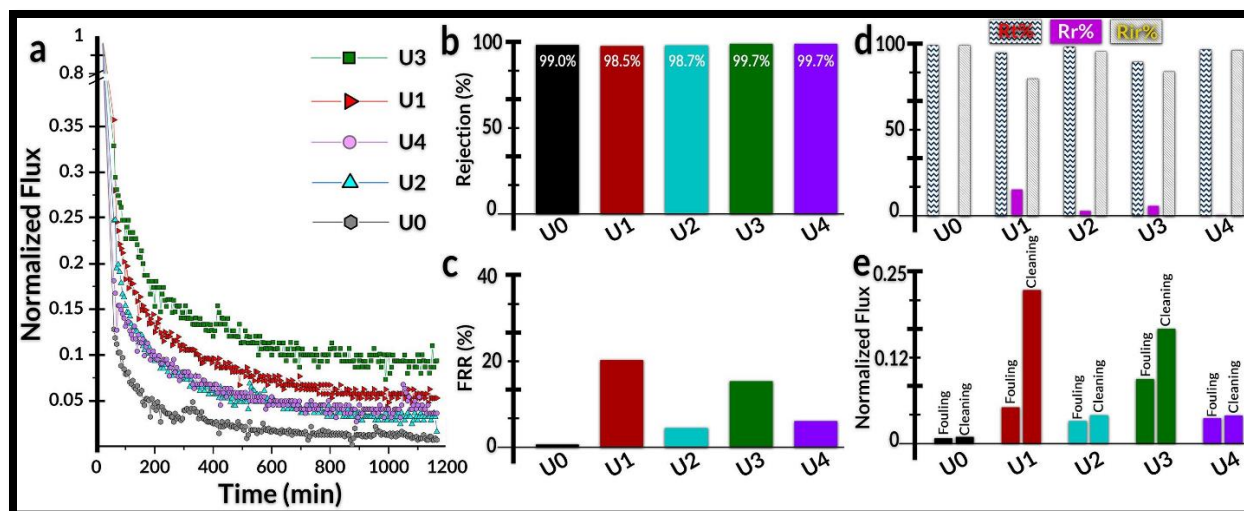
14 The flux of pristine and surface-functionalized membranes was measured in long-term
15 HA filtration tests to evaluate organic fouling and normalized to account for the variations in the
16 initial flux values, as shown in Fig. 21a. As observable, grafting the PSf surfaces with AA and
17 MOFs positively impacted the fouling resistance of the membrane, as these modifications: (i)
18 reduce the rate of initially sharp flux decline; and (ii) hasten the steady-state flux level leading to
19 an increased flux value at the end of the fouling run. The steady fluxes at the end were roughly

1 7X (U1), 3X (U2), 13X (U3), and 5X (U4) the pristine U0 flux. This result was directly in
2 accordance with the wettability results from contact angle measurements especially for U3,
3 which had the largest gain in hydrophilicity. The initial flux decline rate was objectively high for
4 all samples, which was predictable given the composition of the feed solution, comprising HA
5 and divalent cations at high concentrations to promote accelerated fouling conditions. This drop
6 naturally became even more pronounced with the dead-end configuration of the filtration cell,
7 promoting the quick formation of a cake layer upon rejection of HA by the membrane. The
8 initial flux decline of U0 pristine samples was roughly 36%, 30%, 44%, and 19% quicker than
9 U1, U2, U3, and U4, respectively, proving these modifications did indeed hamper fouling
10 noticeably, if not significantly.

11 HA rejection was also measured for each membrane (Fig. 21b). High rejection (>98.5%)
12 was shown by U0 and put as a benchmark; other membranes maintained their pristine-level
13 rejection rates post-modification and some even displayed rates up to 99.7%. As mentioned
14 earlier, higher zeta potential values are correlated with a more potent electrical double layer
15 repulsion and have been reported to positively influence membrane rejection of negatively
16 charged solutes [108]. In that sense, HA rejection order of $U4=U3>U0>U2>U1$ is in strong
17 accordance with the neutral-range zeta potential values in Fig. 10h. Interestingly, same study
18 reported that a stronger zeta potential does not necessarily translate to a less fouling propensity,
19 with roughness and hydrodynamics of permeation playing important roles in that regard. The
20 flux recovery ratio (FRR%) was calculated and plotted in Fig. 21c as a measure to better study
21 the anti-fouling behavior of the membranes; the reversibility of foulant deposition and physical
22 cleaning efficiency were also obtained for a deeper insight and further breakdown of membrane
23 fouling propensity. U1 and U3 with FRR% of 20% and 16%, respectively, suggested a better

1 cleaning behavior compared to other samples. Interestingly, looking into reversible, and
2 irreversible components of total fouling (Fig. 21d) revealed that a higher fouling reversibility
3 was observed for U1 (15%), followed by U3 (6%). Notably, the pristine membrane (U0)
4 demonstrated a near 100% irreversible fouling. Normalized flux values at the end of fouling and
5 during post-cleaning stages are visualized to capture the wholistic effect of antifouling
6 performance and fouling reversibility (Fig. 21e).

7 In summary, U1 outperformed U0 by a wide margin in every performance metric, due to
8 the existence of a hydrophilic AA layer. The use of Ag-MOFs also worked favourably towards
9 antifouling activity and permeation performance of the U3 membranes. The higher surface
10 roughness and lower wettability of U2 led to a relatively more fouling vulnerability and
11 irreversibility of this membrane [74,146,147]. It is worthy of remembrance that U2 was subject
12 to direct deposition of Ag-MOFs (included into the AA solution, without any NMP use this
13 time), proving to cancel out the added positive effects of Ag-MOFs and AA. Also, depositing
14 MOFs on pristine membranes (U4) proved not to be a sufficient strategy for surface
15 modification, ruling out deposition altogether. Instead, U3, obtained by pre-hydrophilizing the
16 material with AA and exploiting this coating to grow uniform Ag-MOFs provided the best
17 overall combination of wettability, roughness, productivity, and rejection. U3 also demonstrated
18 a strong biocidal activity, acting as a strong barrier against microbial deposition and biofilm
19 formation, which would help U3 perform well again biofouling as well.



1
2 **Figure. 21.** (a) Normalized flux of pristine and modified membranes in long term humic acids (HA)
3 fouling filtration; (b) observed rejection of HA; (c) normalized flux recovery ratio (in percentage) after
4 physical cleaning; (d) different components of membrane fouling, categorized into total fouling ($R_t\%$),
5 irreversible fouling ($R_{ir}\%$), and reversible fouling ($R_r\%$); and (e) comparison between fluxes at the end of
6 HA filtration (“fouling”) and DI fluxes following membrane cleaning.

7

8 **3.5 Silver stability on membranes**

9 A great deal of importance has been rightly attributed to the controlled release of silver
10 when Ag-MOFs are immobilized to aspire for effective, stable, and sustainable antibacterial and
11 anti-biofouling activity [2,148]. Kinetics of silver release defines the balance between a contact-
12 based “defensive” bacterial inactivation and a dissolution-based for “offensive” killing [7].
13 Accordingly, the silver release rate was measured for the M1 and M2 TFC membranes, as well
14 as U2, U3, and U4 PSf membranes to obtain a more tangible understanding of silver bond
15 strength within the coordination network of MOFs and by extension, the polymeric membrane
16 (Fig. 22). As can be observed in Fig. 22a, depicting daily measurements of silver release (after 1,
17 7, and 30 days), M1 and M2 membranes performed broadly similarly in terms of initial trend of
18 reduced silver release rate during the first 7 days of monitoring. The following days leading up to
19 the 1-month trial demonstrated that M1 had actually reached a plateau in the first week, with

1 almost no significant subsequent silver release into the solution; however, M2 proved to possess
2 a higher degree of loosely-bound silver even after a spectacular silver loss in day 1, which
3 continued to leach throughout the month, maintaining a positive rate. Please note that these
4 graphs are plotted as silver loss gradient. So, a positive slope for M2 during day 7 to 30 implies
5 that there is an excessive amount of loosely-attached MOFs that even after a week, silver loss
6 actually is worsened in the next 23 days. This could be due to two reasons; 1) too many unstable
7 MOFs are present, and 2) the sheer number of days is longer in the second gradient which could
8 accommodate heavy leaching. A positive slope during such a long period also means that a much
9 longer time is needed for a plateau to be achieved. In absolute terms, M1 was also quite more
10 efficient compared to M2. This observation most probably stems from the difference in
11 modification pathway, imposing a heavier concentration of Ag-MOFs on the M2 surface, which
12 is also in accordance with other characterization data from EDX, indicating a silver content for
13 M2 as almost double that of M1. It was explained that the BPA oxygen-containing functional
14 groups may act as hospitable sites to attach and hold silver ions, which translates to MOF
15 stability on the membrane surface [148]; it is also reasonable to suggest that a competition for
16 attachment to the membrane surface between BPA and Ag-MOFs could end up detrimental to
17 favourable BPA-assisted binding of MOFs, the potential reason why silver on M1 remained
18 more committed to the membrane despite fewer numbers.

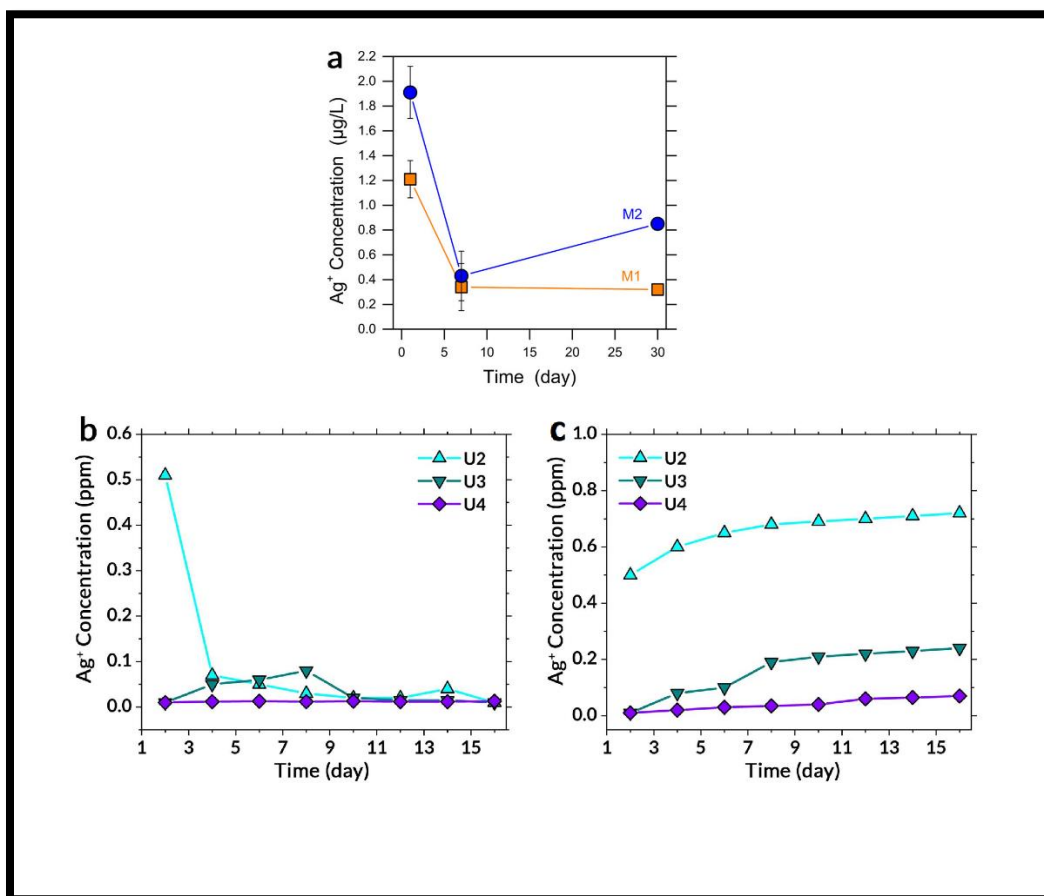
19 Overall, it is worthy of mention that the monthly amount of silver released into the feed
20 for both M1 and M2 is in the order of $\mu\text{g/L}$ (cumulatively $< 4 \mu\text{g/L}$) which sits well below the
21 WHO threshold for drinking water (0.1 mg/L) and most aquatic life in natural waters.

22 From this 1-month monitoring it was obvious that despite the absolute low values of
23 silver depletion for both M1 and M2, M1 was the better candidate in providing a durable Ag^+

1 reservoir, capable of anti(bio)fouling activity, decent bacterial inhibition, with the added benefit
2 of minimal silver wasted.

3 Silver release was monitored and measured daily for U2, U3, and U4 samples during a
4 15-day session as well (Fig. 22b, c). U3 and U4 demonstrated a competitively low amount of
5 release, with continuation of release gradients on a steady and stable path while U2 started from
6 a much higher value of silver release, quickly plummeted after day 1 to reach release gradient
7 values below U3 and more in line with U4. As proposed earlier, AA significantly bolstered Ag-
8 MOFs reception onto the U2 and U3 surfaces by potentially providing hospitable binding sites
9 via carboxyl groups, similar to BPA and PS (via its sulfonic groups) which might be able to
10 justify the higher degree of silver release only in absolute terms compared to the more MOF-
11 barren U4 (Fig. 22c). Again, here there was a similar observation regarding the differences
12 between U2 and U3, reminiscent of that between M1 and M2. While in U3 samples, all the Ag-
13 MOFs are anchored to the membrane through AA, the deposition method used to immobilize
14 MOFs onto U2 could well have left multiple nanoparticles loosely-bound and potentially
15 aggregated, with easily detachable silver ions when exposed to a polar solution such as water.
16 Cumulative release data demonstrated that U3 showed a clear superiority in terms of release rate,
17 amounting to approximately 0.2 ppm over 15 days. These results suggested that UV-grafting
18 could be utilized and (optimized) similarly as chemical grafting and solution deposition, to create
19 long-term silver ion reservoirs on PSf membranes for antibacterial activity in aqueous solutions.
20 Detailed WHO guidelines deem a maximum silver concentration of 0.1 mg/L in drinking water
21 as safe and tolerable for humans, given a regular consumption of said drinking water source for a
22 period of 70 years. Subsequently, only half of the no-observed-adverse-effect-level (NOAEL)
23 threshold of 10 g would be absorbed by the human body. It is noteworthy that U4 performance in

1 terms of silver release was also within the realm of safety guidelines, which totalled a 15-day
2 amount below 0.2 mg/L. It was concluded that these membranes, esp. U3 were relatively low-
3 hazard regarding silver safety issues and able to upkeep the bacteriological quality of water for
4 the short to medium and even long term; hypothetically, these Ag-MOFs could well be
5 regenerated multiple times for an industry-standard operation time span, e.g., 10 years.



6
7 **Figure. 22.** a) results of silver ion leaching experiments from the MOF-modified membranes M1
8 and M2; silver ion leaching results for U2, U3, and U4 membranes, reported in a) daily amounts and
9 b) cumulative amounts for the total duration of 15 days. Please note that silver concentration is
10 actually plotted in terms of gradient, measured between the days of experiment as time points.

11

1 **4. Conclusions**

2 The research conducted for the purposes of this dissertation comprises three studies
3 focused on preparing membranes with maximum utility via pathways optimized for
4 simplification and efficiency. Specifically, the effort was to equip membranes with
5 fouling/biofouling mitigation tools for a smoothly prolonged filtration operation with minimum
6 hindrance in water flux/permeation and avoiding damage to the selective pore structure of the
7 respective active layers. To this end, first component of this research revolved around coating FO
8 membranes with two zwitterion choices, namely, BPA and PS, for a “defensive” antifouling
9 strategy and subsequent immersion under Ag-MOFs solution for an “offensive” biocidal activity
10 against biofouling and biofilm formation. All surface-modified membranes displayed improved
11 resilience against (bio)fouling, declining down to 70% and 85% of initial flux retainment against
12 organic and microbial fouling, respectively. BPA was chosen to further optimize coating
13 strategies which resulted in a maximum of 80% and 90% of initial flux retainment, realized in
14 less than a third of operational time and maintained until the end of filtration. In both studies, FO
15 transport parameters were mostly non-affected or enhanced marginally. To investigate the
16 efficacy of this surface modification strategy on pressure-driven processes, UF membranes were
17 coated with acrylic acid (hydrophilic defense), photo-polymerized under UV irradiation with Ag-
18 MOFs introduced in several pathways. Normalized steady-state water fluxes during a heavy
19 foulant humic acid feed filtration were enhanced up to 13X the pristine membrane as the result of
20 surface modification. Membrane rejection rates remained unaltered or slightly improved. Also,
21 flux recovery ratios following a physical membrane cleaning saw significant increases up to 20%
22 (zero for the UF pristine membrane). Antibacterial analysis for all three studies indicated strong
23 antimicrobial activity against *E.coli* and *S. aureus* planktonic cells; the rates were somewhat

1 wide-ranging spanning from 62% (TFC-PS-MOF against *E.coli*) and 100% (TFC-BPA-MOF
2 against *E.coli*) to 76% (M2 against *E.coli*) in the FO studies and 80% (U2 against *E.coli*), 90%
3 (U3 against *E.coli*), and 95% (both U2 and U3 against *S. aureus*). As stated, the ability to combat
4 biofilm formation from robust biofilm-forming *P. aeruginosa* was also studied in another
5 project; it revealed a near 100% biofilm inhibition when employing Ag-2MI, incorporated into
6 the active layer of the PA FO membrane. A distinctive point in antimicrobial activity suggested
7 by the first FO study is that BPA might be the better host for Ag-MOFs biocides (judging by
8 TFC-BPA-MOF and TFC-PS-MOF performances). However, seeing that a smooth BPA
9 deployment for the Maximum (100%) annihilation rate necessitated the use of an organic solvent
10 for MOF solution dispersion (please note that M2 in the second study displayed a 76%
11 performance, without NMP use), there is the question of how to enhance MOF loading using
12 BPA even further which might possibly help membranes act even stronger and more resiliently
13 against (bio)fouling.

14 This research sheds a light on the efficacy of deploying Ag-MOFs with hydrophilic
15 reinforcements such as zwitterionic or acrylic acid pre-grafts as a successful fouling and
16 biofouling strategy with great material compatibility and minimal disruption to the integrity of
17 the membrane matrix. Overall, the best method seems to be the in-situ growth in order to obtain
18 a uniform layer, highest Ag loading, and less silver leaching while sustaining a stable coating for
19 a prolonged usability.

20

21

22

1 **5. Suggestions**

2 In this research various methods of deploying metal-organic frameworks in combination
3 with hydrophilic coatings were examined with the goal of sustainable (bio)fouling mitigation
4 and biofilm inhibition. The effort was to avoid disruptions to membrane operations by postponing
5 and countering fouling-induced incapacitation. Although stable fluxes were achieved and well-
6 maintained for the 24 h experimentation period, real-life membrane operations last much longer
7 than that, spanning years. Also, despite the efforts to keep methods rather simpler compared to
8 much of the literature, there is still a long way to actually commercialize these techniques and fit
9 them into well-established production protocols. Further research would be warranted to examine
10 the following broad themes:

- 11 ▶ Techno-economic studies on upscaling methods for industrial applications
- 12 ▶ Explore different MOFs possibilities and potencies (different metals, ligands, and
13 resulting topologies)
- 14 ▶ Fine-tune silver release rate and antibacterial activity through improving materials and
15 methods of immobilization (particularly for sensitive industries, e.g., food and beverage)
- 16 ▶ Optimize regeneration for prolonged, minimal-disruption membrane operation
17 (streamlining the process for minimal material use and process duration)
- 18 ▶ Upscaling and industry-fitting the studied modification pathways for incorporation into
19 roll-to-roll membrane production lines

20

1 **References**

- 2 [1] N. Akther, A. Sodiq, A. Giwa, S. Daer, H.A. Arafat, S.W. Hasan, Recent advancements in
3 forward osmosis desalination: A review, *Chem. Eng. J.* 281 (2015) 502–522.
4 doi:10.1016/J.CEJ.2015.05.080.
- 5 [2] M.D. Firouzjaei, S.F. Seyedpour, S.A. Aktij, M. Giagnorio, N. Bazrafshan, A.
6 Mollahosseini, F. Samadi, S. Ahmadalipour, F.D. Firouzjaei, M.R. Esfahani, A. Tiraferri,
7 M. Elliott, M. Sangermano, A. Abdelrasoul, J.R. McCutcheon, M. Sadrzadeh, A.R.
8 Esfahani, A. Rahimpour, Recent advances in functionalized polymer membranes for
9 biofouling control and mitigation in forward osmosis, *J. Memb. Sci.* 596 (2020) 117604.
10 doi:10.1016/j.memsci.2019.117604.
- 11 [3] N.Y. Yip, A. Tiraferri, W.A. Phillip, J.D. Schiffman, M. Elimelech, High Performance
12 Thin-Film Composite Forward Osmosis Membrane, *Environ. Sci. Technol.* 44 (2010)
13 3812–3818. doi:10.1021/es1002555.
- 14 [4] M. Giagnorio, F. Ricceri, A. Tiraferri, Desalination of brackish groundwater and reuse of
15 wastewater by forward osmosis coupled with nanofiltration for draw solution recovery,
16 *Water Res.* 153 (2019) 134–143. doi:10.1016/j.watres.2019.01.014.
- 17 [5] R. Valladares Linares, Z. Li, S. Sarp, S.S. Bucs, G. Amy, J.S. Vrouwenvelder, Forward
18 osmosis niches in seawater desalination and wastewater reuse, *Water Res.* 66 (2014) 122–
19 139. doi:10.1016/j.watres.2014.08.021.
- 20 [6] Y. Chen, W. Xu, H. Zhu, D. Wei, F. He, D. Wang, B. Du, Q. Wei, Effect of turbidity on
21 micropollutant removal and membrane fouling by MIEX/ultrafiltration hybrid process,
22 *Chemosphere.* 216 (2019) 488–498. doi:10.1016/j.chemosphere.2018.10.148.

- 1 [7] M.S. Mauter, Y. Wang, K.C. Okemgbo, C.O. Osuji, E.P. Giannelis, M. Elimelech,
2 Antifouling ultrafiltration membranes via post-fabrication grafting of biocidal
3 nanomaterials, *ACS Appl. Mater. Interfaces.* 3 (2011) 2861–2868.
4 doi:10.1021/am200522v.
- 5 [8] A.W. Mohammad, C.Y. Ng, Y.P. Lim, G.H. Ng, Ultrafiltration in Food Processing
6 Industry: Review on Application, Membrane Fouling, and Fouling Control, *Food*
7 *Bioprocess Technol.* 5 (2012) 1143–1156. doi:10.1007/s11947-012-0806-9.
- 8 [9] Q. She, R. Wang, A.G. Fane, C.Y. Tang, Membrane fouling in osmotically driven
9 membrane processes: A review, *J. Memb. Sci.* 499 (2016) 201–233.
10 doi:10.1016/J.MEMSCI.2015.10.040.
- 11 [10] K. Kimura, Y. Hane, Y. Watanabe, G. Amy, N. Ohkuma, Irreversible membrane fouling
12 during ultrafiltration of surface water, *Water Res.* 38 (2004) 3431–3441.
13 doi:10.1016/j.watres.2004.05.007.
- 14 [11] M.R. Esfahani, S.A. Aktij, Z. Dabaghian, M.D. Firouzjaei, A. Rahimpour, J. Eke, I.C.
15 Escobar, M. Abolhassani, L.F. Greenlee, A.R. Esfahani, A. Sadmani, N. Koutahzadeh,
16 Nanocomposite membranes for water separation and purification: Fabrication,
17 modification, and applications, *Sep. Purif. Technol.* 213 (2019) 465–499.
18 doi:10.1016/j.seppur.2018.12.050.
- 19 [12] H.. Scott. K, *Industrial Membrane Separation Technology*, Springer Netherlands, 1996.
20 doi:10.1007/978-94-011-0627-6.
- 21 [13] M.D. Firouzjaei, S.F. Seyedpour, S.A. Aktij, M. Giagnorio, N. Bazrafshan, A.
22 Mollahosseini, F. Samadi, S. Ahmadalipour, F.D. Firouzjaei, M.R. Esfahani, A. Tiraferri,

- 1 M. Elliott, M. Sangermano, A. Abdelrasoul, J.R. McCutcheon, M. Sadrzadeh, A.R.
2 Esfahani, A. Rahimpour, Recent advances in functionalized polymer membranes for
3 biofouling control and mitigation in forward osmosis, *J. Memb. Sci.* (2019) 117604.
4 doi:10.1016/j.memsci.2019.117604.
- 5 [14] H.-C. Flemming, G. Schaule, T. Griebe, J. Schmitt, A. Tamachkiarowa, Biofouling—the
6 Achilles heel of membrane processes, *Desalination*. 113 (1997) 215–225.
7 doi:10.1016/S0011-9164(97)00132-X.
- 8 [15] J. Zhu, A. Uliana, J. Wang, S. Yuan, J. Li, M. Tian, K. Simoens, A. Volodin, J. Lin, K.
9 Bernaerts, Y. Zhang, B. Van Der Bruggen, Elevated salt transport of antimicrobial loose
10 nanofiltration membranes enabled by copper nanoparticles: Via fast bioinspired
11 deposition, *J. Mater. Chem. A*. 4 (2016) 13211–13222. doi:10.1039/c6ta05661j.
- 12 [16] N. Misdan, W.J. Lau, A.F. Ismail, Seawater Reverse Osmosis (SWRO) desalination by
13 thin-film composite membrane—Current development, challenges and future prospects,
14 *Desalination*. 287 (2012) 228–237. doi:10.1016/J.DESAL.2011.11.001.
- 15 [17] Q. Chen, P. Yu, W. Huang, S. Yu, M. Liu, C. Gao, High-flux composite hollow fiber
16 nanofiltration membranes fabricated through layer-by-layer deposition of oppositely
17 charged crosslinked polyelectrolytes for dye removal, *J. Memb. Sci.* 492 (2015) 312–321.
18 doi:10.1016/j.memsci.2015.05.068.
- 19 [18] A. Rahimpour, S.F. Seyedpour, S. Aghapour Aktij, M. Dadashi Firouzjaei, A. Zirehpour,
20 A. Arabi Shamsabadi, S. Khoshhal Salestan, M. Jabbari, M. Soroush, Simultaneous
21 Improvement of Antimicrobial, Antifouling, and Transport Properties of Forward Osmosis
22 Membranes with Immobilized Highly-Compatible Polyrhodanine Nanoparticles, *Environ.*

- 1 Sci. Technol. 52 (2018) 5246–5258. doi:10.1021/acs.est.8b00804.
- 2 [19] M. Di Vincenzo, M. Barboiu, A. Tiraferri, Y.M. Legrand, Polyol-functionalized thin-film
3 composite membranes with improved transport properties and boron removal in reverse
4 osmosis, J. Memb. Sci. 540 (2017) 71–77. doi:10.1016/J.MEMSCI.2017.06.034.
- 5 [20] L. Yang, Z. Wang, J. Zhang, Highly permeable zeolite imidazolate framework composite
6 membranes fabricated via a chelation-assisted interfacial reaction, J. Mater. Chem. A. 5
7 (2017) 15342–15355. doi:10.1039/C7TA03244G.
- 8 [21] Y.H. La, J. Diep, R. Al-Rasheed, D. Miller, L. Krupp, G.M. Geise, A. Vora, B. Davis, M.
9 Nassar, B.D. Freeman, M. McNeil, G. Dubois, Enhanced desalination performance of
10 polyamide bi-layer membranes prepared by sequential interfacial polymerization, J.
11 Memb. Sci. 437 (2013) 33–39. doi:10.1016/j.memsci.2013.02.044.
- 12 [22] M. Ben-Sasson, K.R. Zodrow, Q. Genggeng, Y. Kang, E.P. Giannelis, M. Elimelech,
13 Surface Functionalization of Thin-Film Composite Membranes with Copper Nanoparticles
14 for Antimicrobial Surface Properties, Environ. Sci. Technol. 48 (2014) 384–393.
15 doi:10.1021/es404232s.
- 16 [23] Z. Yang, Y. Wu, J. Wang, B. Cao, C.Y. Tang, *In Situ* Reduction of Silver by
17 Polydopamine: A Novel Antimicrobial Modification of a Thin-Film Composite Polyamide
18 Membrane, Environ. Sci. Technol. 50 (2016) 9543–9550. doi:10.1021/acs.est.6b01867.
- 19 [24] W. Ding, J. Cai, Z. Yu, Q. Wang, Z. Xu, Z. Wang, C. Gao, Fabrication of an aquaporin-
20 based forward osmosis membrane through covalent bonding of a lipid bilayer to a
21 microporous support, J. Mater. Chem. A. 3 (2015) 20118–20126. doi:10.1039/c5ta05751e.
- 22 [25] H.M. Hegab, A. ElMekawy, T.G. Barclay, A. Michelmore, L. Zou, C.P. Saint, M. Ginic-

- 1 Markovic, Fine-Tuning the Surface of Forward Osmosis Membranes via Grafting
2 Graphene Oxide: Performance Patterns and Biofouling Propensity, *ACS Appl. Mater.*
3 *Interfaces.* 7 (2015) 18004–18016. doi:10.1021/acsami.5b04818.
- 4 [26] M.D. Firouzjaei, A.A. Shamsabadi, S.A. Aktij, S.F. Seyedpour, M. Sharifian, A.
5 Rahimpour, M.R. Esfahani, M. Ulbricht, M. Soroush, Exploiting Synergetic Effects of
6 Graphene Oxide and a Silver-Based Metal-Organic Framework to Enhance Antifouling
7 and Anti-Biofouling Properties of Thin-Film Nanocomposite Membranes, *ACS Appl.*
8 *Mater. Interfaces.* 10 (2018) 42967–42978. doi:10.1021/acsami.8b12714.
- 9 [27] S.B. Darling, Perspective: Interfacial materials at the interface of energy and water, *J.*
10 *Appl. Phys.* 124 (2018) 30901. doi:10.1063/1.5040110.
- 11 [28] S.F. Seyedpour, A. Rahimpour, G. Najafpour, Facile in-situ assembly of silver-based
12 MOFs to surface functionalization of TFC membrane: A novel approach toward long-
13 lasting biofouling mitigation, *J. Memb. Sci.* 573 (2019) 257–269.
14 doi:10.1016/j.memsci.2018.12.016.
- 15 [29] M. Rai, A. Yadav, A. Gade, Silver nanoparticles as a new generation of antimicrobials,
16 *Biotechnol. Adv.* 27 (2009) 76–83. doi:10.1016/j.biotechadv.2008.09.002.
- 17 [30] D. Roy, T.E. Furtak, Evidence for Ag cluster vibrations in enhanced Raman scattering
18 from the Ag/electrolyte interface, *Chem. Phys. Lett.* 124 (1986) 299–303.
19 doi:10.1016/0009-2614(86)85021-7.
- 20 [31] M. Ben-Sasson, X. Lu, E. Bar-Zeev, K.R. Zodrow, S. Nejati, G. Qi, E.P. Giannelis, M.
21 Elimelech, In situ formation of silver nanoparticles on thin-film composite reverse
22 osmosis membranes for biofouling mitigation, *Water Res.* 62 (2014) 260–270.

- 1 doi:10.1016/J.WATRES.2014.05.049.
- 2 [32] P. Babaniamansour, M. Ebrahimian-Hosseiniabadi, A. Zargar-Kharazi, Designing an
3 Optimized Novel Femoral Stem, *J. Med. Signals Sens.* 7 (2017) 170–177.
4 doi:10.4103/jmss.JMSS_1_17.
- 5 [33] D.J. Miller, P.A. Araújo, P.B. Correia, M.M. Ramsey, J.C. Kruithof, M.C.M. van
6 Loosdrecht, B.D. Freeman, D.R. Paul, M. Whiteley, J.S. Vrouwenvelder, Short-term
7 adhesion and long-term biofouling testing of polydopamine and poly(ethylene glycol)
8 surface modifications of membranes and feed spacers for biofouling control, *Water Res.*
9 46 (2012) 3737–3753. doi:10.1016/j.watres.2012.03.058.
- 10 [34] C.S. Ong, P.S. Goh, W.J. Lau, N. Misdan, A.F. Ismail, Nanomaterials for biofouling and
11 scaling mitigation of thin film composite membrane: A review, *Desalination.* 393 (2016)
12 2–15. doi:10.1016/j.desal.2016.01.007.
- 13 [35] S. Kitagawa, R. Kitaura, S.I. Noro, Functional porous coordination polymers, *Angew.*
14 *Chemie - Int. Ed.* 43 (2004) 2334–2375. doi:10.1002/anie.200300610.
- 15 [36] N. Yin, K. Wang, L. Wang, Z. Li, Amino-functionalized MOFs combining ceramic
16 membrane ultrafiltration for Pb (II) removal, *Chem. Eng. J.* 306 (2016) 619–628.
17 doi:10.1016/J.CEJ.2016.07.064.
- 18 [37] J. Quirós, K. Boltes, S. Aguado, R.G. de Villoria, J.J. Vilatela, R. Rosal, Antimicrobial
19 metal–organic frameworks incorporated into electrospun fibers, *Chem. Eng. J.* 262 (2015)
20 189–197. doi:10.1016/J.CEJ.2014.09.104.
- 21 [38] X. Lu, J. Ye, D. Zhang, R. Xie, R.F. Bogale, Y. Sun, L. Zhao, Q. Zhao, G. Ning, Silver
22 carboxylate metal–organic frameworks with highly antibacterial activity and

- 1 biocompatibility, *J. Inorg. Biochem.* 138 (2014) 114–121.
2 doi:10.1016/J.JINORGBIO.2014.05.005.
- 3 [39] K. Martín-Betancor, S. Aguado, I. Rodea-Palomares, M. Tamayo-Belda, F. Leganés, R.
4 Rosal, F. Fernández-Piñas, Co, Zn and Ag-MOFs evaluation as biocidal materials towards
5 photosynthetic organisms, *Sci. Total Environ.* 595 (2017) 547–555.
6 doi:10.1016/j.scitotenv.2017.03.250.
- 7 [40] M. Berchel, T. Le Gall, C. Denis, S. Le Hir, F. Quentel, C. Elléouet, T. Montier, J.-M.
8 Rueff, J.-Y. Salaün, J.-P. Haelters, G.B. Hix, P. Lehn, P.-A. Jaffrès, A silver-based metal–
9 organic framework material as a ‘reservoir’ of bactericidal metal ions, *New J. Chem.* 35
10 (2011) 1000. doi:10.1039/c1nj20202b.
- 11 [41] M. Pejman, M. Dadashi Firouzjaei, S. Aghapour Aktij, P. Das, E. Zolghadr, H. Jafarian,
12 A. Arabi Shamsabadi, M. Elliott, M. Sadrzadeh, M. Sangermano, A. Rahimpour, A.
13 Tiraferri, In Situ Ag-MOF Growth on Pre-Grafted Zwitterions Imparts Outstanding
14 Antifouling Properties to Forward Osmosis Membranes, *ACS Appl. Mater. Interfaces.* 12
15 (2020) 36287–36300. doi:10.1021/acsami.0c12141.
- 16 [42] M. Pejman, M.D. Firouzjaei, S.A. Aktij, P. Das, E. Zolghadr, H. Jafarian, A.A.
17 Shamsabadi, M. Elliott, M.R. Esfahani, M. Sangermano, M. Sadrzadeh, E.K. Wujcik, A.
18 Rahimpour, A. Tiraferri, Improved antifouling and antibacterial properties of forward
19 osmosis membranes through surface modification with zwitterions and silver-based metal
20 organic frameworks, *J. Memb. Sci.* 611 (2020). doi:10.1016/j.memsci.2020.118352.
- 21 [43] G. Wyszogrodzka, B. Marszałek, B. Gil, P. Doroczyński, Metal-organic frameworks:
22 Mechanisms of antibacterial action and potential applications, *Drug Discov. Today.* 21

- 1 (2016) 1009–1018. doi:10.1016/j.drudis.2016.04.009.
- 2 [44] M.D. Firouzjaei, A.A. Shamsabadi, M. Sharifian Gh., A. Rahimpour, M. Soroush, A
3 Novel Nanocomposite with Superior Antibacterial Activity: A Silver-Based Metal
4 Organic Framework Embellished with Graphene Oxide, *Adv. Mater. Interfaces*. 5 (2018)
5 1701365. doi:10.1002/admi.201701365.
- 6 [45] W. Chen, N. Dai, Z. Wang, H. Liu, Q. Yao, Topology-optimized design of microporous
7 filling prosthesis, in: *ACM Int. Conf. Proceeding Ser.*, 2018: pp. 148–153.
8 doi:10.1145/3278198.3278203.
- 9 [46] M. Yi, C.H. Lau, S. Xiong, W. Wei, R. Liao, L. Shen, A. Lu, Y. Wang, Zwitterion-Ag
10 Complexes That Simultaneously Enhance Biofouling Resistance and Silver Binding
11 Capability of Thin Film Composite Membranes, *ACS Appl. Mater. Interfaces*. 11 (2019)
12 15698–15708. doi:10.1021/acsami.9b02983.
- 13 [47] C. Liu, A.F. Faria, J. Ma, M. Elimelech, Mitigation of Biofilm Development on Thin-Film
14 Composite Membranes Functionalized with Zwitterionic Polymers and Silver
15 Nanoparticles, *Environ. Sci. Technol.* 51 (2017) 182–191. doi:10.1021/acs.est.6b03795.
- 16 [48] P. Kaner, E. Rubakh, D.H. Kim, A. Asatekin, Zwitterion-containing polymer additives for
17 fouling resistant ultrafiltration membranes, *J. Memb. Sci.* 533 (2017) 141–159.
18 doi:10.1016/j.memsci.2017.03.034.
- 19 [49] J.F. Jhong, A. Venault, C.C. Hou, S.H. Chen, T.C. Wei, J. Zheng, J. Huang, Y. Chang,
20 Surface zwitterionization of expanded poly(tetrafluoroethylene) membranes via
21 atmospheric plasma-induced polymerization for enhanced skin wound healing, *ACS Appl.*
22 *Mater. Interfaces*. 5 (2013) 6732–6742. doi:10.1021/am401669q.

- 1 [50] Q. Li, Q.Y. Bi, B. Zhou, X.L. Wang, Zwitterionic sulfobetaine-grafted poly(vinylidene
2 fluoride) membrane surface with stably anti-protein-fouling performance via a two-step
3 surface polymerization, *Appl. Surf. Sci.* 258 (2012) 4707–4717.
4 doi:10.1016/j.apsusc.2012.01.064.
- 5 [51] Q. Li, B. Zhou, Q.Y. Bi, X.L. Wang, Surface modification of PVDF membranes with
6 sulfobetaine polymers for a stably anti-protein-fouling performance, *J. Appl. Polym. Sci.*
7 125 (2012) 4015–4027. doi:10.1002/app.36715.
- 8 [52] S. Minko, Grafting on solid surfaces: Grafting to and grafting from methods, in: *Polym.*
9 *Surfaces Interfaces Charact. Modif. Appl.*, Springer Berlin Heidelberg, 2008: pp. 215–
10 234. doi:10.1007/978-3-540-73865-7_11.
- 11 [53] I. Roppolo, A. Chiappone, K. Bejtka, E. Celasco, A. Chiodoni, F. Giorgis, M.
12 Sangermano, S. Porro, A powerful tool for graphene functionalization: Benzophenone
13 mediated UV-grafting, *Carbon N. Y.* 77 (2014) 226–235.
14 doi:10.1016/j.carbon.2014.05.025.
- 15 [54] H. Ma, R.H. Davis, C.N. Bowman, Novel sequential photoinduced living graft
16 polymerization, *Macromolecules.* 33 (2000) 331–335. doi:10.1021/ma990821s.
- 17 [55] M.B.M.Y. Ang, S.H. Huang, M.W. Chang, C.L. Lai, H.A. Tsai, W.S. Hung, C.C. Hu,
18 K.R. Lee, Ultraviolet-initiated graft polymerization of acrylic acid onto thin-film
19 polyamide surface for improved ethanol dehydration performance of pervaporation
20 membranes, *Sep. Purif. Technol.* 235 (2020) 116155. doi:10.1016/j.seppur.2019.116155.
- 21 [56] V. Vatanpour, M. Esmacili, M. Safarpour, A. Ghadimi, J. Adabi, Synergistic effect of
22 carboxylated-MWCNTs on the performance of acrylic acid UV-grafted polyamide

- 1 nanofiltration membranes, *React. Funct. Polym.* 134 (2019) 74–84.
2 doi:10.1016/j.reactfunctpolym.2018.11.010.
- 3 [57] Y. Yi, H. Tu, X. Zhou, R. Liu, Y. Wu, D. Li, Q. Wang, X. Shi, H. Deng, Acrylic acid-
4 grafted pre-plasma nanofibers for efficient removal of oil pollution from aquatic
5 environment, *J. Hazard. Mater.* 371 (2019) 165–174. doi:10.1016/j.jhazmat.2019.02.085.
- 6 [58] F. Israr, D. Chun, Y. Kim, D.K. Kim, High yield synthesis of Ni-BTC metal–organic
7 framework with ultrasonic irradiation: Role of polar aprotic DMF solvent, *Ultrason.*
8 *Sonochem.* 31 (2016) 93–101. doi:10.1016/J.ULTSONCH.2015.12.007.
- 9 [59] A. Zirehpour, A. Rahimpour, A. Arabi Shamsabadi, M. Sharifian Gh., M. Soroush,
10 Mitigation of Thin-Film Composite Membrane Biofouling via Immobilizing Nano-Sized
11 Biocidal Reservoirs in the Membrane Active Layer, *Environ. Sci. Technol.* 51 (2017)
12 5511–5522. doi:10.1021/acs.est.7b00782.
- 13 [60] R. Hu, G. Li, Y. Jiang, Y. Zhang, J.J. Zou, L. Wang, X. Zhang, Silver-zwitterion organic-
14 inorganic nanocomposite with antimicrobial and antiadhesive capabilities, *Langmuir.* 29
15 (2013) 3773–3779. doi:10.1021/la304708b.
- 16 [61] J. Zhao, Y. Zhang, Y. Su, J. Liu, X. Zhao, J. Peng, Z. Jiang, Cross-linked bovine serum
17 albumin composite membranes prepared by interfacial polymerization with stimuli-
18 response properties, *J. Memb. Sci.* 445 (2013) 1–7. doi:10.1016/j.memsci.2013.05.050.
- 19 [62] Z. Liu, Y. Hu, Sustainable Antibiofouling Properties of Thin Film Composite Forward
20 Osmosis Membrane with Rechargeable Silver Nanoparticles Loading, *ACS Appl. Mater.*
21 *Interfaces.* 8 (2016) 21666–21673. doi:10.1021/acsami.6b06727.
- 22 [63] M. Pejman, M. Dadashi Firouzjaei, S. Aghapour Aktij, E. Zolghadr, P. Das, M. Elliott, M.

- 1 Sadrzadeh, M. Sangermano, A. Rahimpour, A. Tiraferri, Effective strategy for UV-
2 mediated grafting of biocidal Ag-MOFs on polymeric membranes aimed at enhanced
3 water ultrafiltration, *Chem. Eng. J.* 426 (2021) 130704. doi:10.1016/j.cej.2021.130704.
- 4 [64] N.A.A. Sani, W.J. Lau, A.F. Ismail, Morphologies and separation characteristics of
5 polyphenylsulfone-based solvent resistant nanofiltration membranes: Effect of polymer
6 concentration in casting solution and membrane pretreatment condition, *Korean J. Chem.*
7 *Eng.* 32 (2015) 743–752. doi:10.1007/s11814-014-0281-2.
- 8 [65] Z. Yang, Y. Dai, S. Wang, H. Cheng, J. Yu, In situ incorporation of a S, N doped
9 carbon/sulfur composite for lithium sulfur batteries, *RSC Adv.* 5 (2015) 78017–78025.
10 doi:10.1039/c5ra15360c.
- 11 [66] A. Tiraferri, N.Y. Yip, A.P. Straub, S. Romero-Vargas Castrillon, M. Elimelech, A
12 method for the simultaneous determination of transport and structural parameters of
13 forward osmosis membranes, *J. Memb. Sci.* 444 (2013) 523–538.
14 doi:10.1016/J.MEMSCI.2013.05.023.
- 15 [67] M. Herzberg, S. Kang, M. Elimelech, Role of extracellular polymeric substances (EPS) in
16 biofouling of reverse osmosis membranes, *Environ. Sci. Technol.* 43 (2009) 4393–4398.
17 doi:10.1021/es900087j.
- 18 [68] Y. Pan, L. Ma, S. Lin, Y. Zhang, B. Cheng, J. Meng, One-step bimodel grafting: Via a
19 multicomponent reaction toward antifouling and antibacterial TFC RO membranes, *J.*
20 *Mater. Chem. A.* 4 (2016) 15945–15960. doi:10.1039/c6ta05746b.
- 21 [69] H.Y. Yu, Y. Kang, Y. Liu, B. Mi, Grafting polyzwitterions onto polyamide by click
22 chemistry and nucleophilic substitution on nitrogen: A novel approach to enhance

- 1 membrane fouling resistance, *J. Memb. Sci.* 449 (2014) 50–57.
2 doi:10.1016/j.memsci.2013.08.022.
- 3 [70] C. Boo, M. Elimelech, S. Hong, Fouling control in a forward osmosis process integrating
4 seawater desalination and wastewater reclamation, *J. Memb. Sci.* 444 (2013) 148–156.
5 doi:10.1016/J.MEMSCI.2013.05.004.
- 6 [71] L.D. Nghiem, S. Hawkes, Effects of membrane fouling on the nanofiltration of trace
7 organic contaminants, *Desalination.* 236 (2009) 273–281.
8 doi:10.1016/J.DESAL.2007.10.077.
- 9 [72] Q. Chen, P. Yu, W. Huang, S. Yu, M. Liu, C. Gao, High-flux composite hollow fiber
10 nanofiltration membranes fabricated through layer-by-layer deposition of oppositely
11 charged crosslinked polyelectrolytes for dye removal, *J. Memb. Sci.* 492 (2015) 312–321.
12 doi:10.1016/J.MEMSCI.2015.05.068.
- 13 [73] K. Gao, Y. Su, L. Zhou, M. He, R. Zhang, Y. Liu, Z. Jiang, Creation of active-passive
14 integrated mechanisms on membrane surfaces for superior antifouling and antibacterial
15 properties, *J. Memb. Sci.* 548 (2018) 621–631. doi:10.1016/j.memsci.2017.10.042.
- 16 [74] F. Gholami, S. Zinadini, A.A. Zinatizadeh, A.R. Abbasi, TMU-5 metal-organic
17 frameworks (MOFs) as a novel nanofiller for flux increment and fouling mitigation in
18 PES ultrafiltration membrane, *Sep. Purif. Technol.* 194 (2018) 272–280.
19 doi:10.1016/j.seppur.2017.11.054.
- 20 [75] M.D. Firouzjaei, A.A. Shamsabadi, S.A. Aktij, S.F. Seyedpour, M. Sharifian Gh., A.
21 Rahimpour, M.R. Esfahani, M. Ulbricht, M. Soroush, Exploiting Synergetic Effects of
22 Graphene Oxide and a Silver-Based Metal–Organic Framework To Enhance Antifouling

- 1 and Anti-Biofouling Properties of Thin-Film Nanocomposite Membranes, *ACS Appl.*
2 *Mater. Interfaces.* 10 (2018) 42967–42978. doi:10.1021/acsami.8b12714.
- 3 [76] C.Y. Tang, Y.N. Kwon, J.O. Leckie, Effect of membrane chemistry and coating layer on
4 physiochemical properties of thin film composite polyamide RO and NF membranes. I.
5 FTIR and XPS characterization of polyamide and coating layer chemistry, *Desalination.*
6 242 (2009) 149–167. doi:10.1016/j.desal.2008.04.003.
- 7 [77] A. Soroush, W. Ma, Y. Silvino, M.S. Rahaman, Surface modification of thin film
8 composite forward osmosis membrane by silver-decorated graphene-oxide nanosheets,
9 *Environ. Sci. Nano.* 2 (2015) 395–405. doi:10.1039/c5en00086f.
- 10 [78] G. O’Toole, H.B. Kaplan, R. Kolter, Biofilm Formation as Microbial Development, *Annu.*
11 *Rev. Microbiol.* 54 (2000) 49–79. doi:10.1146/annurev.micro.54.1.49.
- 12 [79] The Handbook of Infrared and Raman Characteristic Frequencies of Organic ... - Daimay
13 Lin-Vien, Norman B. Colthup, William G. Fateley, Jeanette G. Grasselli - Google Books,
14 (n.d.).
15 [https://books.google.it/books?hl=en&lr=&id=bYWNSi6abvwc&oi=fnd&pg=PP1&dq=Lin-](https://books.google.it/books?hl=en&lr=&id=bYWNSi6abvwc&oi=fnd&pg=PP1&dq=Lin-Vien,+D.,+et+al.,+The+handbook+of+infrared+and+Raman+characteristic+frequencies+of+organic+molecules.+1991:+Elsevier.&ots=yobt0Mv_i2&sig=AlnUqNz-oRgUUyQIyryi3Ke347A&redir_esc=y#v=onepage&q=Lin-Vien%2C D.%2C et al.%2C The handbook of infrared and Raman characteristic frequencies of organic molecules. 1991%3A Elsevier.&f=false)
16 [n-](https://books.google.it/books?hl=en&lr=&id=bYWNSi6abvwc&oi=fnd&pg=PP1&dq=Lin-Vien,+D.,+et+al.,+The+handbook+of+infrared+and+Raman+characteristic+frequencies+of+organic+molecules.+1991:+Elsevier.&ots=yobt0Mv_i2&sig=AlnUqNz-oRgUUyQIyryi3Ke347A&redir_esc=y#v=onepage&q=Lin-Vien%2C D.%2C et al.%2C The handbook of infrared and Raman characteristic frequencies of organic molecules. 1991%3A Elsevier.&f=false)
17 [Vien,+D.,+et+al.,+The+handbook+of+infrared+and+Raman+characteristic+frequencies+](https://books.google.it/books?hl=en&lr=&id=bYWNSi6abvwc&oi=fnd&pg=PP1&dq=Lin-Vien,+D.,+et+al.,+The+handbook+of+infrared+and+Raman+characteristic+frequencies+of+organic+molecules.+1991:+Elsevier.&ots=yobt0Mv_i2&sig=AlnUqNz-oRgUUyQIyryi3Ke347A&redir_esc=y#v=onepage&q=Lin-Vien%2C D.%2C et al.%2C The handbook of infrared and Raman characteristic frequencies of organic molecules. 1991%3A Elsevier.&f=false)
18 [of+organic+molecules.+1991:+Elsevier.&ots=yobt0Mv_i2&sig=AlnUqNz-](https://books.google.it/books?hl=en&lr=&id=bYWNSi6abvwc&oi=fnd&pg=PP1&dq=Lin-Vien,+D.,+et+al.,+The+handbook+of+infrared+and+Raman+characteristic+frequencies+of+organic+molecules.+1991:+Elsevier.&ots=yobt0Mv_i2&sig=AlnUqNz-oRgUUyQIyryi3Ke347A&redir_esc=y#v=onepage&q=Lin-Vien%2C D.%2C et al.%2C The handbook of infrared and Raman characteristic frequencies of organic molecules. 1991%3A Elsevier.&f=false)
19 [oRgUUyQIyryi3Ke347A&redir_esc=y#v=onepage&q=Lin-Vien%2C D.%2C et al.%2C](https://books.google.it/books?hl=en&lr=&id=bYWNSi6abvwc&oi=fnd&pg=PP1&dq=Lin-Vien,+D.,+et+al.,+The+handbook+of+infrared+and+Raman+characteristic+frequencies+of+organic+molecules.+1991:+Elsevier.&ots=yobt0Mv_i2&sig=AlnUqNz-oRgUUyQIyryi3Ke347A&redir_esc=y#v=onepage&q=Lin-Vien%2C D.%2C et al.%2C The handbook of infrared and Raman characteristic frequencies of organic molecules. 1991%3A Elsevier.&f=false)
20 [The handbook of infrared and Raman characteristic frequencies of organic molecules.](https://books.google.it/books?hl=en&lr=&id=bYWNSi6abvwc&oi=fnd&pg=PP1&dq=Lin-Vien,+D.,+et+al.,+The+handbook+of+infrared+and+Raman+characteristic+frequencies+of+organic+molecules.+1991:+Elsevier.&ots=yobt0Mv_i2&sig=AlnUqNz-oRgUUyQIyryi3Ke347A&redir_esc=y#v=onepage&q=Lin-Vien%2C D.%2C et al.%2C The handbook of infrared and Raman characteristic frequencies of organic molecules. 1991%3A Elsevier.&f=false)
21 [1991%3A Elsevier.&f=false](https://books.google.it/books?hl=en&lr=&id=bYWNSi6abvwc&oi=fnd&pg=PP1&dq=Lin-Vien,+D.,+et+al.,+The+handbook+of+infrared+and+Raman+characteristic+frequencies+of+organic+molecules.+1991:+Elsevier.&ots=yobt0Mv_i2&sig=AlnUqNz-oRgUUyQIyryi3Ke347A&redir_esc=y#v=onepage&q=Lin-Vien%2C D.%2C et al.%2C The handbook of infrared and Raman characteristic frequencies of organic molecules. 1991%3A Elsevier.&f=false) (accessed October 25, 2019).
- 22 [80] Y. Fan, C.J. Cornelius, Raman spectroscopic and gas transport study of a pentablock

- 1 ionomer complexed with metal ions and its relationship to physical properties, *J. Mater.*
2 *Sci.* 48 (2013) 1153–1161. doi:10.1007/s10853-012-6853-9.
- 3 [81] A. Kaldor, A.G. Maki, A.J. Dorney, I.M. Mills, The assignment of ν_2 and ν_4 of SO_3 , *J.*
4 *Mol. Spectrosc.* 45 (1973) 247–252. doi:10.1016/0022-2852(73)90155-0.
- 5 [82] N. Sundaraganesan, S. Ilakiamani, H. Saleem, P.M. Wojciechowski, D. Michalska, FT-
6 Raman and FT-IR spectra, vibrational assignments and density functional studies of 5-
7 bromo-2-nitropyridine, *Spectrochim. Acta - Part A Mol. Biomol. Spectrosc.* 61 (2005)
8 2995–3001. doi:10.1016/j.saa.2004.11.016.
- 9 [83] M. Chisanga, H. Muhamadali, D.I. Ellis, R. Goodacre, Surface-Enhanced Raman
10 Scattering (SERS) in Microbiology: Illumination and Enhancement of the Microbial
11 World, *Appl. Spectrosc.* 72 (2018) 987–1000. doi:10.1177/0003702818764672.
- 12 [84] K. Singh, S. Devi, H.C. Bajaj, P. Ingole, J. Choudhari, H. Bhrambhatt, Optical Resolution
13 of Racemic Mixtures of Amino Acids through Nanofiltration Membrane Process, *Sep. Sci.*
14 *Technol.* 49 (2014) 2630–2641. doi:10.1080/01496395.2014.911023.
- 15 [85] S. Rafiq, Z. Man, S. Maitra, A. Maulud, F. Ahmad, N. Muhammad, Preparation of
16 asymmetric polysulfone/polyimide blended membranes for CO_2 separation, *Korean J.*
17 *Chem. Eng.* 2011 2810. 28 (2011) 2050–2056. doi:10.1007/S11814-011-0053-1.
- 18 [86] R. Liu, Z. Xian, S. Zhang, C. Chen, Z. Yang, H. Li, W. Zheng, G. Zhang, H. Cao,
19 Electrochemical-reduction-assisted assembly of ternary Ag
20 nanoparticles/polyoxometalate/graphene nanohybrids and their activity in the
21 electrocatalysis of oxygen reduction, *RSC Adv.* 5 (2015) 74447–74456.
22 doi:10.1039/c5ra12556a.

- 1 [87] J.A. Melero, R. van Grieken, G. Morales, M. Paniagua, Acidic mesoporous silica for the
2 acetylation of glycerol: Synthesis of bioadditives to petrol fuel, *Energy and Fuels*. 21
3 (2007) 1782–1791. doi:10.1021/ef060647q.
- 4 [88] S. Kitagawa, R. Kitaura, S. Noro, Functional Porous Coordination Polymers, *Angew.*
5 *Chemie Int. Ed.* 43 (2004) 2334–2375. doi:10.1002/anie.200300610.
- 6 [89] V. Kochkodan, N. Hilal, A comprehensive review on surface modified polymer
7 membranes for biofouling mitigation, *Desalination*. 356 (2015) 187–207.
8 doi:10.1016/j.desal.2014.09.015.
- 9 [90] X. Gu, S. Bi, L. Guo, Y. Zhao, T. Li, M. Liu, P. Chen, Y. Wu, Facile Fabrication of
10 Ordered Component-Tunable Heterobimetallic Self-Assembly Nanosheet for Catalyzing
11 “click” Reaction, *ACS Omega*. 2 (2017) 5415–5433. doi:10.1021/acsomega.7b00364.
- 12 [91] J. Li, Y. Xie, Y. Zhong, Y. Hu, Facile synthesis of Z-scheme Ag₂CO₃/Ag/AgBr ternary
13 heterostructured nanorods with improved photostability and photoactivity, *J. Mater.*
14 *Chem. A*. 3 (2015) 5474–5481. doi:10.1039/c4ta06075j.
- 15 [92] K. Fatyeyeva, J. Bigarré, B. Blondel, H. Galiano, D. Gaud, M. Lecardeur, F. Poncin-
16 Epailard, Grafting of p-styrene sulfonate and 1,3-propane sultone onto Laponite for
17 proton exchange membrane fuel cell application, *J. Memb. Sci.* 366 (2011) 33–42.
18 doi:10.1016/j.memsci.2010.09.023.
- 19 [93] W. Song, B. Hong, S. Hong, Y. Lai, J. Li, Y. Liu, Effect of prop-1-ene-1,3-sultone on the
20 performances of lithium cobalt oxide/graphite battery operating over a wide temperature
21 range, *Int. J. Electrochem. Sci.* 12 (2017) 10749–10762. doi:10.20964/2017.11.84.
- 22 [94] W. Yao, Z. Zhang, J. Gao, J. Li, J. Xu, Z. Wang, Y. Yang, Vinyl ethylene sulfite as a new

- 1 additive in propylene carbonate-based electrolyte for lithium ion batteries, *Energy*
2 *Environ. Sci.* 2 (2009) 1102–1108. doi:10.1039/b905162g.
- 3 [95] J. Zhao, Y. Zhang, Y. Su, J. Liu, X. Zhao, J. Peng, Z. Jiang, Cross-linked bovine serum
4 albumin composite membranes prepared by interfacial polymerization with stimuli-
5 response properties, *J. Memb. Sci.* 445 (2013) 1–7. doi:10.1016/j.memsci.2013.05.050.
- 6 [96] J. Ye, F. He, J. Nie, Y. Cao, H. Yang, X. Ai, Sulfur/carbon nanocomposite-filled
7 polyacrylonitrile nanofibers as a long life and high capacity cathode for lithium-sulfur
8 batteries, *J. Mater. Chem. A* 3 (2015) 7406–7412. doi:10.1039/c4ta06976e.
- 9 [97] A. Abdul Razzaq, Y. Yao, R. Shah, P. Qi, L. Miao, M. Chen, X. Zhao, Y. Peng, Z. Deng,
10 High-performance lithium sulfur batteries enabled by a synergy between sulfur and carbon
11 nanotubes, *Energy Storage Mater.* 16 (2019) 194–202. doi:10.1016/j.ensm.2018.05.006.
- 12 [98] M. Pejman, M. Dadashi Firouzjaei, S. Aghapour Aktij, P. Das, E. Zolghadr, H. Jafarian,
13 A. Arabi Shamsabadi, M. Elliott, M. Sadrzadeh, M. Sangermano, A. Rahimpour, A.
14 Tiraferri, In Situ Ag-MOF Growth on Pre-Grafted Zwitterions Imparts Outstanding
15 Antifouling Properties to Forward Osmosis Membranes, *ACS Appl. Mater. Interfaces*. 12
16 (2020) 36287–36300. doi:10.1021/acsami.0c12141.
- 17 [99] G. Xue, Q. Dai, S. Jiang, Chemical Reactions of Imidazole with Metallic Silver Studied
18 by the Use of SERS and XPS Techniques, *J. Am. Chem. Soc.* 110 (1988) 2393–2395.
19 doi:10.1021/ja00216a009.
- 20 [100] B.J. Matsoso, K. Ranganathan, B.K. Mutuma, T. Lerotholi, G. Jones, N.J. Coville,
21 Synthesis and characterization of boron carbon oxynitride films with tunable composition
22 using methane, boric acid and ammonia, *New J. Chem.* 41 (2017) 9497–9504.

- 1 doi:10.1039/c7nj01886j.
- 2 [101] J. Yang, H. Bai, X. Tan, J. Lian, IR and XPS investigation of visible-light photocatalysis-
3 Nitrogen-carbon-doped TiO₂ film, *Appl. Surf. Sci.* 253 (2006) 1988–1994.
4 doi:10.1016/j.apsusc.2006.03.078.
- 5 [102] I. Kusunoki, M. Sakai, Y. Igari, S. Ishidzuka, T. Takami, T. Takaoka, M. Nishitani-Gamo,
6 T. Ando, XPS study of nitridation of diamond and graphite with a nitrogen ion beam,
7 *Surf. Sci.* 492 (2001) 315–328. doi:10.1016/S0039-6028(01)01430-3.
- 8 [103] A. Zirehpour, A. Rahimpour, M. Ulbricht, Nano-sized metal organic framework to
9 improve the structural properties and desalination performance of thin film composite
10 forward osmosis membrane, *J. Memb. Sci.* 531 (2017) 59–67.
11 doi:10.1016/j.memsci.2017.02.049.
- 12 [104] M.K. Sinha, M.K. Purkait, Preparation and characterization of novel pegylated
13 hydrophilic pH responsive polysulfone ultrafiltration membrane, *J. Memb. Sci.* 464 (2014)
14 20–32. doi:10.1016/J.MEMSCI.2014.03.067.
- 15 [105] B. Saini, S. Khuntia, M.K. Sinha, Incorporation of cross-linked poly(AA-co-ACMO)
16 copolymer with pH responsive and hydrophilic properties to polysulfone ultrafiltration
17 membrane for the mitigation of fouling behaviour, *J. Memb. Sci.* 572 (2019) 184–197.
18 doi:10.1016/J.MEMSCI.2018.11.017.
- 19 [106] X. Lu, S. Romero-Vargas, C. Castrillón, D.L. Shaffer, J. Ma, M. Elimelech, In Situ
20 Surface Chemical Modification of Thin-Film Composite Forward Osmosis Membranes
21 for Enhanced Organic Fouling Resistance, *Environ. Sci. Technol.* 47 (2013) 12219–
22 12228. doi:10.1021/es403179m.

- 1 [107] B. Mi, M. Elimelech, Organic fouling of forward osmosis membranes: Fouling
2 reversibility and cleaning without chemical reagents, *J. Memb. Sci.* 348 (2010) 337–345.
3 doi:10.1016/J.MEMSCI.2009.11.021.
- 4 [108] E.M. Vrijenhoek, S. Hong, M. Elimelech, Influence of membrane surface properties on
5 initial rate of colloidal fouling of reverse osmosis and nanofiltration membranes, *J. Memb.*
6 *Sci.* 188 (2001) 115–128. doi:10.1016/S0376-7388(01)00376-3.
- 7 [109] M.F. Ismail, B. Khorshidi, M. Sadrzadeh, New insights into the impact of nanoscale
8 surface heterogeneity on the wettability of polymeric membranes, *J. Memb. Sci.* 590
9 (2019) 117270. doi:10.1016/j.memsci.2019.117270.
- 10 [110] M. Drahansky, M.. Paridah, A. Moradbak, A.. Mohamed, F. abdulwahab taiwo Owolabi,
11 M. Asniza, S.H.. Abdul Khalid, Re-derivation of Young’s Equation, Wenzel Equation,
12 and Cassie-Baxter Equation Based on Energy Minimization Kwangseok, *Intech. i* (2016)
13 13. doi:http://dx.doi.org/10.5772/57353.
- 14 [111] B. Deng, M. Yu, X. Yang, B. Zhang, L. Li, L. Xie, J. Li, X. Lu, Antifouling
15 microfiltration membranes prepared from acrylic acid or methacrylic acid grafted
16 poly(vinylidene fluoride) powder synthesized via pre-irradiation induced graft
17 polymerization, *J. Memb. Sci.* 350 (2010) 252–258. doi:10.1016/j.memsci.2009.12.035.
- 18 [112] L. Shen, Y. Zhang, W. Yu, R. Li, M. Wang, Q. Gao, J. Li, H. Lin, Fabrication of
19 hydrophilic and antibacterial poly(vinylidene fluoride) based separation membranes by a
20 novel strategy combining radiation grafting of poly(acrylic acid) (PAA) and electroless
21 nickel plating, *J. Colloid Interface Sci.* 543 (2019) 64–75. doi:10.1016/j.jcis.2019.02.013.
- 22 [113] A. Tiraferri, C.D. Vecitis, M. Elimelech, Covalent Binding of Single-Walled Carbon

- 1 Nanotubes to Polyamide Membranes for Antimicrobial Surface Properties, ACS Appl.
2 Mater. Interfaces. 3 (2011) 2869–2877. doi:10.1021/am200536p.
- 3 [114] M. Dadashi Firouzjaei, F. Akbari Afkhami, M. Rabbani Esfahani, C.H. Turner, S. Nejati,
4 Experimental and molecular dynamics study on dye removal from water by a graphene
5 oxide-copper-metal organic framework nanocomposite, J. Water Process Eng. 34 (2020)
6 101180. doi:10.1016/j.jwpe.2020.101180.
- 7 [115] S.R. Munishwar, P.P. Pawar, S. Ughade, R.S. Gedam, Size dependent effect of electron-
8 hole recombination of CdS quantum dots on emission of Dy³⁺ ions in boro-silicate
9 glasses through energy transfer, J. Alloys Compd. 725 (2017) 115–122.
10 doi:10.1016/j.jallcom.2017.07.146.
- 11 [116] F. Xiang, B. Li, Y. Li, J. Zhou, W. Gan, Preparation of silver-coated glass frit and its
12 application in silicon solar cells, Chinese Phys. B. 25 (2016) 078110. doi:10.1088/1674-
13 1056/25/7/078110.
- 14 [117] S.F. Seyedpour, A. Arabi Shamsabadi, S. Khoshhal Salestan, M. Dadashi Firouzjaei, M.
15 Sharifian Gh, A. Rahimpour, F. Akbari Afkhami, M.R. Shirzad Kebria, M.A. Elliott, A.
16 Tiraferri, M. Sangermano, M.R. Esfahani, M. Soroush, Tailoring the Biocidal Activity of
17 Novel Silver-Based Metal Azolate Frameworks, ACS Sustain. Chem. Eng. (2020).
18 doi:10.1021/acssuschemeng.0c00201.
- 19 [118] Z. Xiu, Q. Zhang, H.L. Puppala, V.L. Colvin, P.J.J. Alvarez, Negligible Particle-Specific
20 Antibacterial Activity of Silver Nanoparticles, Nano Lett. 12 (2012) 4271–4275.
21 doi:10.1021/NL301934W.
- 22 [119] N. Rani, A. Sharma, R. Singh, Imidazoles as Promising Scaffolds for Antibacterial

- 1 Activity: A Review, Mini-Reviews Med. Chem. 13 (2013) 1812–1835.
2 doi:10.2174/13895575113136660091.
- 3 [120] W. Zhai, M. Wang, J. Song, L. Zhang, X.M. Li, T. He, Fouling resistance of 3-[[3-
4 (trimethoxysilane)-propyl] amino] propane-1-sulfonic acid zwitterion modified poly
5 (vinylidene fluoride) membranes, Sep. Purif. Technol. 239 (2020) 116589.
6 doi:10.1016/j.seppur.2020.116589.
- 7 [121] J. Zhu, J. Hou, Y. Zhang, M. Tian, T. He, J. Liu, V. Chen, Polymeric antimicrobial
8 membranes enabled by nanomaterials for water treatment, J. Memb. Sci. 550 (2018) 173–
9 197. doi:10.1016/j.memsci.2017.12.071.
- 10 [122] A.C. Fonseca, R.S. Summers, A.R. Greenberg, M.T. Hernandez, Extra-cellular
11 polysaccharides, soluble microbial products, and natural organic matter impact on
12 nanofiltration membranes flux decline, Environ. Sci. Technol. 41 (2007) 2491–2497.
13 doi:10.1021/es060792i.
- 14 [123] J. Lin, X. Chen, C. Chen, J. Hu, C. Zhou, X. Cai, W. Wang, C. Zheng, P. Zhang, J. Cheng,
15 Z. Guo, H. Liu, Durably Antibacterial and Bacterially Antiadhesive Cotton Fabrics Coated
16 by Cationic Fluorinated Polymers, ACS Appl. Mater. Interfaces. 10 (2018) 6124–6136.
17 doi:10.1021/acsami.7b16235.
- 18 [124] K. Zodrow, L. Brunet, S. Mahendra, D. Li, A. Zhang, Q. Li, P.J.J. Alvarez, Polysulfone
19 ultrafiltration membranes impregnated with silver nanoparticles show improved
20 biofouling resistance and virus removal, Water Res. 43 (2009) 715–723.
21 doi:10.1016/j.watres.2008.11.014.
- 22 [125] X. Liu, S. Qi, Y. Li, L. Yang, B. Cao, C.Y. Tang, Synthesis and characterization of novel

- 1 antibacterial silver nanocomposite nanofiltration and forward osmosis membranes based
2 on layer-by-layer assembly, *Water Res.* 47 (2013) 3081–3092.
3 doi:10.1016/j.watres.2013.03.018.
- 4 [126] H.C. Pappas, S. Phan, S. Yoon, L.E. Edens, X. Meng, K.S. Schanze, D.G. Whitten, D.J.
5 Keller, Self-Sterilizing, Self-Cleaning Mixed Polymeric Multifunctional Antimicrobial
6 Surfaces, *ACS Appl. Mater. Interfaces.* 7 (2015) 27632–27638.
7 doi:10.1021/acsami.5b06852.
- 8 [127] M. Dadashi Firouzjaei, M. Pejman, M. Sharifian Gh, S. Aghapour Aktij, E. Zolghadr, A.
9 Rahimpour, M. Sadrzadeh, A. Arabi Shamsabadi, A. Tiraferri, M. Elliott, Functionalized
10 Polyamide Membranes Yield Suppression of Biofilm and Planktonic Bacteria while
11 Retaining Flux and Selectivity, *Sep. Purif. Technol.* 282 (2021) 119981.
12 doi:10.1016/j.seppur.2021.119981.
- 13 [128] L. Sarango, J. Benito, I. Gascón, B. Zornoza, J. Coronas, Homogeneous thin coatings of
14 zeolitic imidazolate frameworks prepared on quartz crystal sensors for CO₂ adsorption,
15 *Microporous Mesoporous Mater.* 272 (2018) 44–52.
16 doi:10.1016/J.MICROMESO.2018.06.018.
- 17 [129] S. Zhao, L. Zou, C.Y. Tang, D. Mulcahy, Recent developments in forward osmosis:
18 Opportunities and challenges, *J. Memb. Sci.* 396 (2012) 1–21.
19 doi:10.1016/j.memsci.2011.12.023.
- 20 [130] N.T. Hancock, T.Y. Cath, Solute Coupled Diffusion in Osmotically Driven Membrane
21 Processes, *Environ. Sci. Technol.* 43 (2009) 6769–6775. doi:10.1021/es901132x.
- 22 [131] W.A. Phillip, J.S. Yong, M. Elimelech, Reverse Draw Solute Permeation in Forward

- 1 Osmosis: Modeling and Experiments, *Environ. Sci. Technol.* 44 (2010) 5170–5176.
2 doi:10.1021/es100901n.
- 3 [132] Q. She, X. Jin, C.Y. Tang, Osmotic power production from salinity gradient resource by
4 pressure retarded osmosis: Effects of operating conditions and reverse solute diffusion, *J.*
5 *Memb. Sci.* 401–402 (2012) 262–273. doi:10.1016/J.MEMSCI.2012.02.014.
- 6 [133] D.L. Shaffer, J.R. Werber, H. Jaramillo, S. Lin, M. Elimelech, Forward osmosis: Where
7 are we now?, *Desalination*. 356 (2015) 271–284. doi:10.1016/j.desal.2014.10.031.
- 8 [134] M.H. Zhao, X.P. Chen, Q. Wang, Wetting failure of hydrophilic surfaces promoted by
9 surface roughness, *Sci. Rep.* 4 (2014). doi:10.1038/srep05376.
- 10 [135] J. Wu, W. Lin, Z. Wang, S. Chen, Y. Chang, Investigation of the Hydration of Nonfouling
11 Material Poly(sulfobetaine methacrylate) by Low-Field Nuclear Magnetic Resonance,
12 *Langmuir*. 28 (2012) 7436–7441. doi:10.1021/la300394c.
- 13 [136] L. Shen, X. Zhang, J. Zuo, Y. Wang, Performance enhancement of TFC FO membranes
14 with polyethyleneimine modification and post-treatment, *J. Memb. Sci.* 534 (2017) 46–58.
15 doi:10.1016/J.MEMSCI.2017.04.008.
- 16 [137] S.F. Seyedpour, M. Dadashi Firouzjaei, A. Rahimpour, E. Zolghadr, A. Arabi
17 Shamsabadi, P. Das, F. Akbari Afkhami, M. Sadrzadeh, A. Tiraferri, M. Elliott, Toward
18 Sustainable Tackling of Biofouling Implications and Improved Performance of TFC FO
19 Membranes Modified by Ag-MOF Nanorods, *ACS Appl. Mater. Interfaces*. 12 (2020)
20 38285–38298. doi:10.1021/acsami.0c13029.
- 21 [138] High Resolution XPS of Organic Polymers: The Scienta ESCA300 Database (Beamson,
22 G.; Briggs, D.), *J. Chem. Educ.* 70 (1993) A25. doi:10.1021/ed070pa25.5.

- 1 [139] S. Kim, Y.S. Yun, Y.E. Choi, Development of waste biomass based sorbent for removal
2 of cyanotoxin microcystin-LR from aqueous phases, *Bioresour. Technol.* 247 (2018) 690–
3 696. doi:10.1016/j.biortech.2017.09.164.
- 4 [140] A. Mohtasebi, T. Chowdhury, L.H.H. Hsu, M.C. Biesinger, P. Kruse, Interfacial Charge
5 Transfer between Phenyl-Capped Aniline Tetramer Films and Iron Oxide Surfaces, *J.*
6 *Phys. Chem. C.* 120 (2016) 29248–29263. doi:10.1021/acs.jpcc.6b09950.
- 7 [141] S. Yuan, G. Xiong, A. Roguin, S. Hin, C. Choong, Amelioration of Blood Compatibility
8 and Endothelialization of Polycaprolactone Substrates by Surface-Initiated Atom Transfer
9 Radical Polymerization, in: *Adv. Biomater. Sci. Biomed. Appl., InTech*, 2013.
10 doi:10.5772/52646.
- 11 [142] E.M. Vrijenhoek, S. Hong, M. Elimelech, Influence of membrane surface properties on
12 initial rate of colloidal fouling of reverse osmosis and nanofiltration membranes, *J. Memb.*
13 *Sci.* 188 (2001) 115–128. doi:10.1016/S0376-7388(01)00376-3.
- 14 [143] M. Elimelech, W.A. Phillip, The future of seawater desalination: Energy, technology, and
15 the environment, *Science* (80-.). 333 (2011) 712–717. doi:10.1126/science.1200488.
- 16 [144] Y. Mo, A. Tiraferri, N.Y. Yip, A. Adout, X. Huang, M. Elimelech, Improved antifouling
17 properties of polyamide nanofiltration membranes by reducing the density of surface
18 carboxyl groups, *Environ. Sci. Technol.* 46 (2012) 13253–13261. doi:10.1021/es303673p.
- 19 [145] D. Ma, S.B. Peh, G. Han, S.B. Chen, Thin-Film Nanocomposite (TFN) Membranes
20 Incorporated with Super-Hydrophilic Metal-Organic Framework (MOF) UiO-66: Toward
21 Enhancement of Water Flux and Salt Rejection, *ACS Appl. Mater. Interfaces.* 9 (2017)
22 7523–7534. doi:10.1021/acsami.6b14223.

- 1 [146] F. Mohammadnezhad, M. Feyzi, S. Zinadini, A novel Ce-MOF/PES mixed matrix
2 membrane; synthesis, characterization and antifouling evaluation, *J. Ind. Eng. Chem.* 71
3 (2019) 99–111. doi:10.1016/j.jiec.2018.09.032.
- 4 [147] S. Yang, Q. Zou, T. Wang, L. Zhang, Effects of GO and MOF@GO on the permeation
5 and antifouling properties of cellulose acetate ultrafiltration membrane, *J. Memb. Sci.* 569
6 (2019) 48–59. doi:10.1016/j.memsci.2018.09.068.
- 7 [148] M.D. Firouzjaei, A.A. Shamsabadi, S.A. Aktij, S.F. Seyedpour, M.S. Gh., A. Rahimpour,
8 M.R. Esfahani, M. Ulbricht, M. Soroush, Exploiting Synergetic Effects of Graphene
9 Oxide and a Silver-Based Metal–Organic Framework To Enhance Antifouling and Anti-
10 Biofouling Properties of Thin-Film Nanocomposite Membranes, *ACS Appl. Mater.*
11 *Interfaces.* 10 (2018) 42967–42978. doi:10.1021/ACSAMI.8B12714.
- 12